University of Arkansas, Fayetteville

# ScholarWorks@UARK

Graduate Theses and Dissertations

12-2018

# Fabrication and Characterization of Electrochemical Glucose Sensors

Mohammed Marie
*University of Arkansas, Fayetteville*

Follow this and additional works at: https://scholarworks.uark.edu/etd

Part of the Electronic Devices and Semiconductor Manufacturing Commons, Engineering Physics Commons, and the Semiconductor and Optical Materials Commons

Fabrication and Characterization of Electrochemical Glucose Sensors

A dissertation submitted in partial fulfillment
of the requirements for the degree of
Doctor of Philosophy in Microelectronics-Photonics

by

Mohammed Marie
University of Baghdad
Bachelor of Science in Physics, 2001
University of Tikrit
Master of Science in Physics, 2007

December 2018
University of Arkansas

This dissertation is approved for recommendation to the Graduate Council.


_____
Omar Manasreh, Ph.D.
Dissertation director


_____          _____
Simon Ang, Ph.D.                              Jiali Li, Ph.D.
Committee Member                              Committee Member


_____          _____
Jingxian Wu, Ph.D.                            Rick Wise, Ph.D.
Committee Member                              Ex-Officio Member

The following signatories attest that all software used in this dissertation was legally licensed for the use by Mohammed Marie for research purposes and publication.


_____          _____
Mohammed Marie, Student                   Dr. Omar Manasreh, Dissertation Director


This dissertation was submitted to http://www.turnitin.com for plagiarism review by the TurnItIn company's software. The signatories have examined the report on this dissertation that was returned by TurnItIn and attest that, in their opinion, the items highlighted by the software are incidental to common usage and are not plagiarized material.


_____          _____
Dr. Rick Wise, Program Director           Dr. Omar Manasreh, Dissertation Director

**Abstract**

Electrochemical sensors based on the nanostructure of the semiconductor materials are of tremendous interest to be utilized for glucose monitoring. The sensors, based on the nanostructure of the semiconductor materials, are the third generations of the glucose sensors that are fast, sensitive, and cost-effect for glucose monitoring.

Glucose sensors based on pure zinc oxide nanorods (NRs) grown on different substrates, such ITO, FTO, and Si/SiO$_2$/Au, were investigated in this research. Silicon nanowire (NW)-based glucose sensors were also studied. First, an enzyme-based glucose sensor was fabricated out of glass/ITO/ZnO NRs/BSA/GO$_x$/nafion membrane. The sensor was tested amperometrically at different glucose concentrations. The device showed a high sensitivity and a lower limit of detection in the order of 10.911 mA/cm$^2$ mM and 0.22 μM, respectively. In addition, the device exhibited a fast and a sharp amperometric time response of ~3 s with different glucose concentrations.

The high surface-to-volume ratio provided by the ZnO NRs was investigated by characterizing the sensor with and without the ZnO NRs grown on Si/SiO$_2$/Au substrates. The sensor showed almost a negligible amperometric response to the changes in the glucose concentrations without ZnO NRs. After applying the ZnO NRs, the sensor exhibited a linear response to the glucose concentrations from 1-8 mM. Furthermore, very clear oxidation peaks were observed at the scan rates of 100 and 200 mV/s in the presence of 2 mM of the glucose. The device showed no dependency on different scan rates without applying the ZnO NRs.

An enzyme-free glucose sensor was fabricated based on ZnO NRs grown on FTO and modified with Fe$_2$O$_3$. The device showed a high sensitivity and a wide amperometric linear response on the order of 0.052 μA/cm$^2$ and from 100-400 mg/dL, respectively. Reactive ion

etching and nanosphere lithography methods were utilized to grow the Si NWs vertically on top of a silicon wafer. The sensor showed a high linearity from 1-9 mM for changes in glucose concentrations. In addition, the high surface-to-volume ratio provided by the Si NWs helped in adsorbing higher concentrations of the enzyme.

**Acknowledgements**

I would like to express my deep thankfulness to my academic advisor Dr. Omar Manasreh for his unlimited help, support, guidance, and advices throughout my Ph.D. research. His way of giving the students the lead makes me more confident and independent.

I would like also to say a big thank you to my committee members for their help and support to make this work successful. Thank you very much to Dr. Rick Wise, Dr. Simon Ang. Dr. Jingxian Wu, and Dr. Jiali Li. Special thanks to Professor Ken Vickers who was there for any help and guidance I needed.

Many thanks go to my research group in the optoelectronics lab in the Electrical Engineering Department. Thank you to Ramesh Vasan, Ahmad Nusir, Hayder Salman, Yahia Makableh, Jony Sarker, Sanghamitra Mandal, Seung Yong Lee, Raad Haleoot, and Wafaa Gebril.

My deep appreciation and gratitude go to my wife, Fatima Ibrihem, for her unlimited support and unlimited patience. Without her support and encouragement, it would be impossible to finish this work.

I owe deep thanks to my extended family for their support and encouragement. The honest supplications of my mother, brothers, and sisters helped me to face all the difficulties while studying abroad.

**Taken from author's published works**

**Chapter 2** is partially produced from my published papers in Sensors, Chemosensors, and Nanotechnology. **Chapter 3** is mainly produced from my published papers in Sensors, Chemosensors, and Nanotechnology.

1. **M. Marie**, S. Mandal, and O. Manasreh, "An Electrochemical Glucose Sensor Based on Zinc Oxide Nanorods," Sensors, vol. 15, no. 8, pp. 18714-18723, Aug 2015.

2. **M. Marie** and M. O. Marasreh, "Investigation of the Influence of the As-Grown ZnO Nanorods and Applied Potentials on an Electrochemical Sensor for In-Vitro Glucose Monitoring," Chemosensors, vol. 5, no. 1, 2017.

3. **M. Marie**, A. Manoharan, A. Kuchuk, S. Ang, and M. O. and Manasreh, "Vertically grown zinc oxide nanorods functionalized with Ferric oxide for in-vivo and non-enzymatic glucose detection," *Nanotechnology,* vol. 29, no. 11, 2018.

**Dedication**

To my mother with my deep love and compassion

To my father's soul in the heaven

To my beloved wife and children (Abdulmuhaimin, Omar, Abdulmelik, and Razan)

To my brothers and sisters (my supporters)

**Table of Contents**

# List of Figures

**List of Tables**

**List of Abbreviations**

| | |
|---|---|
| ZnO NRs | Zinc oxide nanorods |
| Si NWs | Silicon nanowires |
| Ag NPs | Silver nanoparticles |
| PBS | Phosphate buffer solution |
| $GO_x$ | Glucose oxidase |
| Au NPs | Gold nanoparticles |
| LOD | Lower limit of detection |
| FAD | Flavin adenine dinucleotide |
| $H_2O_2$ | Hydrogen peroxide |
| HF | Hydrofluoric acid |
| MOSFET | Metal oxide semiconductor field effect transistor |
| $C_{dl}$ | Double layer capacitor |
| $R_{sol}$ | Solution resistor |
| $C_{di}$ | Dielectric capacitor |
| $M_{ox}$ | Oxidation of mediator |
| $M_{red}$ | Reduction of mediator |
| SEM | Scanning electron microscopy |
| XRD | X-ray diffraction |
| PDMS | polydimethylsiloxane |
| $SiO_2$ | Silicon dioxide |
| CVD | Chemical vapor deposition |
| ITO | Indium tin oxide |

| | |
|---|---|
| FTO | Fluorine doped tin oxide |
| II-VI | Groups 2 and 6 in the periodic table |
| eV | Electron volte |
| PIE | Piezoelectric |
| CuO | Copper oxide |
| mM | Millimolar |
| RPM | Rotation per minute |
| DI water | Deionized water |
| M | Molar |
| TOAB | Tetraoctylammonium bromide |
| sccm | Standard cubic centimeter per minute |
| ICP | Inductive coupled plasma |
| RF | Radio frequency |
| RIE | Reactive ion etching |

**Chapter 1  Introduction**

**1.1  Diabetes mellitus**

Millions of people are affected by diabetes mellitus all over the world. Heart attacks and kidney failure are direct serious health problems associated with the diabetes [1-6]. The number of diabetic people is directly correlated proportional with aging, the growth of population, obesity, and the availability of clean and healthy food and water resources [7]. Diabetes mellitus is expected to increase rapidly in the coming years especially in the undeveloped countries based on the World Health Organization.  In 2005, around 347 million patients were clinically diagnosed as diabetic people, and the number is expected to be doubled by 2030 [5].

Diabetes mellitus can be mainly categorized into two types, type1 and type 2 diabetes [8,9]. The first type of diabetes is the insufficient production of insulin by the pancreas, and it requires a continuous compensation of insulin to regulate the glucose level in the blood. The destruction of β cells in the blood is a major reason to have a type 1 diabetes mellitus. Beta cells are responsible for storing and releasing insulin in the blood to regulate the glucose concentrations.

When the glucose concentration level in the blood is higher than the normal concentration, β cells secrete some of their stored insulin [10, 11]. The other type of diabetes is classified as insulin resistance and it is known as type 2 diabetes [12, 13]. It occurs when the produced insulin is not recognized by the body leading to a high concentration of glucose in the blood. Studies showed that this type of diabetes might be controlled by taking some drugs and following certain diets and daily physical activities [14].

### 1.2 Glucose detection methods

### 1.2.1 Invasive method of glucose detection

Glucose sensors are devices that convert the biological reaction inside the body into an electrical signal, which can be detected easily. Those glucose sensors can be wearable, portable, or as an installed setup [15-17]. The biological sensors are designed to react with the biological elements in the body, such as enzymes, proteins, or other electroactive species in the blood. Generally, glucose sensors are nontoxic devices allowing them to be used widely to monitor glucose safely and accurately. Glucose concentration in the blood is well-known by glycemia. Higher and lower glucose concentrations are known as hyperglycemia and hypoglycemia, respectively [18]. There are three major approaches to evaluate the concentrations of glucose in the blood: fully invasive, minimally invasive, and noninvasive [19]. The invasive one requires a finger prick to extract enough blood from the person with diabetes. The extracted blood is then placed on the strip test, which is the glucose sensor, and the strip test is connected to the glucose meter to read out the concentrations of the glucose using units of either mg/dL or mmol/L.

### 1.2.2 Minimally invasive approaches of glucose sensing

Minimally invasive approaches relay on subcutaneous glucose monitoring. This way of glucose monitoring is based on analyzing the interstitial fluids which are underneath the skin and determining the concentrations of glucose in the extracted fluid. Minimally invasive glucose detection focuses on extracting the required fluid underneath the skin without damaging the blood vessel [20]. Minimally invasive approaches of glucose detection work based on several mechanisms, such as amperometric and enzymatic based sensors [21, 22], microneedle array-based glucose sensors, carbon nanotube-based sensors, and florescence-based glucose sensors [23]. The idea is to extract the interstitial fluids from some less sensitive areas in the body, such

2

as forearm, upper arm, and thigh [24].

Those areas in the body are less sensitive than the finger prick. Continuous monitoring of glucose can be done using either minimally invasive or fully non-invasive methods [25]. One way to carry out the minimally invasive method for glucose detection is by analyzing the refractive index of the interstitial fluid. To extract the interstitial fluid underneath the skin, the skin is treated ultrasonically by applying a continuous source of ultrasound. This procedure helps in enhancing the permeability of the skin by creating new passages that the interstitial fluid will pass through. The interstitial fluid is then extracted by using a vacuum pump which is connected to the resonance sensor. The extracted interstitial fluid is analyzed through the refractive index on the surface of the resonance sensor and the concentrations of glucose can be detected easily [26]. The time of the ultrasound that the patients need to use for minimally invasive monitoring of glucose varies depending on several parameters.

Another way to fabricate a minimally invasive glucose sensor is the microneedle array. The working electrode of the minimal invasive glucose sensor is designed using a negative photoresist called SU8 50 and the design is metallized with platinum to form the working electrode [27]. These kinds of devices are produced to monitor the glucose concentrations using the interstitial fluid continuously while reducing the pain as low as possible. The microneedle array-based minimally invasive method of glucose monitoring can also be inserted underneath the skin of the diabetic patients [28, 29]. These kinds of minimally invasive sensors function based on the correlation between the concentrations of glucose in the interstitial fluid and the concentrations of glucose in the blood [30, 31].

### 1.2.3 Fully noninvasive method of glucose detection

The other approach to monitor diabetes and to measure the concentrations of glucose is

3

the fully noninvasive method. This way to monitor glucose was given tremendous attention since glucose concentrations are monitored without extracting blood from diabetic patients [32]. In addition, using the fully noninvasive method, diabetic people have the opportunity to monitor their glucose concentrations continuously and easily from home without any need to visit their doctors regularly. Several different approaches for noninvasively monitoring of glucose have been investigated, such as electrochemical, optical, electrical, and ultrasound [33, 34]. Each fully noninvasive approach of glucose monitoring has some advantages and disadvantages. Since there is no subcutaneous measurement by using the fully noninvasive method to monitor and to detect the changes in the glucose concentrations, sensitivity, selectivity, and accuracy are the major issues in this method. Furthermore, the lower limit of detection is another problem to be determined noninvasively. The most accurate and effective approach of detecting glucose noninvasively is by using the electrochemical enzyme glucose sensors [35].

The working mechanism of detecting glucose noninvasively depends mainly on the capability of the glucose sensor to detect the sodium ions in the blood [36]. Sodium ions are the major molecules in the interstitial fluids underneath the skin. The mechanism of detection is well-known by the reverse ionotophoresis by applying a mild electric current into the skin to extract the interstitial fluids to the surface of the skin. Due to the natural negative charge of the skin at the neutral pH, sodium ions will be attracted to the positive electrode of the sensor that sticks on the skin. The sodium ions will extract the other interstitial fluid underneath the skin to the surface of the skin [37-39]. Glucose is one of the electroactive species in the interstitial fluid underneath the skin. The electrochemical sensors that are used to detect the glucose noninvasively among several other electroactive species are the enzymatic based sensors. The role of the enzyme in this detection method is to increase the selectivity of the sensor toward

glucose molecules to avoid any contamination in the detected signal since the concentrations of

the glucose in the blood is much higher than the concentration of the glucose in the interstitial

fluids. Ultrasonic energy is used to determine the concentration of the glucose in the blood.

However, the drawback of this method is the size of the sensor which makes it difficult to be

used as a wearable sensor. In addition, the method depends on using a biological sensor, which

makes it a costly approach for glucose detection [40].

Optical coherence tomography is another noninvasive method for glucose detection. It

works based on detecting the reflected scattered light from the target molecules. The changes in

the scattered light due to the changes in the refractive index of the targeted molecules are

detected and analyzed to determine the concentrations of glucose in the blood [41, 42]. This

method of glucose concentration detection consists of a low-coherent light, a source, a reference

arm, and a sensitive detector to detect the backscattered light. Near-infrared light sources are

used in the optical coherence tomography method. In this method, the infrared light can penetrate

the skin up to 1 mm. The output signal from the detector can be written as:

$$I_d(\tau)=I_s+I_r+2(I_s \times I_r)^{1/2} \mid V_{tc}(\tau) \mid \cos (2\pi v\tau), \qquad \text{(Equation 1.1)}$$

where $I_s$ is the intensity of the light in the sample, $I_r$ is the intensity of the light in the reference

arm, $V_{tc}$ is the temporal coherent function, and $v$ is the frequency of the incident light [43]. From

Equation 1, the detected signal is in direct proportion to the intensities of the light in the

reference arm and the sample that is under investigation. The selectivity is one of the hurdles

faced when using this method of detection. The changes in the properties of the backscattered

light can be influenced by other electroactive species in the interstitial fluid in the tissues

underneath the skin [44]. Thus, the detected signal might not be associated only with the

concentrations of glucose. In addition, the complex structure, the thickness of the skin, and the

5

big differences between the concentrations of the glucose in the blood and in the interstitial fluids underneath the skin make the signal-to-noise ratio very low. Thus, it is difficult to increase the sensitivity and the selectivity of such methods of glucose detection.

## 1.3 Drawbacks of the minimally and fully noninvasive approaches

The low sensitivity and specificity of the minimally and fully noninvasive methods of glucose detection is one of the big hurdles that makes it difficult to accurately sense glucose concentrations for diabetic people. One of the reasons for the low sensitivity and selectivity is the low signal-to-noise ratio. Low signal-to-noise ratio means that the detected signal has a high noise because of the influence of the other electroactive species in the blood. To enhance the selectivity and the sensitivity of the minimally invasive and fully invasive glucose detection methods, a high signal-to-noise ratio must be obtained [45, 46 -25]. The other issue with the fully and minimally invasive measurements of glucose is the calibration. Real blood samples must be taken from the patient before using the noninvasive devices to monitor glucose. The blood samples are used as references to ensure the accuracy of the noninvasive measurement and to compare the results. The majority of the minimally and fully invasive measurements of glucose require a complex calibration process to ensure the accuracy of the measurement [47]. Three hours of calibration and four measuremets each hour are required to calibrate the NBM-200G noninvasive system of glucose detection [48]. Two to three days of calibration are nessesary to calibrate another noninvasive system called Pendra [49].

Predicting the concentrations of glucose multiple times for diabetic people is dificult using the noninvasive techniques [50]. This comes from the big difference between the glucose in the interstitial fluids and the concentrations of the glucose in the blood. This is a major challenge for the minimally and fully noninvasive methods of glucose detection, especially for

optical-based noninvasive techniques [51]. Since people with diabetes are required to follow a certain diet and medications, it is essential that diabetic people have very accurate data by using the continuous glucose monitoring system. Having non-accurate measurements of the concentration of the glucose in the blood might lead diabetic people to have several complications, such as heart attacks, kidney failure, brain damage, and vision problems. Furthermore, all the noninvasive methods of glucose detection require a continuous calibration, which means that people with diabetes still have to puncture their fingers to extract a blood sample. The physiological differences between the concentrations of glucose in the blood and in the interstitial fluids have lead people to come up with other techniques to overcome the sensitivity and selectivity problems. One of these techniques is the dynamic concentration correction. It is about the ability of transferring the mass of glucose between the interstitial fluids underneath the skin and the blood during the noninvasive and optical measurements of the glucose [52].

## 1.4  The enzyme glucose oxidase, $GO_x$

Glucose oxidase, $GO_x$ and PQQ-glucose dehydrogenases are two families of enzymes that have been used widely in electrochemical glucose sensors. There are several differences between the two families of the enzymes, such as their oxidation and reduction potential, their chemical structure, their capabilities to react with glucose, their cofactors, and their apparent Michaelis-Menten constants [53].  Glucose oxidase is the most commonly used enzyme in the electrochemical glucose sensors. The enzyme, $GO_x$, is a biocompatible chemical material that can be used safely in biological and electrochemical sensors. It has a complex chemical structure and the specificity of the enzyme toward glucose makes it a great candidate to be used in the enzymatic glucose sensors. However, the lifetime of the enzyme is an issue that limits the

lifetime of the enzymatic glucose sensors. The glucose sensors using the enzyme, $GO_x$, in general suffer from a short lifetime since $GO_x$ is sensitive to temperature, humidity, and other harsh environments. To avoid the degradation of the biological activities of the enzyme glucose oxidase due to temperature, humidity, chemical solvents, and other harsh environment conditions, the working electrodes of the sensor must be stored in specific places under specific conditions. Because of the biological degradation activities of the enzyme, the reproducibility of the enzymatic glucose electrochemical sensors has become a big issue. The protein, flavin adenine dinucleotide (FAD), which is in the center of $GO_x$, works as an electron acceptor during the electrochemical reaction of glucose sensing.

## 1.5  Electrochemical glucose sensors

Electrochemical sensors are the most used devices for glucose detection [2]. Electrochemical glucose sensors can be divided into three groups based on the measurement principles, which are potentiometric measurements, amperometric measurements, and impedimetric measurements. In addition, those sensors are categorized into three generations according to the electron transfer mechanism, first, second, and third generations. The third generation is divided into two groups, enzymatic and non-enzymatic electrochemical sensors.

## 1.5.1  The structure of the enzymatic electrochemical glucose sensors

The enzymatic glucose sensors are the most used devices for glucose sensing and in the continuous glucose monitoring systems. The enzymatic glucose sensors consist of three different electrodes. The working, or the sensing, electrode is the part of the enzymatic sensor in which the electrochemical reaction takes place and it is the electrode that is modified by the enzyme. The counter electrode, which is mainly made of a platinum metal, is used in the electrochemical glucose sensors to enable the oxidation and reduction reaction on the surface of the working

electrode. The third electrode in the electrochemical sensor is the reference electrode. The most common used reference electrode is silver/silver chloride (Ag/AgCl). It is very necessary to control the oxidation and the reduction potential during the sensing measurement of the glucose in the blood in order to assure a high sensitivity and a high selectivity of the electrochemical sensor.

The reference electrode, Ag/AgCl, is well-known by its oxidation potential, which is around 0.1 volt. Thus, using Ag/AgCl in the electrochemical sensors during the sensing process keeps the electrochemical reaction under control and helps in controlling the applied potential over the working electrode. Controlling the applied potential during the sensing measurement leads to enhanced selectivity by eliminating the influence of the other electrochemical species in the blood besides glucose. At high applied potentials, there is a big chance that other components, such as ascorbic acid, uric acid, cholesterol, and so on, will be oxidized and influence the sensed signal. This is a main reason for the low signal to noise ratio that most glucose sensors suffer from.

**1.5.2 Electrochemical sensors based on the measurement principle**

**1.5.2.1 Potentiometric measurement**

This kind of measurement is utilized when the concentration of glucose in the analytical solution under the test is within the physiological range of glucose in the blood. It works based on measuring the potential difference between the sensing and the reference electrodes in the electrochemical cell at zero current flow between the two electrodes [54-56]. The reference electrode is usually made of Ag/AgCl, which has a very stable potential during the electrochemical measurements. Whereas, the potential at the working electrode varies depending on the concentration of the glucose in the analytical solution. The potential difference between

9

the two electrodes is detected as a function to the glucose concentrations. The recorded potential

is calculated according to Nernst equation [57].

$$E = E_{\text{o}} \frac{RT}{\eta F} lnQ \qquad \text{(Equation 1.2)}$$

In Equation 1.2, $E$ is the output potential difference measured at zero, a negligible current

flows between the two electrodes, $E_{\text{o}}$ is the constant potential provided to the cell by the

reference electrode, $R$ is the universal gas constant, $T$ is the temperature in Kelvin, $\eta$ is number of

charge, $F$ is Faraday constant, and $Q$ is the ratio of the concentration of ions in the anode and in

the cathode. Potentiometric measurements are used in MOSFET-based glucose sensors, ion-

selective electrode-based sensors, and so on.

### 1.5.2.2 Amperometric measurement

Amperometric measurement of electrochemical glucose sensors is one of the most used

and sensitive methods to characterize these sensors [58]. In these electrochemical measurements,

the sensed signal is the current that is associated with the concentrations of the targeted

molecules in the analytical solution. The measurement is carried out by applying a fixed

potential between the two or three electrodes in the electrochemical cell [59]. In this

measurement, the glucose is oxidized on the surface of the working electrode and usually these

types of electrochemical measurements are carried out with three electrodes, which are the

working (sensing), the reference, and the counter electrodes. The presence of the reference

electrode is essential to control the potential voltage applied to the surface of the sensing

electrode. The sensed signal (current) is in direct proportional to the concentrations of the

glucose in the analytical solution. The linearity of the sensed current out of the amperometric

measurement reflects the sensitivity of the electrochemical glucose sensor toward the changes in

the glucose concentrations.

### 1.5.2.3  Impediametric measurements

The impedance-based glucose sensor is one of the methods that can be used to monitor glucose in the electrochemical sensors. The glucose detection mechanism works based on detecting the changes in the dielectric constant of the analyte [60]. The changes in the dielectric constant of the samples are associated with the changes in the glucose concentrations. The only problem that this approach faces is the double-layer capacitor, which is created from the interaction between the ions and molecules of the analytical solution with the surface of the electrode (electrode-electrolyte interaction). This problem can be solved by reducing the surface of the electrodes during the fabrication process [61-63]. The measured impedance is represented by the solution resistance, the dielectric capacitance, and the double-layered capacitors as in Equations 1.3 and 1.4.

$$Z_1 = \sqrt{R_{sol}^2 + \frac{1}{(\pi f C_{dl})^2}} \qquad \text{(Equation 1.3)}$$

$$Z_2 = \frac{1}{2\pi f C_{di}} \qquad \text{(Equation 1.4)}$$

After taking the measurements of different concentrations of glucose, the output impedance is analayzed at three different ranges of frequencies: low, medium, and high. As can be seen from Equation 1.3, at the low frequency regime, $Z_1$, the changes in the output impedance which are associated with the changes in the glucose concentrations in the analytical solution depend on the double layer capacitance $C_{dl}$. This might increase the noise in the detected impedance. At the high frequency regime, $Z_2$ (Equation 1.4) is the dominant parameter because the electric current passes through the solution without being affected by the double layered capacitors [62].  In the equivalent circuit in Figure 1.1 below, there are two double layered capacitors, $C_{dl}$, which are formed by the interference between the electrode and the electrolyte. Those capacitors are in series with the solution resistance, $R_{sol}$. The double layered capacitors are

in parallel with the analytical solution capacitors, $C_{di}$.
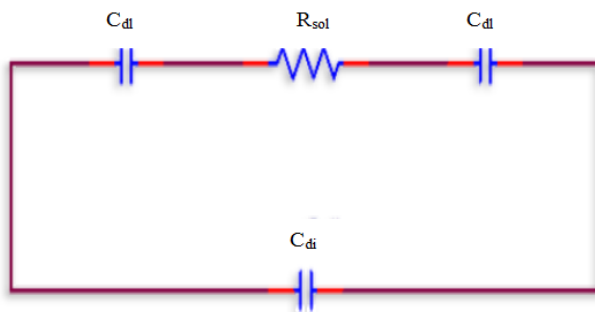


Figure 1.1. The equivalent circuit of the impedance analyzer method of glucose detection.

## 1.6 Electrochemical sensors based on electron transfer mechanism

### 1.6.1 The first generation of electrochemical glucose sensors

In the first generation of electrochemical glucose sensors, the electrode is modified by the enzyme, mostly glucose oxidase. The oxygen is the main mediator in between the electrode and the enzyme to help in oxidizing glucose in the analytical solution [64]. The enzyme, $GO_x$, has the flavin adenine dinucleotide (FAD) as a co-factor in its chemical structure. The FAD center is the responsible protein of the direct transfer of electrons between glucose oxidase and the surface of the working electrode in the presence of glucose. The reduction of oxygen to hydrogen peroxide is enhanced by several proteins, such as FAD and $FADH_2$. The FAD in the center of the enzyme $GO_x$, works as an electron acceptor, so it will be oxidized to $FADH_2$ by accepting the electrons from the glucose during electrochemical reaction.

Glucose oxidase is the specific enzyme for glucose detection due to its ability to react with glucose and produce hydrogen peroxide, $H_2O_2$, and gluconolactone. Hydrogen peroxide is oxidized to hydrogen, oxygen, and free electrons. The concentration of the hydrogen peroxide is associated with the concentration of the glucose in the analytical solution.  Also, the

12

concentration of glucose is determined by the concentration of the reduced oxygen. The produced electrons on the surface of the working electrode at different glucose concentrations can be detected amperometrically as an output current. The chemical structure of the D-glucose is as shown in Figure 1.2, and the electrochemical reaction is represented by Equations 1.5 to 1.9. In addition, the electrochemical reaction is illustrated schematically in Figure 1.3 [65]. The first generation of the electrochemical glucose sensors suffers from the lack of oxygen during the electrochemical reaction. This limited the effectiveness of use of these kinds of glucose sensors and triggered the attention to find a suitable replacement of the oxygen and to create a way to oxidize glucose without depending on the presence and concentration of the oxygen during the electrochemical reaction.

$$\text{Glucose} + \text{FAD-GO}_x \longrightarrow \text{FADH}_2\text{-GO}_x \qquad \text{(Equation 1.5)}$$

$$\text{FADH}_2\text{-GO}_x + O_2 \longrightarrow \text{FAD-GO}_x + H_2O_2 \qquad \text{(Equation 1.6)}$$

$$H_2O_2 \longrightarrow O_2 + 2H^+ + 2e \qquad \text{(Equation 1.7)}$$

The electrochemical reaction can be described as it follows:

$$\text{Glucose} + O_2 \xrightarrow{\text{GO}_x} \text{gluconic acid} + H_2O_2 \qquad \text{(Equation 1.8)}$$

$$H_2O_2 \longrightarrow O_2 + 2H^+ + 2e^- \qquad \text{(Equation 1.9)}$$

In both sets of electrochemical equations, the final step is that the hydrogen peroxide is oxidized to oxygen, hydrogen, and two free electrons.
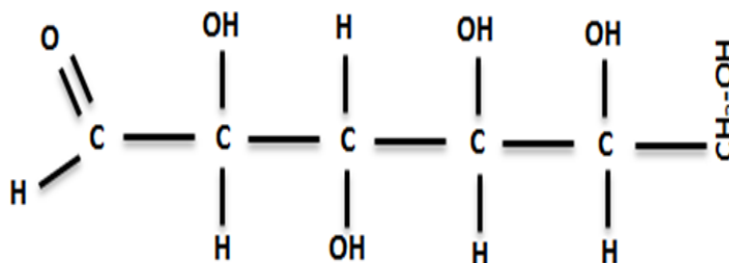


Figure 1.2. The chemical struture of D-glucose with the chemical formula $C_6H_{12}O_6$.
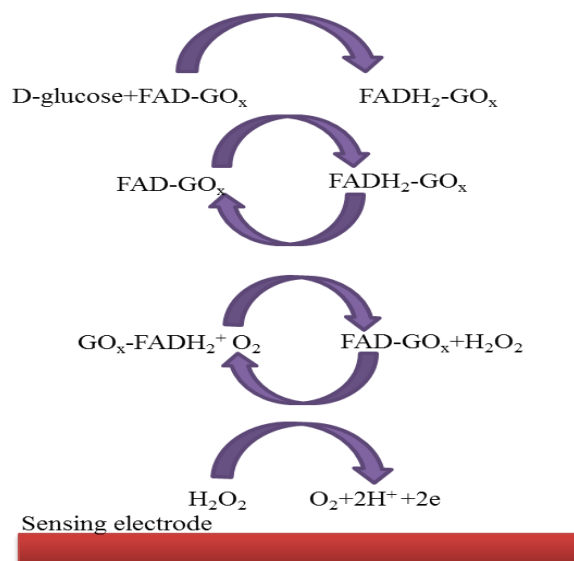
Figure 1.3. The electrochemical reaction of the first generation of the enzymatic electrochemical glucose sensors on the surface of the working electrode in the presence of different glucose concentrations [65].

### 1.6.2 The second generation of electrochemical glucose sensors

The second genetation of electrochemical glucose sensors works based on replacing the oxygen with artificial mediators [66]. It is not possible to directly tranfer the produced electrons by the enzyme itself due to the high barrier surrounding the FAD in the enzyme center created by the protein layer in the FAD. Therefore, artificial mediators are used to help in transferring the generated electrons from the enzyme center to the surface of the electrode. There are several artificial mediators that can be used as electron acceptors in the structure of the electrochemical glucose sensors, such as fericyanide, some organic and conductive salts, transition metal compounds, and ferrocene [67-69]. The electron transfer process between the center of the enzyme and the surface of the working electrode can be described in Figure 1.4 by the schematic structure [70]. In Figure 1.4, $M_{(ox)}$ is the oxidation mode of the artificial mediator. Whereas, $M_{(red)}$ is the reduction mode of the same mediator. The artificial mediator is oxidized in the

14

surface of the electrode producing free electrons. The concentration of the oxidized mediator is in direct proportional to the concentration of glucose in the analytical solution.

$$\text{Glucose} + GO_{x(ox)} \longrightarrow \text{Gluconic acid} + GO_{x(red)}$$

$$GO_{x(red)} + 2M_{(ox)} \longrightarrow GO_{x(ox)} + 2M_{(red)} + 2H^+$$

$$2M_{(red)} \longrightarrow 2M_{(ox)} + 2e^-$$
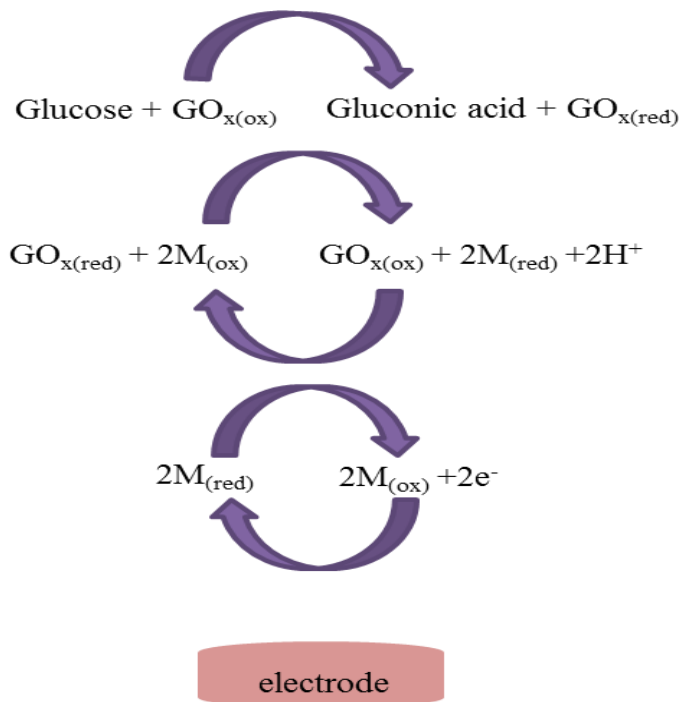
electrode

Figure 1.4. The electrochemical reaction of the second generation of the enzymatic electrochemical glucose sensors on the surface of the working electrode in the presence of different glucose concentrations [70].

### 1.6.3 The third generation of electrochemical glucose sensors

The working mechanisim of the third generation of electrochemical glucose sensors is to transfer the electrons directly from the center of the $GO_x$ to the surface of the electrode without using a mediator. This direct transfer is achieved by fabricating nanostructured materials based the working electrode [69, 71]. The drawback with the direct electron transfer is the sensitivity and selectivity of the enzyme. In the next sections, the third generation of the elctrochemical sensors will be discussed, and it will be divided into two groups: enzymatic and non-enzymatic glucose sensors.

## 1.7 Silicon nanowire-based enzymatic electrochemical sensors

Silicon nanowires have attracted tremendous attention due to their unique optical, electrical, and structural properties [72]. Silicon nanowires have been employed to construct several nano-devices, such as glucose sensors [73], field effect transistors [74], photodetectors [75], and photovoltage devices [76]. Silicon nanowires on silicon substrates can be grown using different methods, such as metal-assisted etching, nanosphere lithography, and electroless etching. Electrochemical glucose sensors are fabricated out of silicon nanowires arrays [77]. Silicon nanowires have a high affinity with several metals which enables fabricating modified working electrodes to be used in the electrochemical glucose sensors. For instance, the successful decoration of gold nanoparticles on the surface of the grown silicon nanowires enables construction of an enzymatic electrochemical glucose sensor based on the hybrid nanostructure [78].

Those kinds of enzymatic electrochemical sensors are sensitive, selective, and have a fast response to changes in the glucose concentrations. The high selectivity of the electrochemical glucose sensors based on the nanostructure of silicon is because of the high specificity of the enzyme glucose oxidase towards the glucose. Furthermore, due to the high surface-to-volume ratio provided by the silicon nanowires, more $GO_x$ is adsorbed by the electrochemical sensing area of the sensor. In other words, the silicon nanowires help in enhancing the active area of the enzymatic electrochemical sensor [79]. Silicon nanowires can be applied in the electrochemical glucose sensors to enhance the performance of the glucose sensors based on MOSFETs [74]. An example of Si NW-based glucose electrochemical sensors is illustrated in Figure 1.5.

From the figure, the drain and source are protected by the polydimethylsiloxane (PDMS) transparent insulator. The solution that contains the different glucose concentrations should not

16
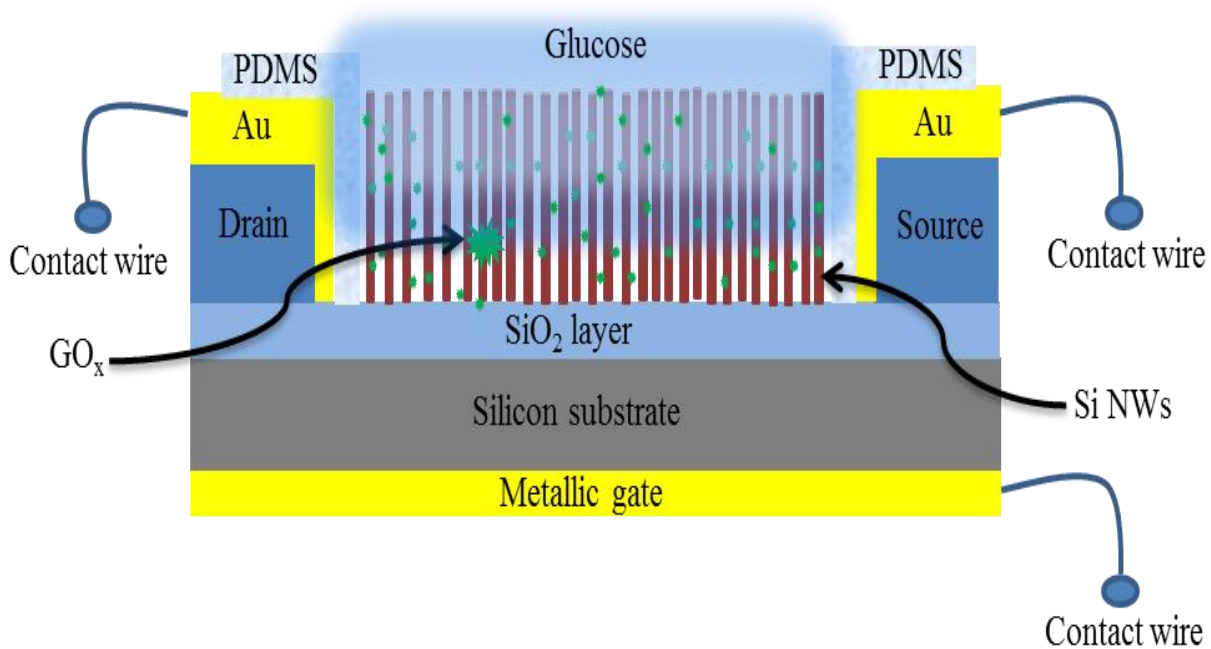
Figure 1.5. The schematic structure of a silicon nanowire-based enzymatic electrochemical glucose sensor that works based on the principle of a metal-oxide-semiconductor field effect transistor (MOSFET).

be in contact with the drain and source to avoid any short contact in the circuit during the measurements. The thickness of the oxide layer ($SiO_2$) varies and depends on the type of measurements and other parameters. The silicon dioxide thickness is usually deposited to be from 100-300 nm. The silicon substrate might be either n or p-type depending on the properties of the nanostructure of the semiconductor material in between the channel. The drain, source, and the gate are formed by depositing gold metal using different methods of deposition, such as electron-beam evaporator, sputtering system, or chemical vapor deposition (CVD). During the electrochemical measurements, a drain-source potential is applied for glucose detection and the MOSFET is biased by applying a fixed voltage to the gate in the back of the structure. The drain-source current is extracted as a function to either drain-source voltage or as a function to gate-source voltage.

## 1.8 ZnO nanorod-based enzymatic electrochemical sensors

The nanostructures of zinc oxide at different morphologies have been investigated to fabricate electrochemical sensors for glucose monitoring. A zinc oxide nanorod (ZnO NR)-based working electrode is utilized to detect glucose directly without a mediator. The surface of the as-grown ZnO NRs is immobilized with $GO_x$ and the immobilized structure is covered with a nafion membrane to enhance the stability of the structure. Figure 1.6 shows the working electrode of the ZnO NR-based electrochemical glucose sensor [80].
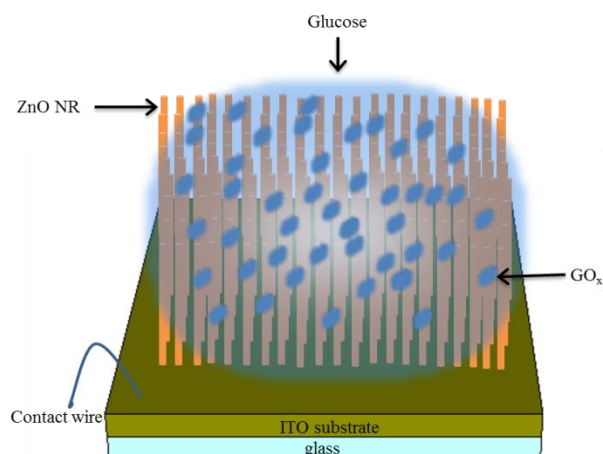


Figure 1.6. The schematic structure of the working electrode based on ZnO NRs modified with $GO_x$ on a conductive ITO substrate. Reprinted with permission from Marie et al. [80].

## 1.9 The non-enzymatic electrochemical glucose sensors

Although the enzymatic electrochemical glucose sensors are sensitive, selective, and easy to fabricate, reproducibility is a big problem since the biological activities of the electrochemical sensors depend on the enzyme, glucose oxidase [81, 82]. The non-enzymatic electrochemical sensors for glucose monitoring have, in general, longer lifetime compared with the enzymatic devices. However, the selectivity and the sensitivity of the non-enzymatic glucose sensors are lower than those of the enzymatic devices. To overcome the short lifetime of the working electrodes of the enzymatic electrochemical glucose sensors, several approaches have been

employed. All the efforts are directed toward replacing the enzyme glucose oxidase by manipulating the structure of the surface of the working electrode. The working electrode in the non-enzymatic electrochemical glucose sensors is modified in different ways to create microenvironment areas to host the glucose molecules.

Non-enzymatic electrochemical glucose sensors based on the nanostructure of materials specifically semiconductor materials, have attracted tremendous attention to produce highly efficient, highly selective, and highly sensitive glucose sensors [83]. The nanostructure material-based electrochemical glucose sensor is one of the desirable approaches that helps in enhancing the performance, increasing the accuracy, reducing the cost, decreasing the harmfulness, increasing the flexibility, and providing high level of safety for the users [84]. The nanostructure of semiconductor materials has unusual electrical, optical, mechanical, and structural properties that can be implemented to replace the enzyme-based glucose sensors.

## 1.10  Zinc oxide nanostructure for enzyme-free glucose sensors

Many toxic materials can be replaced with ZnO since this material is considered one of the nontoxic materials. The position of the interstitial zinc atoms and the vacancies atoms of oxygen make n-type is the natural doping of zinc oxide. Zinc oxide is of the group $II - VI$ in the periodic table [85]. Different morphologies of zinc oxide nanostructure have been studied along with different growth methods. In recent years, the nanostructure of zinc oxide is one of the most preferred semiconductor materials for biomedical applications, such as enzymatic and non-enzymatic electrochemical glucose sensors, DNA sequencing, pH sensors, gas sensors, pacemakers, and oximeter sensors. There are two main crystal structures of the ZnO semiconductor – the hexagonal wurtzite and cubic zinc blende – and the most stable structure is hexagonal wurtzite as shown in Figure 1.7 [86]. Zinc oxide has high sensitivity to chemical

materials at room temperature. The surface oxidation due to the oxygen vacancies on the ZnO

surface has an impact on the optical properties of ZnO nanostructures [87]. Zinc oxide has a

high isoelectric point (IEP) of 9.5, which makes it a great absorber for materials with lower IEP

[88]. The high affinity between zinc oxide and other semiconductors and metals enables creating

different hybrid nanostructures and thus has resulted in many non-enzymatic electrochemical

glucose sensors. The zinc oxide nanostructure works as a hosting medium that adsorbs other

nanomaterials, especially nanoparticles such as gold, platinum, and silver. Good examples of the

high affinity and the hybrid structure are ZnO-CuO, ZnO-Ag, ZnO-$Fe_2O_3$, ZnO-nafion, and

ZnO-Ag and Au nanoparticles.
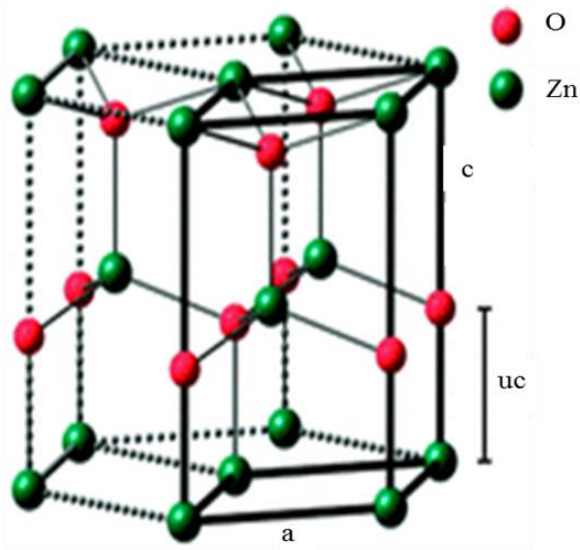


Figure 1.7. Hexagonal wurtzite structure of zinc oxide [86].

Cubic zincblende of ZnO is a stable structure if it is grown on cubic lattice structured

substrates [89]. Zinc oxide semiconductor has some favorable features, such as an acceptable

level of transparency, high electron mobility, and high luminescence at room temperature. Zinc

oxide has a direct band gap of 3.37 eV; this allows ZnO to absorb the wavelengths at the edge of

20

the visible region [90]. In other words, the photons with high energies and short wavelengths are absorbed by the ZnO nanostructure, and this increases the stability of zinc oxide. The piezoelectric phenomenon of ZnO makes it a favorable material for biological and medical applications. For instance, pacemaker devices that can be injected inside small areas of human bodies are considered one of the major applications based on the piezoelectric effect. The nanorod and nanotube structure of ZnO have been investigated extensively. The excellent control of the synthesis procedure to obtain the nanostructure of zinc oxide makes it very desirable for physics, chemistry, and materials science as well [91].

Table 1.1 is a comparison between enzymatic and non-enzymatic electrochemical sensors using different working electrodes.

Table 1.1 Summary of the different types of electrochemical glucose sensors based on the detection method: enzymatic and non-enzymatic.

| Type of sensing electrode | Sensing method | Sensitivity | Linear response  mM |
|---|---|---|---|
| Si NWs-Ag NPs | Enzymatic | - | (0.1-0.8) mM [78] |
| ZnO NRs-Au nanocomposite | Enzymatic | 1492 µA/mM $cm^2$ | (0.1-33) µM [92] |
| ZnO NRs-Graphene heterostructure | Enzymatic | 17.64 µA/mM |  (0.2-1.6) mM [93] |
| ZnO NWs-CuO NPs | Non-enzymatic | 3066.4 µA/mM $cm^2$ | Up to 1.6 mM [94] |
| $ZnO$-$Fe_2O_3$-nafion membrane | Non-enzymatic | 0.052 µA $cm^{-2}$ $(mg/dL)^{-1}$ | (100-400) mg/dL [95] |
| ZnO NRs powder surface-Carbon | Non-enzymatic | 2.97 µA/$cm^2$ mM | 0.1-10 mM [96] |
| CuO nanoparticles inkjet printed on electrode | Non-enzymatic | 2762 µA/$cm^2$ mM | 0.05-18.45 mM [97] |

**Chapter 2  Materials and devices growth, fabrication, and characterization techniques**

**2.1  Introduction**

Chapter Two is divided into two major sections. The first part of the chapter will be the growth and characterization of nanomaterials. Whereas, the second section of the chapter is about the fabrication of the devices and techniques used to characterize the fabricated devices. The growth of different nanostructures of materials, such as the growth of zinc oxide nanorods on different substrate — ITO, FTO, glass, and silicon substrate-coated gold — will be discussed in detail. In addition, the modification of ZnO NRs with ferric oxide using the dip-coating technique is summarized. The growth of silicon nanowires is explained in the chapter. Different growth methods were utilized to grow Si NWs horizontally and vertically. For instance, metal-assisted wet etching technique and nanospheres lithography method are discussed. In addition, a photolithography method was carried out with a photomask to etch silicon substrates horizontally. Device fabrication using the photolithography method and the electrochemical set-up are covered in this chapter.

Materials characterization techniques are discussed in detail. Different characterization methods, such as scanning electron microscopy, Raman spectroscopy, UV-visible-near IR spectrophotometer, x-ray diffraction, optical profiling, and microscope images were used to characterize the grown materials. Device characterization method, such as Keithley series Sourcemeter 2410 (Tektronix, Inc, Beaveron, OR), Gamry potentiostat (Gamry Instruments, Warninster, PA), and Semiconductor Simulator (Tektronix, Inc, Beaveron, OR) were used to test the fabricated devices. An electrochemical set-up consisting of three electrodes configuration was constructed to carry out the characterization tests, such as cyclic voltammetry, time response, amperometric response, and Michaelis-Menten constant.

## 2.2 Hydrothermal growth of ZnO nanorods

## 2.2.1 Growth of seed layer

Different growth methods can be utilized to grow ZnO NRs and the hydrothermal growth is one of the desired methods. The hydrothermal growth method can be controlled easily at low temperatures [98-100, 80]. Controlling the aspect ratio of the as-synthesized ZnO NRs is one of the most important parameters that make this method of growth a desirable approach. In the hydrothermal growth method, there are two parameters, the growth time and the growth temperature. The method is divided into two parts, the growth of the seed layers and the preparation of the growth solution.

To prepare the seed layer solution, or sol-gel solution, 0.5 M of the precursor, zinc acetate dehydrate ($Zn(CH_3COOH)_2 \cdot 2H_2O$), was mixed with 10 mL of methoxyethanol ($CH_3H_8O_2$ 99%), which is an organic compound known as a colorless solvent [80]. Both the precursor and the organic compound were placed on the hot plate at 75 °C under a continuous stirring at 300 rotations per minute (rpm) for one hour. A certain volume of ethanolamine, 0.3 mL of which is an organic chemical compound with high viscosity, was added to the mixture in order to increase the viscosity, to accelerate the dissolvent of the precursor in the organic compound, and to stabilize the chemical reaction. The addition of the 0.3 mL of the ethanolamine had to be after around 30 minutes of chemical reaction between the precursor zinc acetate dehydrate and the solvent methoxyethanol ($CH_3H_8O_2$ 99%). The addition of the ethanolamine was performed very slowly drop-by-drop to ensure the high solubility of the precursor zinc acetate dehydrate in the solvent methoxyethanol ($CH_3H_8O_2$ 99%). The mediator ethanolamine is also known as 2-aminoethanol or monoethanolamine and it has two abbreviations, ETA and MEA.

The viscosity of the sol-gel solution is controlled by the volume of the ethanolamine. In fact, it is very important to have the sol-gel solution at a certain viscosity in order to ensure a high quality film of the seed layer on the surface of the substrate. An ultrasound bath for one hour was carried out to ensure the homogeneity of the solution. It is worth mentioning that in most of the growth cases, mixing the precursor with the solvent at 300 rpm was not enough to ensure that there were no undissolved particles even if after sonication. Another important step was carried out which was the filtering of the mixture using 0.25 µm filter. The seed layer solution had to be kept at room temperature at least 24 hours before it could be used in the synthesis procedure. The seed layer solution had a lifetime around a month after the first synthesis. After one month, the seed layer solution started to degrade because of the degradation of the precursor zinc acetate dehydrate ($Zn(CH_3COOH)_2 \cdot 2H_2O$).

## 2.2.2 Synthesis of the growth solution

To complete the growth of ZnO NRs using the hydrothermal and sol-gel method, the growth solution was prepared using two different precursors. Zinc nitrate hexahydrate ($Zn(NO_3)_2 \cdot 6H_2O$) was used in the synthesis [80]. Zinc nitrate hexahydrate is an inorganic chemical compound and it is soluble in water and some other polar solvents. The powder phase of the zinc nitrate hexahydrate has a white color and since it has the hexahydrate in its chemical structure, it is normal to store it at room temperature. The inorganic chemical compound was used without any further purification. The other chemical that was used in the synthesis procedure of the growth solution was the hexamethylenetetramine. It is an organic chemical compound that has a high solubility in water and other polar solvents. Hexamethylenetetramine has a cage-like crystal structure, and it can be used in several applications, such as medical applications. It is used in treatments of some urinary tract infections as a medical salt.

To prepare the growth solution at 0.05 molarity, 0.025 M of zinc nitrate hexahydrate $(Zn(NO_3)_2 \cdot 6H_2O)$ was dissolved in a 10 mL of deionized water. In addition, a 0.025 M of hexamethylenetetramine was also dissolved in 10 mL of deionized water separately. The two prepared precursors were placed on a magnetic stirrer are stirred for one hour separately in a glass vial container at 300 rpm at room temperature. A micropipette was utilized to mix the two precursors together using a dropwise method. The two mixed solutions were stirred together for another hour to ensure the homogeneity between them and to ensure that all the salt was dissolved completely in the deionized water. It is worth mentioning that the pH of the growth solution must be kept at 7 to synthesize ZnO NRs.

For different morphologies of ZnO nanostructure, such as nanotubes, nanoneedles, and nanowires, the pH of the growth solution was increased by using some strong base solutions, such as ammonium hydroxide $(NH_3OH)$, sodium hydroxide (NaOH), and potassium hydroxide (KOH). The lifetime of the prepared solution was very critical and the growth solution had to be used immediately to avoid any degradation of its biological activities. To grow ZnO NRs with different aspect ratios, one can manipulate the growth time. A flow chart of the growth of ZnO NRs is shown in Figure 2.1. The density and the diameters of the as-grown ZnO NRs were controlled by the viscosity and thickness of the sol-gel (seed layer) solution and the annealing temperature, whereas the morphology and the length of the as-synthesized ZnO NRs were controlled by the pH of the growth solution and the growth time, respectively.

## 2.3 Modification of ZnO NRs with ferric oxide

The precursor $Fe_2(NO_3)_3 9H_2O$ was utilized to modify the surface of ZnO NRs with ferric oxide $(Fe_2O_3)$ using the dip-coating method. [95]. 0.1g of $Fe_2(NO_3)_3 9H_2O$ was dissolved in 30 mL of DI water. The mixture was placed on a magnetic stirrer to ensure complete dissolution of
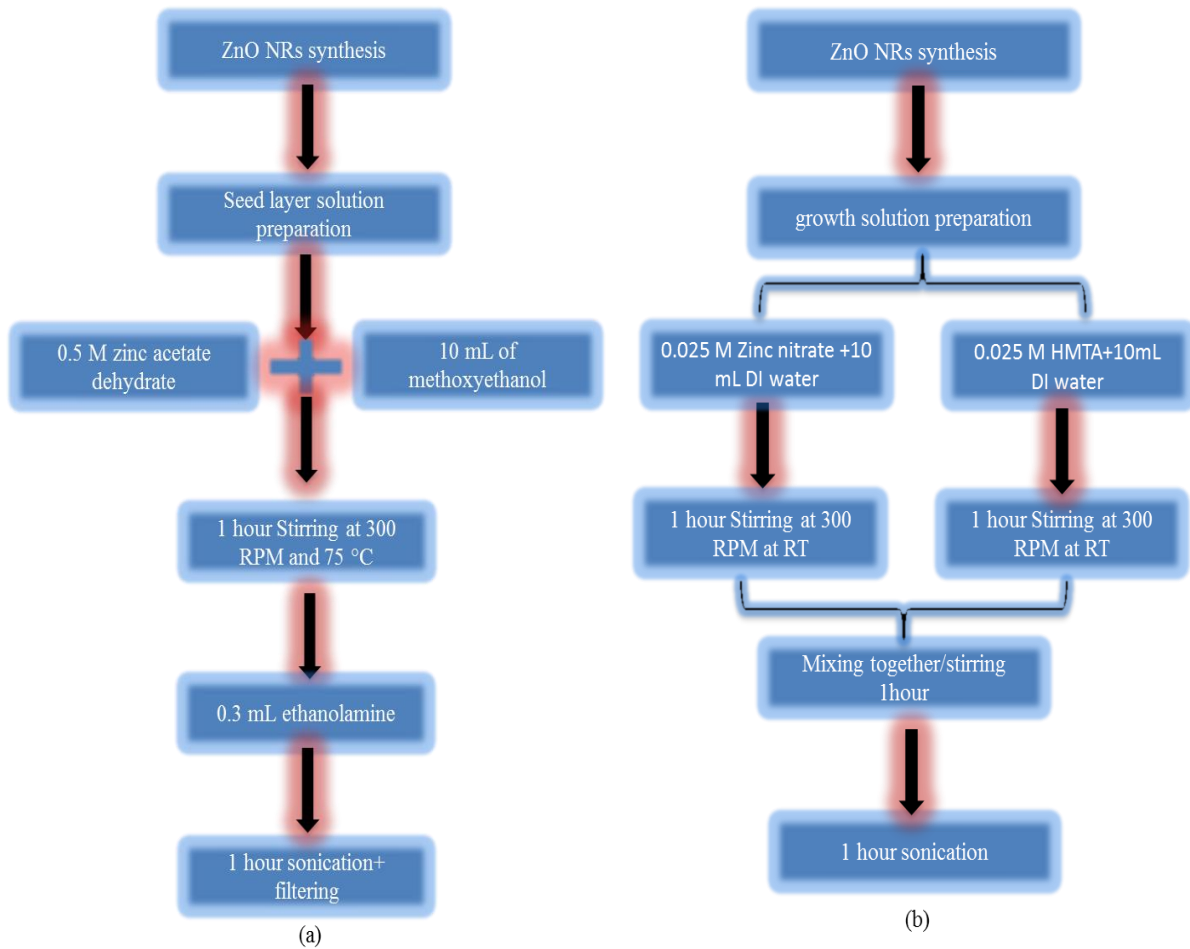
Figure 2.1.Flow chart of the synthesis procedure of ZnO NRs consisting of two major steps: (a) the seed layer growth; and, (b) the growth solution preparation.

the precursor in the water. To modify the surface of the as-grown ZnO NRs with ferric oxide, the dip-coater machine was utilized. After several trial and error methods, the down speed was chosen to be 100 mm/min. The up speed was 25 mm/min, which was very important to determine the thickness of the ferric oxide on top of the surface of ZnO NRs. The dwell time was varied between 60 sec to 3 min, and 1 min dwell time was selected. The dry time was chosen to be 180 sec and the recipe was run for one cycle. A one hour annealing time was chosen at 250 °C in air. It is worth mentioning that reducing the up speed helped immobilize the surface of the as-synthesized ZnO NRs uniformly.

**2.4  Growth of silver nanoparticles**

**2.4.1  Growth of Ag NPs in toluene**

Silver colloidal nanoparticles were grown by two phase synthesis similar to that of gold nanoparticle synthesis. Tetraoctylammonium bromide (TOAB) was used as a phase transfer agent in order to separate the two phases during the synthesis — the aqueous and the organic phases. In order to avoid silver bromide (AgBr) formation, excessive sodium nitrate ($NaNO_3$) salt was added. For the synthesis of Ag nanoparticles in toluene:

1. 30 ml of 5.0 M $NaNO_3$ solution was prepared by dissolving 12.749 g $NaNO_3$ in 30 ml deionized water.

2. For the preparation of the organic phase, 50 ml of tetraoctylammonium bromide (TOAB) solution in toluene was prepared by dissolving 1.367 g of TOAB.

3. The prepared sodium nitrate solution in step one was added slowly to TOAB solution and stirred vigorously for 1 to 2 hours.

4. After the organic and the aqueous phases were dissolved completely and a homogenous solution was obtained, the two phases were separated by an extraction step. The aqueous phase was discarded from the solution.

5. The organic phase was washed one more time with deionized water and the phase separation step was carried out to separate the two phases of the solution.

6. The aqueous phase was discarded again. Thus, the bromide ions were removed from the organic phase of the synthesis.

7. Afterwards as a silver precursor, 7.5 mL of 30 mM of silver nitrate ($AgNO_3$) solution was added to the organic solution and stirred vigorously to mix the two phases and to transfer the silver ions into organic phase that had the tetraoctylammonium bromide.

8. Meanwhile, 0.4 M ice cold sodium borohydride (NaBH$_4$) solution was prepared and added very slowly drop-wise to the organic phase solution and the final solution was stirred vigorously for 1 to 2 hours.

9. The organic phase turned out to be yellow, and it was extracted and washed several times carefully with DI water and the organic phase was separated again.

10. Finally, to have silver nanoparticles Ag NPs dispersed alone in the toluene solution, the organic phase was dried with sodium sulfate (Na$_2$SO$_4$) salt to remove traces of the DI water drops from toluene solution. Figure 2.2 shows the growth setup of the Ag NPs.
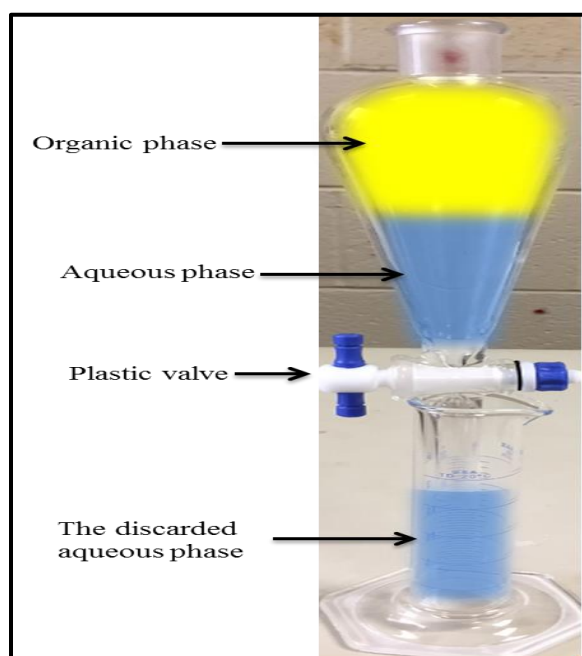


Figure 2.2. The aqueous and the organic phases of the synthesis procedure of silver nanoparticles.

## 2.4.2 Growth of Ag NPs in DI water

Silver nanoparticles can also be grown in deionized water. The growth procedure of the Ag NPs in DI water is simple and cost-effective. Also, the size of the synthesized Ag NPs is

under control. However, DI water is still a strong polar solvent and this makes it difficult to separate the charges in the Ag NPs. The colloidal growth of Ag NPs was carried out as follows:

1. 0.02 gm of sodium citrate ($C_6H_5Na_3O_7.H_2O$) was dissolved in 2 mL of DI water and stirred for one hour to ensure the complete solubility of the sodium citrate in the DI water.

2. 0.0033 gm, that makes 1mM of silver nitrate ($AgNO_3$), was dissolved in 20 mL of DI water and stirred for 30 minutes to ensure the homogenous solubility of the $AgNO_3$ in the DI water.

3. The solution was heated to boiling with continuous stirring.

4. Sodium citrate solution was added to silver nitrate solution drop-by-drop and the mixture was mixed together for around 30 minutes.

5. The color of the new mixture turned to bright yellow and this was evidence of the accumulation of the positive silver ions $Ag^+$ in the solution. Both procedures of synthesizing silver nanoparticles were utilized and were successful to produce Ag NPs.

## 2.5  Growth of silicon nanowires

### 2.5.1  Metal-assisted wet etching of Si NWs

Silicon nanowires (Si NWs) were grown using a p-type silicon substrate that had 100 nm oxide thicknesses on the surface by using the metal assisted etching (MAE). The oxide layer was removed using a concentrated hydrofluoric acid (HF 48%). The samples were immersed in the HF solution for 5 seconds followed by cleaning with DI water to stop any further etching. The samples then were dried with a nitrogen gas and placed in a plastic box at room temperature. The etching recipe and procedure were as follows:

1. p-type silicon wafers (boron dopant) were utilized for the etching.

2. The p-type silicon wafer had the following features: crystal orientation was (100) $\pm0.5^\circ$, resistivity = 1-10 ohm-cm, thickness = 500 ± 25 μm, diameter = 100 ± 0.5 mm.

3. The silicon wafers were diced to have areas of $1 \times 1$ cm$^2$.

4. The samples were dipped in trichloroethane solution in an ultrasound bath for 10 minutes following by etching with DI water. Then, the cleaned samples were sonicated in an ethanol solvent for another 10 minutes followed by rising with DI water. Finally, the samples were placed in acetone inside the ultrasound bath for 10 minutes and cleaned with DI water.

5. To remove any oxide layer that might formed by the cleaning process, a dilute HF solution was prepared by mixing 1:10 ratio of HF: DI water. The samples were immersed in the solution for one minute followed by washing with DI water and drying with nitrogen.

6.  A molarity of 4.6 of HF was prepared by taking 5 mL of 48% HF and 27 mL of DI water.

7. A volume of 2 mL of the oxidizer, hydrogen peroxide ($H_2O_2$), was added to the final solution.

8. To have the catalyst metal, 0.115 gm, which makes the molarity of $AgNO_3$ equals to 20 mM, was added to the mixture of HF:DI water: $H_2O_2$. The samples were then placed in the etching solution at 90 $^{\circ}$C for different times starting at 10 minutes and depending on the desired length and diameter of the silicon nanowires.

9. The etching rate using this procedure was expected to be 67 nm/min.

10. To remove the silver metal from the surface of the etched Si NWs, a concentrated nitric acid $HNO_3$ was used in the process and the etched samples were immersed in the solution for 30 minutes.

11. The final step in the etching method was washing the etched samples by DI water and

drying with nitrogen. The metal assisted etching method to grow Si NWs is schematically illustrated in Figure 2.3.
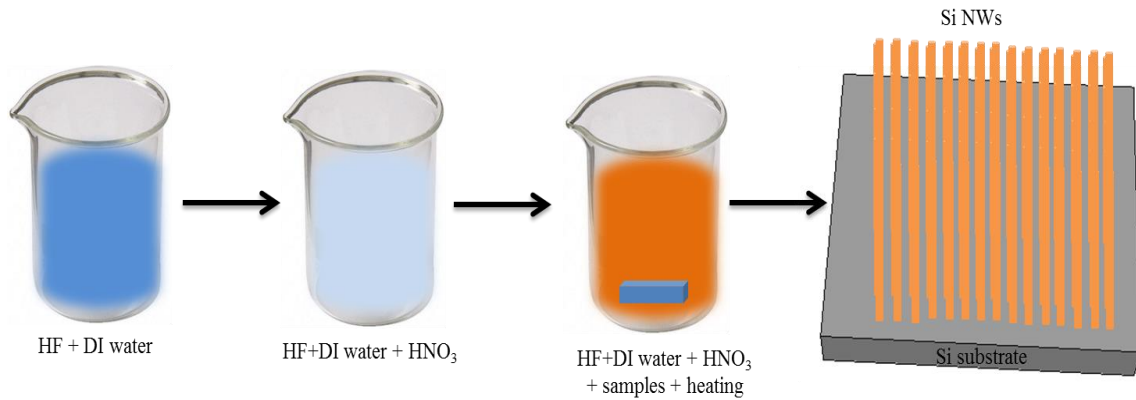


Figure 2.3. The step-by-step metal-assisted etching method to synthesize vertically aligned Si NWs using HF and AgNO$_3$ on top of p-type silicon wafers.

**2.5.2 Silicon nanowires based on nanospheres lithography method**

Nanosphere lithography is one of the desired approaches to grow Si NWs using dry and wet etching. The nanospheres help in controlling the diameters and the length of the etched Si NWs by acting as a photomask.  Synthesis of Si NWs procedure was carried out as the follows:

1. The n-type silicon samples were treated with RCA cleaning solution to change the surface from hydrophobic to hydrophilic. The concentrations used are summarized in Table 2.1.

2. An ultrasound bath was used to clean the samples with different solvents. Trichloroethane solvent was used in the cleaning and the silicon wafers were dipped in the solution for 10 minutes followed by cleaning with DI water. The ethanol solvent was used to clean the samples for another 10 minutes inside the ultrasnic bath followed by washing with DI water. Acetone was then used to clean the samples for 10 minutes and

31

the samples were rinsed with DI water then dried with nitrogen.

3.  The nanospheres were diluted with ethanol to the ratio of 2:1 ethanol: nanoshperes.

4.  The nanospheres were placed in an ultrasonic bath for 1 minute to ensure uniform dispersion of the nanospheres in the ethanol.

5.  The diluted nanospheres were spun-coated on top of the cleaned silicon samples at 300 rpm to form the close-packed surface.

6.  The reactive ion etching (RIE) system was used to control the diameter of the nanospheres on top of the silicon samples using plasma etching. The plasma etching changes the surface of the coated nanospheres from a close packed to a non-close packed surface.

7.  The etching recipe used to reduce the diameters of the nanospheres was: RF power of 50 W, ICP power of 30 W, $O_2$ flow rate of 50 sccm, chamber pressure of 100 mTorr, and 20-25 minutes etch time.

8.  The e-beam evaporator was used to deposit 15 nm of gold on top of the samples coated with the non-close packed surface.

9.  The wet etching method was used to etch the silicon underneath the gold. In other words, the areas not protected by the nanospheres were etched by the etching solution. To start the procedure, the etchant solution was prepared by adding 27 mL of DI water to 5 mL to the 48% HF solution. That brought the molarity of the etchant solution to 4.6 M. The etching rate obtained from this process was 67nm/min.

10. The covered areas with the nanospheres were protected from the etchant solution. The areas uncovered by the nanospheres were etched and the remaining un-etched areas formed the silicon nanowires on top of the silicon substrates.

11. The length of the etched Si NWs was controlled by changing the etching time using the HF solution as described above. Whereas, the diameters of the etched Si NWs were controlled by the dry etching time. The longer the wet etching time, the smaller the diameters were of the Si NWs.

12. The coated nanospheres were removed by placing the etched samples inside the toluene solvent for 30 minutes following by washing the samples with DI water and drying them with nitrogen.

13. The gold thin film was removed from the surface of the samples by using aqua regia solution. The solution was prepared as follows: 4 mL of HCl (hydrochloric acid) and 1 mL of nitric acid ($HNO_3$).

14. The samples were dipped in the aqua regia solution at 110 $^{\circ}$C until the gold was completely removed from the surface. Table 2.1 is a summary of the aqua regia preparation. Afterward, the samples were washed with DI water to stop any further reaction and dry with $N_2$. Figure 2.4 is the step by step fabrication method of Si NWs using Nanospheres lithography and RIE system. To remove the gold from the surface of the sample, aqua regia solution was prepared as summarized in Table 2.2.

Table 2.1. The RCA cleaning to change the surface of the silicon wafers from hydrophobic to hydrophilic.

| NH$_3$ (Ammonia) 25% | H$_2$O$_2$ hydrogen peroxide 30% | H$_2$O | Time (min) | Temperature (°C) |
|---|---|---|---|---|
| 10 mL | 8.5 mL | X | 30 | 90 |

Table 2.2. The aqua regia solution to remove the gold from the surface of the etched Si NWs.

| HCl 39% (hydrochloric acid) | HNO$_3$ 30% (nitric acid) | Time (min) | Temperature (°C) |
|---|---|---|---|
| 4 mL | 1 mL | 5 | 100 |
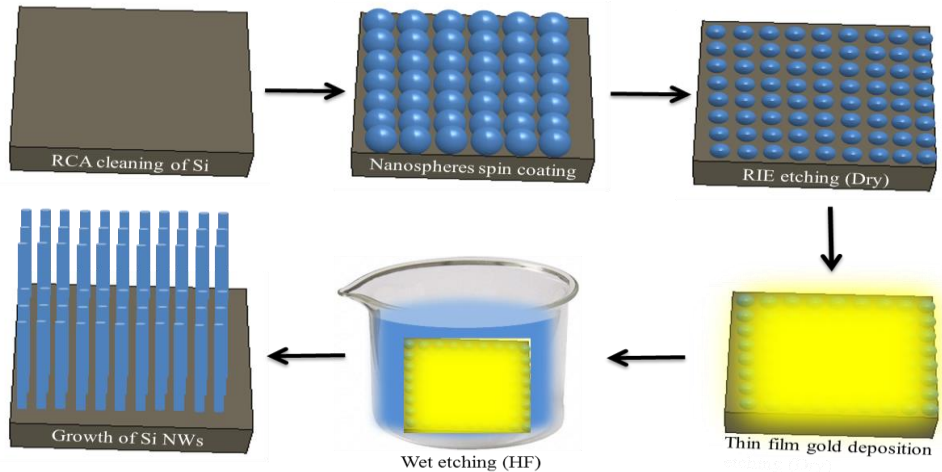


Figure 2.4 The schematic diagram of the nanosphere lithography procedure to synthesize vertically grown Si NWs on top of a silicon substrate.

### 2.5.3  Horizontal growth of Si NWs by photolithography

Silicon nanowires are grown horizontally using a p-type silicon substrate through the photolithography process using a photomask. The synthesis of the horizontally aligned Si NWs was performed as follows:

1. A photomask consisting of a horizontally aligned array was designed using chromium on the top of the mask.

2. The length of the Si NWs was 300 µm and the width of each Si NW was 3 µm.The distance between the Si NWs was 3 µm as well.

3. The total area of the Si NWs was calculated to 3000 × 3997 µm$^2$.

34

4. The samples were cleaned with different solvents using an ultrasonic bath. The p-type silicon samples were dipped in trichloroethane solution in an ultrasonic bath for 10 minutes following by cleaning with DI water. Then, the cleaned samples were placed in an ethanol solvent for another 10 minutes inside the ultrasonic bath followed by washing with DI water. The samples were placed in acetone inside the ultrasonic bath for another10 minutes followed by cleaning with DI water and drying with nitrogen.

5. A positive photoresist AZP 4330-RS (AZ Electronics USA Corp, Somerville, NJ) was utilized and spun coated on top of the cleaned samples using the spin coater machine at 7000 rpm for 1 minute and a ramp speed of 2000 rpm. The spin coating recipe to deposit the photoresist on top of the silicon substrates was optimized based on the designed dimensions of the Si NWs in the photomask. A speed of 7000 rpm resulted in 3 µm thickness of the positive photoresist used.

6. The coated samples with photoresist were placed on a hot plate for 3 minutes for soft baking at 110 °C to prepare the samples for the ultra violet (UV) light source and to help distribute the photoresist evenly on top of the samples.

7. It is worth mentioning that the silicon samples were located on the surface of the chuck of the spin coater directly without using a substrate holder. This helped obtain an even distribution of the photoresist and in transferring the pattern effectively and successfully from the photomask to the surface of the silicon substrates.

8. A mask aligner attached to the UV-light source was used to expose the baked photoresist to the light. The UV-light went through the uncovered parts of the structure in the photomask.

9. Since the photoresist used was a positive type, the UV-light broke the bonds of the photoresist and it made it easy to develop the exposed photoresist.

10. A developer solution was prepared by mixing 300 mL of DI water with 100 mL of the AZ 400 K developer. The exposed samples were immersed inside the developer solution for 18 seconds.

11. It is worth mentioning that the developing time was inversely proportional to the spin coating speed of the photoresist. In other words, the thickness of the photoresist was inversely proportional to the developing time.

12. The immersed samples were shaken inside the developer solution very gently to help in removing the exposed photoresist from the silicon surface until one could see the pattern on top of the silicon substrates

13. The well-developed samples were placed directly in DI water to stop any further developing and to clean the surface of the silicon substrate.

14. Finally, the pattern on top of the silicon substrates was washed carefully with DI water and dried with nitrogen.

15. The samples were hard-baked on a hot plate for one hour at 150 $^\circ$C. This helped in making the photoresist hard enough to resist the etching process by using the sulfur hexafluoride ($SF_6$) gas.

16. The RIE system was used to perform the dry etching process to fabricate the 3 μm width and 3000 μm length Si NWs. Here, it is very important to note that there was no need to deposit any metal, such as gold or silver, to perform the etching on top of the samples. The photoresist acts as a mask on top of the silicon wafers.

17. The dry etching recipe to etch the uncovered areas of the silicon samples by the hard baked photoresist was as follows: RF power was 50 W, inductively coupled plasma power (ICP) was 30 W, the flow rate of $O_2$ was 50 sccm, the $SF_6$ gas flow rate was 50 sccm, the chamber

pressure was 100 mTorr, and the etching time was 5 minutes.

18. The 5 minutes etching time was chosen based on several trial-and-error attempts. It was noticed that an etching time more than 5 minutes etched the entire sample and the hard-baked photoresist could not resist the $SF_6$. In addition, less than 5 minutes etching time was less effective and did not reach the desired etching depth of the Si NWs.

19. The obtained Si NWs out of the dry RIE etching method had a sharp edges and a width very close to 3μm since the dry etching by RIE system provided anisotropic etching. This was very important to increase the electroactive area of the glucose sensor.

20. The etched samples were immersed in a photoresist stripper solution on a hot plate at 90 °C for 1 hour in order to remove all the remaining photoresist on top of the synthesized Si NWs. A schematic diagram of the fabrication procedure is shown in Figure 2.5.
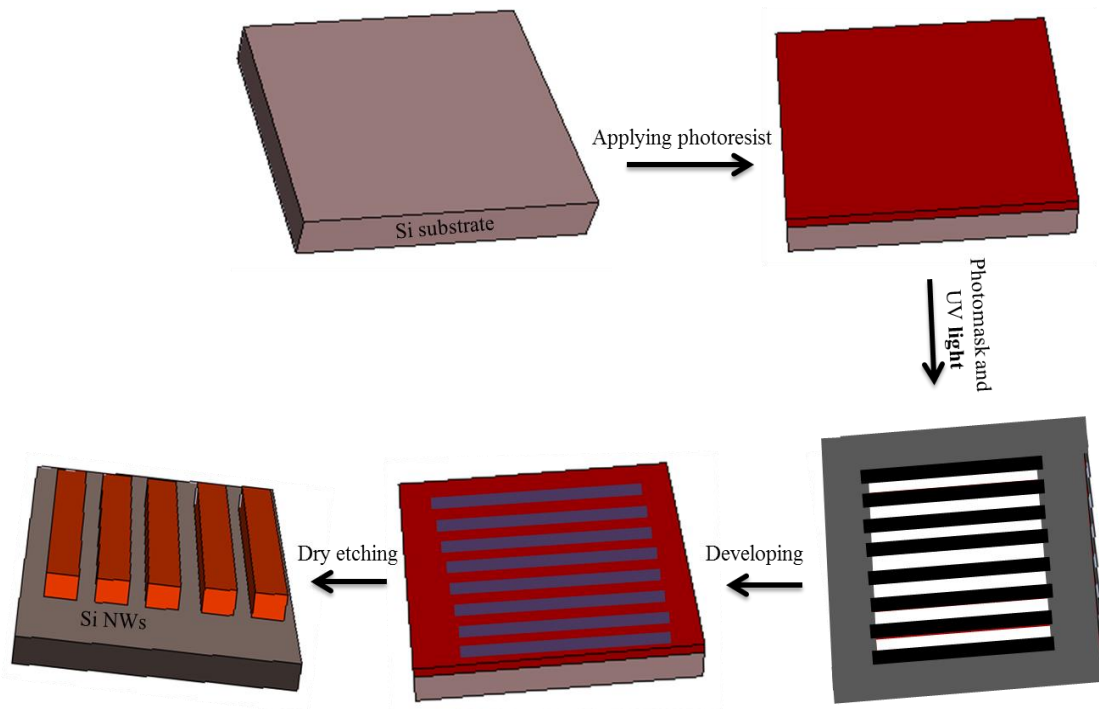


Figure 2.5. The schematic structure of the horizontal growth method of Si NWs using the RIE system with $SF_6$ gas.

## 2.6 Materials characterization

The grown materials were characterized using different techniques, such as SEM, UV-visible spectrophotometer, Raman spectroscopy, and x-ray diffraction (XRD).

## 2.6.1 Scanning electron microscopy (SEM)

FEI xT Nova NanoLab 200 scanning electron microscopy (SEM) (ThermoFisher Scientific, Waltham, MA) was utilized to characterize the grown ZnO NRs on top of the ITO substrates. An electron metallic filament was used to generate the electrons. The metallic filament is known as the gun. The electromagnetic field lenses inside the SEM system were utilized to direct the electrons to the surface of the sample. Those electrons formed in a beam shape. The electron beam that hits the surface of the sample was accelerated. The energetic electrons hit the surface of the sample and there were two possible mechanisms. Some of the electrons penetrated the surface of the samples and diffused inside the material as can be seen in Figure 2.6. The rest of the electrons reacted with the surface of the material and generated what can be called secondary electrons. The generated secondary electrons that reflect from the surface of the sample were detected by the detector connected to a display. The detected electrons created an image of the surface of the sample. The samples that were tested by the SEM system should be conductive. Otherwise, a thin film of a conductive material could be deposited on the surface.

Images of the samples at different magnifications can be obtained by the SEM system to analyze the surface structure of the material. The chamber of the SEM system is pumped down to avoid any interruption by other molecules inside the SEM chamber. The SEM system provides a large area of the surface of the material, which is very important especially for the nanowires and nanorods structures. In these nanostructures, the alignment, the length and the diameters are
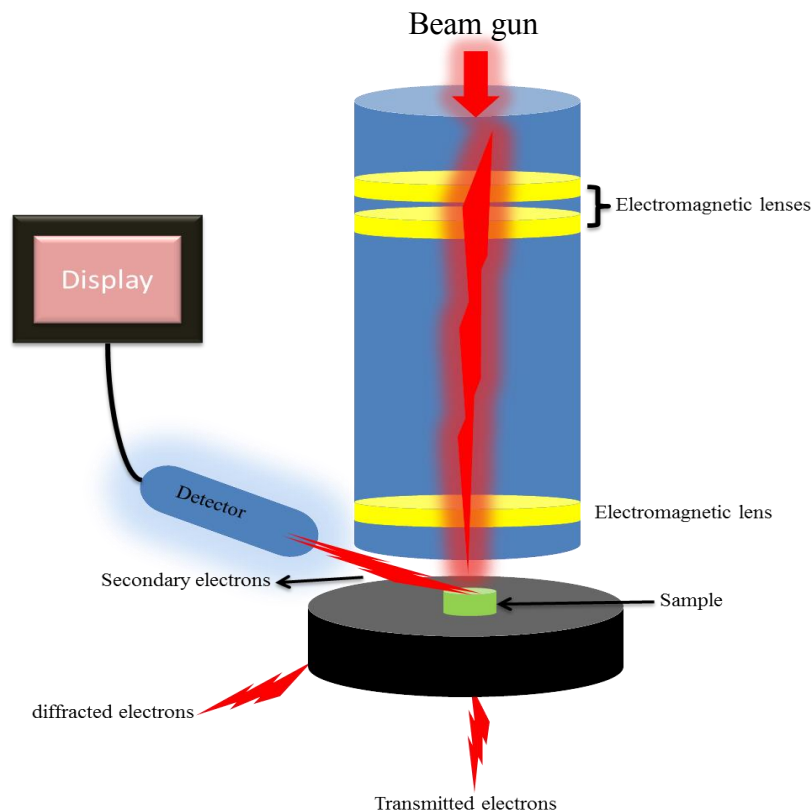
Figure 2.6. Schematic of the SEM system and working principle of taking the SEM images of the nanostructures of the materials.

the most important parameters to evaluate the growth of the materials.  It is difficult to observe

the coupling between two nanostructures of materials when there is a big difference between

their grain sizes.  It is important to mention that when the accelerated electrons hit the surface of

the material, different groups of electrons are generated, such as the backscattered electrons,

Auger electrons, diffracted electrons, and transmitted electrons. The secondary electrons are the

most important groups in all of these groups because these electrons interacted with the surface

of the material. High resolution images of the as-synthesized ZnO NRs were obtained by the

SEM characterization technique, and very important parameters, such as the lengths, the

diameters, the alignment, and the density of nanorods were precisely measured.

### 2.6.2 UV-visible spectrophotometer characterization

UV-visible-near infrared spectroscopy was utilized to characterize the as-synthesized ZnO NRs, the grown silver nanoparticles, and the etched silicon nanowires. A schematic of the system used is shown in Figure 2.7. The band gap of ZnO nanostructure is in the order of 3.37 eV and the optical exciton peak should be observed at the edge of the visible region and according to Planck's Equation:

$$E = h\nu \qquad \text{(Equation 2.1)}$$

Where E is the energy, h is Planck constant, and $\nu$ is the frequency of the light. Since

$$\nu = \frac{c}{\lambda} \qquad \text{(Equation 2.2)}$$

where $c$ is the speed of the light and $\lambda$ is wavelength of the light, Equation 2.1 can be rewritten as:

$$E = \frac{hc}{\lambda} \qquad \text{(Equation 2.3)}$$

The absorbance of the synthesized materials was measured in the range of 200 to 1100 nm, which covered the entire visible region of the spectrum. The as- synthesized ZnO NRs and the etched silicon nanowires were characterized as sold materials. Whereas, the synthesized Ag NPs were characterized while they were dispersed in toluene.  It was very important to determine the size of the Ag NPs before using them in the fabrication process of a glucose sensor. The exciton peak in the absorbance spectrum provided an idea about the size of the synthesized nanoparticles. The solid samples were placed in the sample holder and the slit height was adjusted to ensure that the spectrum of the light was passing through and hitting the samples. For ZnO NRs grown on ITO, the absorbance of a blank ITO was measured as a baseline. Whereas, for the etched Si NWs, a bulk silicon sample was utilized as a baseline. The working mechanism of UV-visible-near IR spectroscopy is based on Beer-Lambert law:

$$I = I_\text{o}\, e^{-\alpha x} \qquad\qquad \text{(Equation 2.4)}$$

where $I$ is the transmitted intensity, $I_\text{o}$ is the incident intensity, $\alpha$ is the absorption coefficient, and $x$ is the thickness of the material. Absorbance can be calculated by manipulating the above equation, as follows:

$$A = \log_{10}\frac{I}{I_\text{o}} \qquad\qquad \text{(Equation 2.5)}$$

Herein, when the transmitted intensity is equal to the incident one, $\frac{I}{I_\text{o}} = 1$ and log 1 is zero, which means no absorbance. Figure 2.7 shows the setup of the utilized Cary 500 UV-visible-NIR spectrophotometer (Varian, Inc, Palo Alto, CA).
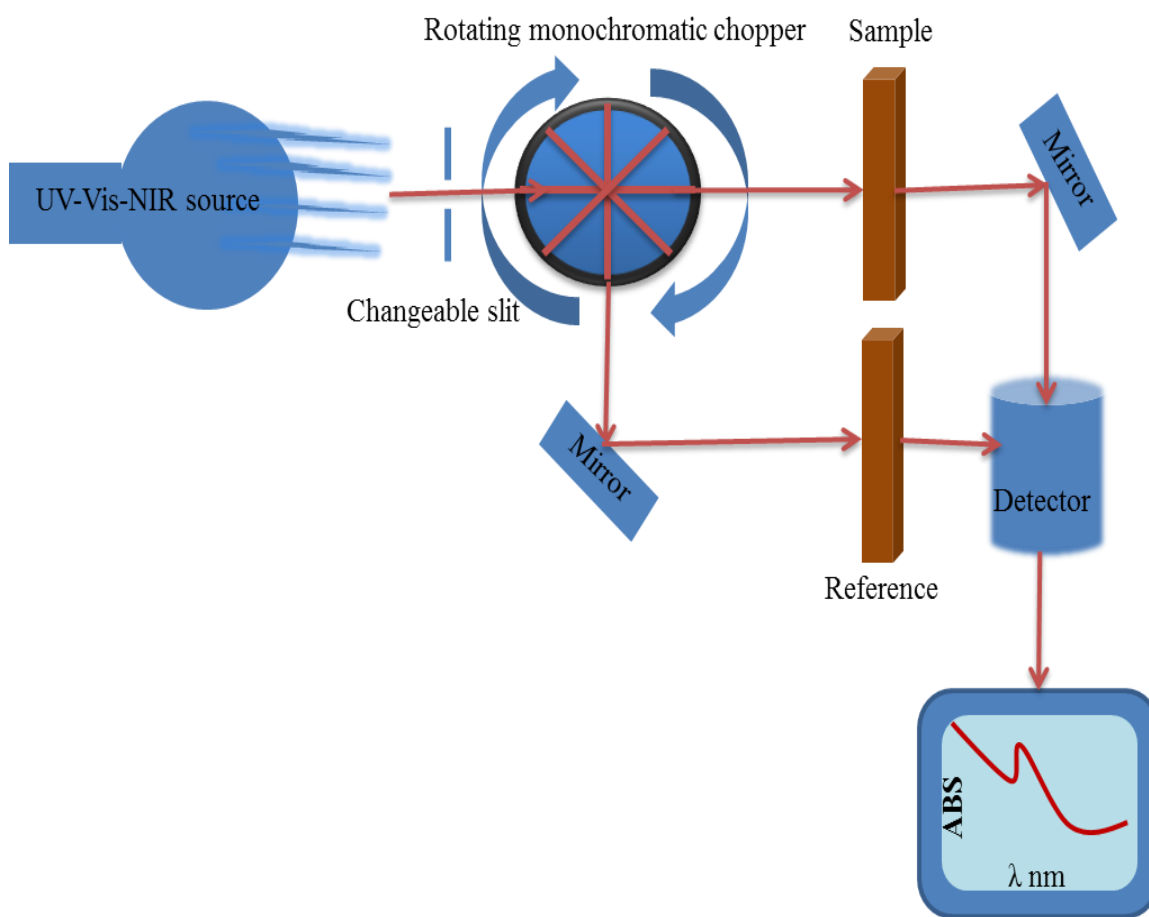


Figure 2.7. The schematic diagram illustrating the working mechanism of the UV-visible-near infrared spectrophotometer utilized to characterize the grown nanomaterials.

### 2.6.3  Raman spectroscopy characterization

Lattice vibration (phonon vibration) of the ZnO NRs can be studied using Raman spectroscopy as illustrated in Figure 2.8. Raman spectroscopy can be explained as an inelastic scattering of monochromatic light (usually laser) in the nanostructure of the material. Raman scattering is divided into Stoke and anti-Stoke scattering or lines. For Stoke lines, the scattered light has energy lower than the incident light. Whereas, for the anti-Stoke lines, the energy of the scattered light is higher than the energy of the incident light. Each material has its specific vibration or phonon modes and Raman spectroscopy is used as a finger print. For the as-synthesized ZnO NRs, Raman Spectroscopy type LabRAM HR (Horiba, Edison, NJ) with a blue laser that has a wavelength 472 nm was utilized to observe phonon vibrations. The spectrum used was determined to be from 200 to 800 cm$^{-1}$ and the noise was reduced by increasing the number of cycles. The blue laser was focused as much as possible on the surface of the as-grown ZnO NRs and all the obtained peaks were marked based on their different vibrations.
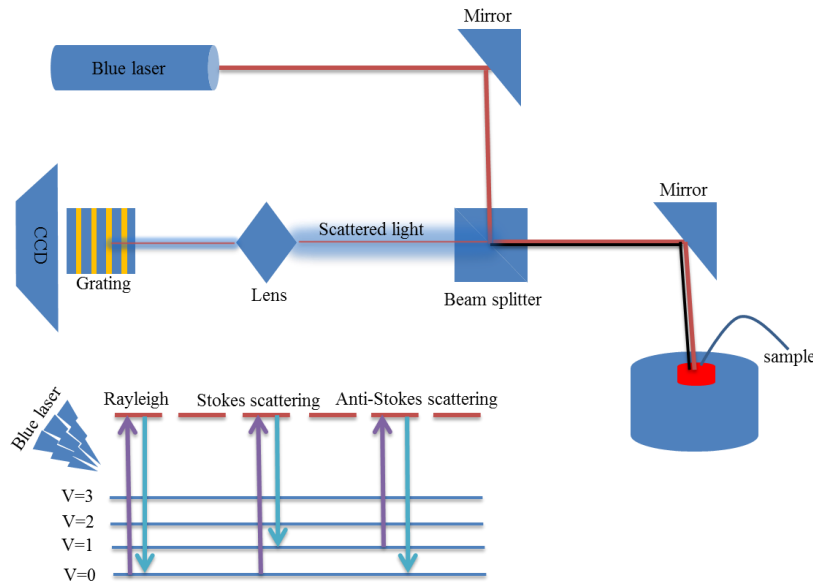


Figure 2.8. A schematic of Raman spectroscopy and the working mechanism.

### 2.6.4 X-ray diffraction (XRD) characterization

X-ray diffraction characterization is carried out to determine the crystal structure of the synthesized ZnO NRs before and after modification with ferric oxide. A Philips x-ray diffractometer (Philips, Amsterdam, Netherlands) with wavelength 1.54 Å was utilized to characterize the grown nanostructure of the material. The working mechanism of the XRD system is shown in Figure 2.9. The grain size and the crystal structure of the synthesized ZnO NRs were determined, which was very important to have the most stable hexagonal wurtzite structure of ZnO NRs. In addition, the texture coefficient was calculated from the XRD pattern. The impurity level was also investigated from the measurement. The peaks of the conductive ITO and FTO substrates were determined from the XRD pattern. Miller indices, which determine the crystal planes, were also determined from the peaks of the XRD pattern. In the XRD measurement, the lattice constant of the grown material could be calculated to determine the distance between the two atoms of the crystal lattice. The XRD measurement works based on Bragg's law which is

$$n\lambda = 2d\sin\theta \qquad\qquad \text{(Equation 2.6)}$$

where $\lambda$ is the wavelength of the incident light, d is the distance between the two atomics layers, and n is an integer number. Diffraction occurs when the wavelength of the incident light is equal or twice as large as the distance between the two atomic levels.
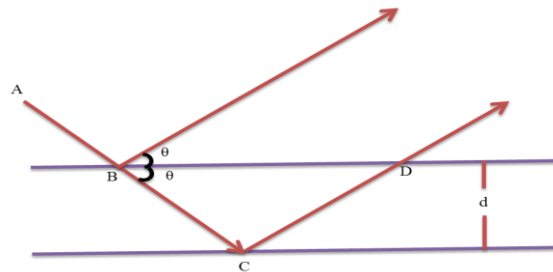


Figure 2.9. The working mechanism of the x-ray diffraction measurement based on Bragg's law.

## 2.7 Device fabrication and characterization

### 2.7.1 ZnO NRs grown on ITO-based enzymatic glucose sensor.

1. Indium tin oxide substrates were cut and cleaned as it was explained in the previous section with an area of $1 \times 1$ cm$^2$ [80].

2. A small area of the ITO substrate was covered with tape to protect the area for contact during the characterization process of the sensor.

3. Three layers of the prepared sol-gel solution were spun coated on top of the cleaned and prepared ITO substrates at 3000 rpm for each layer. After deposition of the first layer on top of the ITO substrates, the sample was annealed at 110 $^{\circ}$C for 5 minutes followed by the deposition of the second layer. After deposition of the second layer of the sol-gel solution, the sample was annealed at 110 $^{\circ}$C for 3 minutes followed by deposition of the third and final layer. It is worth mentioning that all three layers were deposited at 3000 rpm using the spin coater machine [80].

4. After the three layers of the sol-gel solution were deposited, the tape that was used to cover a small area for metal contact was peeled off to keep the uncoated area by the sol-gel solution clean and uncontaminated.

5. The samples were annealed for 1 hour at 110 $^{\circ}$C on a hot plate at room temperature.

6. The annealing step was very crucial since it helped the sol-gel solution be uniformly distributed on top of the ITO substrate. Otherwise, the distribution of the seed layers solution on the ITO would be random, and this would have affected the growth of the ZnO NRs in terms of the density, length, and diameter. SEM images of as-synthesized ZnO NRs grown on top of the ITO substrates based on a non-annealed sol-gel solution are provided in Chapter 3.

7. After one hour of annealing, the samples were left to cool naturally and the coated layers could be seen on top of the ITO surface.

8. A glass slide was cleaned very carefully and the annealed samples were pasted onto the glass slide and immersed upside down in the growth solution in a 20 mL screw glass vial, before being placed in a furnace.

9. The growth time and temperature were chosen to be 4 h and 90 $^\circ$C, respectively, and then the samples were taken out of the furnace and cooled naturally.

10. The samples then rinsed with deionized water three to four times to stop any further growth of ZnO NRs and the samples were dried at 300 $^\circ$C at room temperature for 15 min to evaporate all the water molecules from the surface of the grown samples.

11. To prepare the working electrode for further treatments, the as-synthesized ZnO NRs on top of the ITO substrates were placed in phosphate buffer solution (PBS) with a pH level of 7.4, and left in the air to increase the absorbance of the surface of the electrode by generating a hydrophilic surface.

12. Different concentrations of the enzyme glucose oxidase ($GO_x$) were produced and used to immobilize the working electrode. An investigation study was carried out to determine the best concentration of $GO_x$ that could be used to immobilize the surface of the working electrode.

13. A 40 mg/unit of $GO_x$ was prepared by dissolving a concentration of 40 mg/mL of $GO_x$ in 0.01 M of PBS. The mixture was stirred on a magnetic stirrer for 1 h to ensure the complete solubility of $GO_x$ in the PBS.

14. A volume of 1 μL of the prepared $GO_x$ was dropped on top of the surface of the as-synthesized ZnO NRs using a micropipette and the immobilized working electrode was

stored in the refrigerator at 4 °C for 6 h.

15. The non-adsorbed $GO_x$ by ZnO NRs was removed from the surface of the working electrode, using a covalent method with a higher ionic solution. A concentration of 4.4 M of PBS with pH 7.0 that provides 80 mM of ionic strength was used to remove the excess non-adsorbed $GO_x$.

16. The working electrode was rinsed in the prepared solution five times, for 20 s each time. Removing the non-adsorbed $GO_x$ helped to increase the stability and the life time of the working electrode by decreasing the biological degradation of the enzyme.

17. The last modification step of the working electrode was completed by covering the surface of the electrode with a nafion membrane. A volume of 1 μL of the nafion solution was dropped on the surface of the working electrode, and the electrode was left to dry for 2 h at 4 °C. The schematic diagram of the working electrode is illustrated in Figure 2.10.
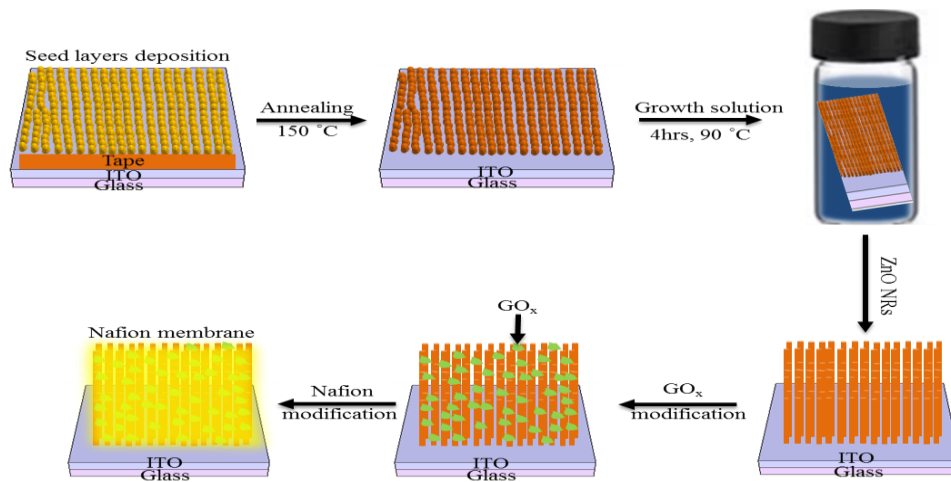


Figure 2.10. The schematic diagram of the fabrication and modification process of the working electrode of the enzymatic electrochemical sensor [80].

It explains step by step the growth of the ZnO NRs and the modification of the electrode with glucose oxidase and nafion membrane. Figure 2.11 shows the three electrodes

system used in the electrochemical setup during the electrochemical characterization of the fabricated sensors.
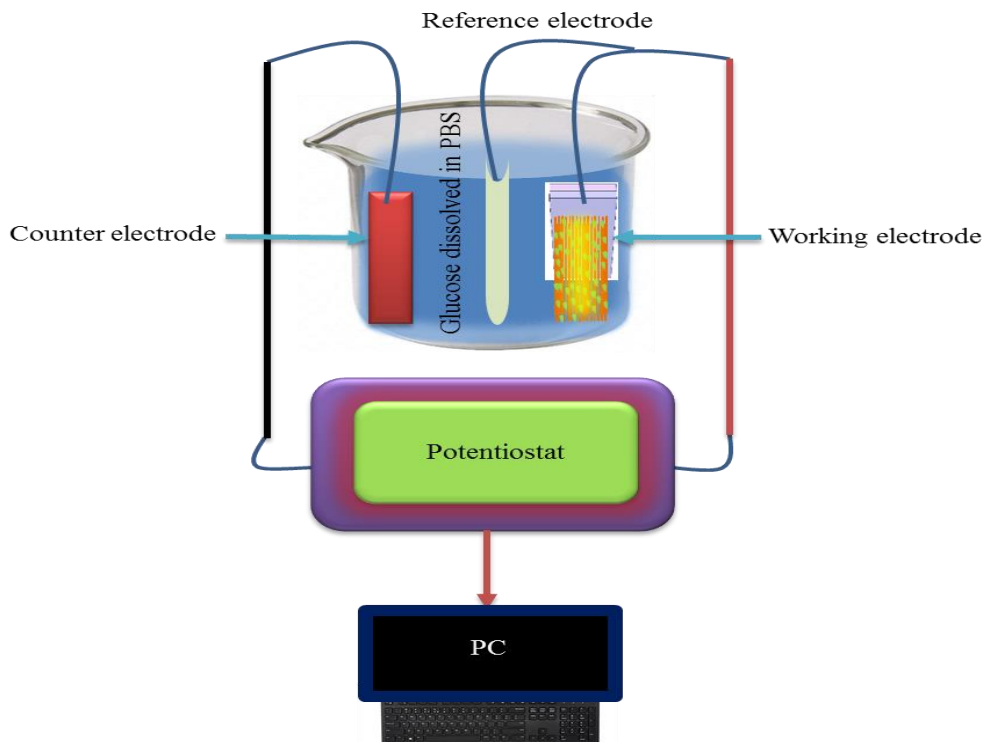


Figure 2.11. The three electrodes used in the electrochemical measurements to test the fabricated glucose sensors with different glucose concentrations.

### 2.7.2  ZnO NRs grown on Si/SiO$_2$/Au based enzymatic glucose sensor.

To fabricate the working electrode of the enzymatic electrochemical sensor, ZnO NRs were grown on Si/SiO$_2$/Au substrate [101]. The fabrication process was as follows:

1.  The same cleaning process described in the previous section was carried out to clean the Si/SiO$_2$ substrate.

2.  The silicon wafer was coated with a 100 nm SiO$_2$ layer using a thermal oxidation method.

3.  The silicon wafers were diced into 0.5×0.5 cm$^2$ specimens and a small area for contact as covered with tape to prevent any growth of ZnO NRs on top of it.

47

4. A 100 nm of gold thin film was deposited on the surface of the cleaned samples using an

   e-beam evaporator. The deposition rate was 1.5 Å/s with a pressure $2.5 \times 10^{-7}$ Torr .

   After a smooth thin film of gold was obtained on the surface of $Si/SiO_2$ substrate, ZnO

   NRs were grown on top of the structure $Si/SiO_2/Au$ using the same previously described

   hydrothermal and sol-gel methods of growth.

5. The working electrode was immobilized with glucose oxidase and a nafion membrane as

   a final modification steps to fabricate the enzyme electrochemical glucose sensor. The

   modifications with $GO_x$ and nafion membrane were performed using the same method

   explained in the previous section.

6. The fabricated working electrode was used with other electrodes to test the

   electrochemical sensor with different glucose concentrations. The schematic diagram of

   the working electrode based on ZnO NRs grown on $Si/SiO_2/Au$ is shown in Figure 2.12.
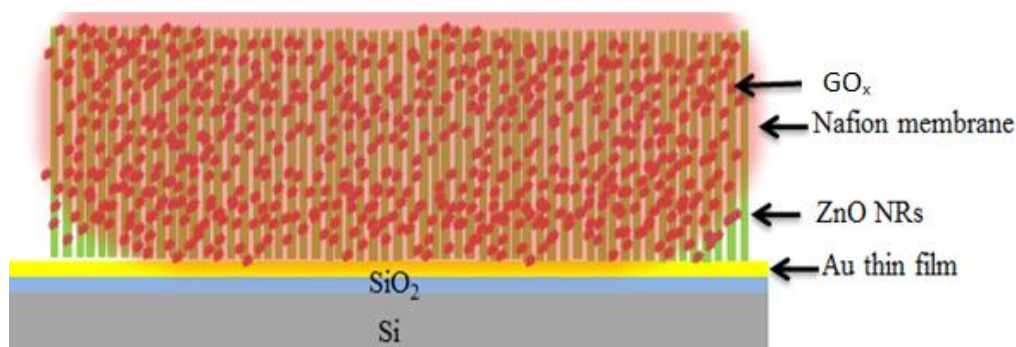


Figure 2.12. The schematic diagram of the working electrode based on the vertically grown ZnO NRs on top of $Si/SiO_2/Au$ substrate for the enzymatic glucose sensor.

### 2.7.3 ZnO NR-coated ferric oxide for enzyme-free glucose

To fabricate a non-enzymatic electrochemical glucose sensor, vertically grown ZnO NRs

on top of an FTO substrate were modified by the ferric oxide as was explained in the materials

48

growth section (Sec. 2.3). The enzyme, $GO_x$ was replaced by ferric oxide to directly oxidize the

glucose on the surface of the working electrode. The fabricated working electrode was casted

with a nafion membrane using a drop cast method to increase the stability of the working

electrode. A three electrode station was utilized to test the enzyme-free electrochemical sensor.

The schematic diagram of the working electrode is illustrated in Figure 2.13 [95].
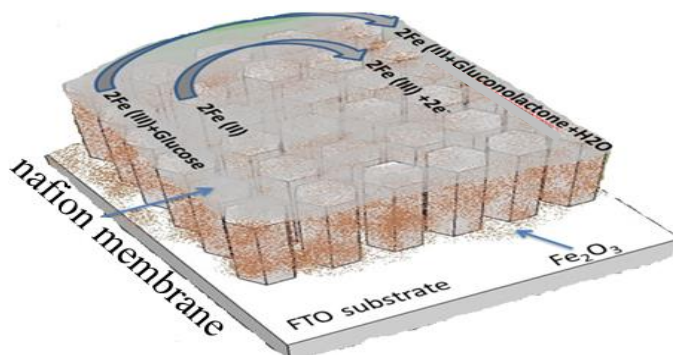


Figure 2.13. Schematic diagram of the working electrode of the enzyme-free electrochemical
sensor based on vertically grown ZnO NRs modified with ferric oxide and coated with a nafion
membrane. Reprinted with permission from Marie et al. [95].

## 2.8  Vertically etched Si NWs by nanosphere lithography and RIE based glucose sensor.

The nanosphere lithography method explained in the materials growth section (2.5.2) was

utilized to etch Si NWs vertically using a silicon wafer. Nanosphere lithography and the RIE

method were carried out. The vertically etched Si NWs were modified with the enzyme $GO_x$ and

nafion membrane. To successfully immobilize the etched Si NWs with the enzyme glucose

oxidase, the grown Si NWs were immersed in the PBS solution to create a hydrophilic surface

for the enzyme. Afterward, a volume of 1 µL of the enzyme was dropped on top of the Si NWs

and the samples were kept overnight in the refrigerator at 4 °C. Next, the working electrode was

coated with a nafion membrane to enhance the stability of the electrode and to increase the ion

49

exchange capability between the center of the enzyme and the surface of the working electrode. Coating the working electrode with the nafion membrane helped in preventing any unwanted reaction by the other electroactive species in the analytical solution. This helped in increase the signal-to-noise ratio of the working electrode.

## 2.9  Device characterization

The fabricated electrochemical glucose sensors were characterized using Gamry potentiostat, Keithley 2410 SourceMeter and a Keithley 4200 semiconductor characterization system. Different tests were carried out to characterize the fabricated devices. Different concentrations of glucose were dissolved in a phosphate buffer solution with pH 7.4 to run the electrochemical measurements at room temperature. A three electrode station was prepared containing the working electrode, the counter electrode, and the reference electrode, which was immersed in between the two electrodes inside the electrochemical cell.

### 2.9.1  Amperometric response

The amperometric test was performed to evaluate the performance of the fabricated electrochemical sensors for both enzymatic and enzyme-free devices. It is one of the most important tests to study the amperometric response of the glucose sensors for different glucose concentrations. The test was performed by fixing the potential between the working (sensing) electrode, the counter electrode, and the reference electrode at a certain value and changing the glucose concentrations continuously.

#### 2.9.1.1  The sensitivity of the glucose sensor

One of the most important factors to evaluate the performance of the glucose sensors that can be extracted from the linear amperometric response is the sensitivity of the sensor. From the amperometric characterization one can extract the linearity of the fabricated electrochemical

50

glucose sensors for different glucose concentrations. The linear response to high concentrations of glucose reflects the high sensitivity of the sensor toward the changes in the glucose concentrations. The sensitivity of the glucose sensor is the slope of the linear amperometric measurement, which is the current density as a function of the changes in the glucose concentration.

### 2.9.1.2  Time response

The time response is another way to characterize the electrochemical sensors. It tests the time that the fabricated sensor needs to respond to the changes in the glucose concentration until it reaches steady-state current. The time response is extracted from the amperometric measurement. Changes in the glucose concentration are made continuously and the average of each 20, 30, or 50 values of the sensed current is calculated. The time of each value is set to be 1 second. It is worth mentioning that the shorter the time response, the higher the ability of the glucose sensor to respond to the changes in the glucose concentration.

### 2.9.1.3  The apparent Michaelis-Menten constant

The apparent Michaelis-Menten constant test is one of the very important tests that can be extracted from the amperometric characterization technique of the electrochemical glucose sensor. It is performed by fixing the applied potential between the three electrodes and changing the concentrations of the glucose continuously. The apparent Michaelis-Menten constant provides an indication of the affinity between the enzyme glucose oxidase and the surface of the working electrode. In the case of the enzyme-free glucose sensor, the apparent Michaelis-Menten constant is used to test the affinity between the surface of the working electrode and the nanomaterial used to modify the surface. To extract Michaelis-Menten constant out of the amperometric measurement, the inverse of the current density was plotted as a function of the

inverse of the changes in glucose concentration. The apparent Michaelis-Menten constant was evaluated using the Lineweaver-Burk equation [102, 103].

$$\frac{1}{i} = \left(\frac{K_M^{app}}{i_{max}}\right)\left(\frac{1}{c} + \frac{1}{i_{max}}\right) \qquad \text{(Equation 2.7)}$$

where $i$ is the current, $K_M^{app}$ is apparent Michaelis-Menten constant, $i_{max}$ is the maximum current at the saturation region, and $c$ is the D-glucose concentrations.

## 2.9.2 Cyclic voltammetry characterization

Cyclic voltammetry is one of the tests used to examine the oxidation and reduction mechanisms of the glucose. In this characterization, the applied potential was swept against the reference electrode from -1 to 1 volt. To determine the sensing ability of the sensor, the tests were performed in the absence and in the presence of glucose. The testes were carried out at different scanning rates of 50, 100, 200, 300, 400, and 500 mV/s. In the absence of glucose in the analytical solution, the enzymatic and non-enzymatic sensors exhibited no dependency on the level of the swept voltage and on the different scan rates.

**Chapter 3  Results and discussion**

**3.1  Introduction**

In this chapter, materials characterization results will be discussed in detail as well as how the nanomaterials used affected the performance of the fabricated electrochemical sensors. The other section of the chapter contains the results of the devices characterized made from grown nanomaterials.

**3.2  ZnO characterization results**

**3.2.1  Scanning electron microscopy (SEM)**

**3.2.1.1  First synthesis trial of ZnO NRs on ITO surfaces**

Scanning electron microscopy (SEM) was utilized to examine the as-synthesized ZnO NRs before and after annealing. The alignment, density, lengths, and diameters of the as-synthesized ZnO NRs are the most crucial parameters that affect the performance of the electrochemical glucose sensors fabricated out of ZnO NRs. All these parameters have a direct influence on the signal-to-noise ratio of the fabricated sensors and on the amount of the enzyme, $GO_x$, that is used to modify the surface of the working electrode. In addition, for the enzyme-free glucose sensors, these parameters affect the coupling between the surface of ZnO NRs and the other nanostructure semiconductor materials.

In the first trial of synthesizing ZnO NRs on top of the ITO substrates to be used as a working electrode for the enzymatic electrochemical sensor, the SEM images showed a cloudy surface of the ZnO NRs which can be seen in Figure 3.1 a,b, and c for different magnifications. The red circles indicate the spots of chemicals which were left on the surface of the synthesized nanostructure. To better observe the cloudy spots on the surface, an SEM image was obtained at 120210 x magnification as can be seen in Figure 3.1c. This cloudy surface was due to the

accumulation of the hydroxyl group in the surface during the growth procedure. Also, it was because of the long growth time of the as-grown ZnO NRs. The first growth trial was 6.5 hours at 120 $^\circ$C, which might have led to formation of an oxide layer on the top surface of the nanostructure. Also, the drying time after the growth of ZnO NRs was very important. For the first trial, the ZnO NRs grown on top of ITO substrates were dried at 300 $^\circ$C for 15 minutes. Another reason behind the clustered chemicals on top of the as-synthesized ZnO NRs could have been the solvent, methoxyethanol. This solvent must be stored in the glove box under nitrogen ambient. The chemical was stored at room temperature when it was used to synthesize the seed layer solution. As can be clearly seen from Figure 3.1 a, b, and c, the SEM images showed well-aligned and a highly dense ZnO NRs; the density and alignment of the nanostructure was more clear at 65000 x and 120210 x nm magnifications. In addition, for the first synthesis trial, the hexagonal structure of the as-synthesized ZnO NRs was very clear in the SEM images. For glucose sensing applications, a very clear and uncontaminated surface of the as-synthesized ZnO NRs is highly desired. As a result, the growth procedure of ZnO NRs was adjusted by reducing the growth time from 6.5 hours to 4 hours followed by a careful cleaning step to clean and remove all the residuals from the surface of ZnO NRs.

### 3.2.1.2 Second synthesis trial of ZnO NRs on ITO surfaces

To remove the unwanted chemicals from the surface of the as-synthesized ZnO NRs, a second synthesis attempt was carried out. In this trial, the growth temperature was kept at 90 $^\circ$C and the growth time was reduced to 4 hours. In addition, the surface of the as-grown ZnO NRs was cleaned very carefully four to five times with DI water and dried with nitrogen. Furthermore, the drying time was increased from 15 to 30 minutes at 300 $^\circ$C. Another adjustment to the growth process of ZnO NRs was storing the organic solvent, methoxyethanol, in the glove
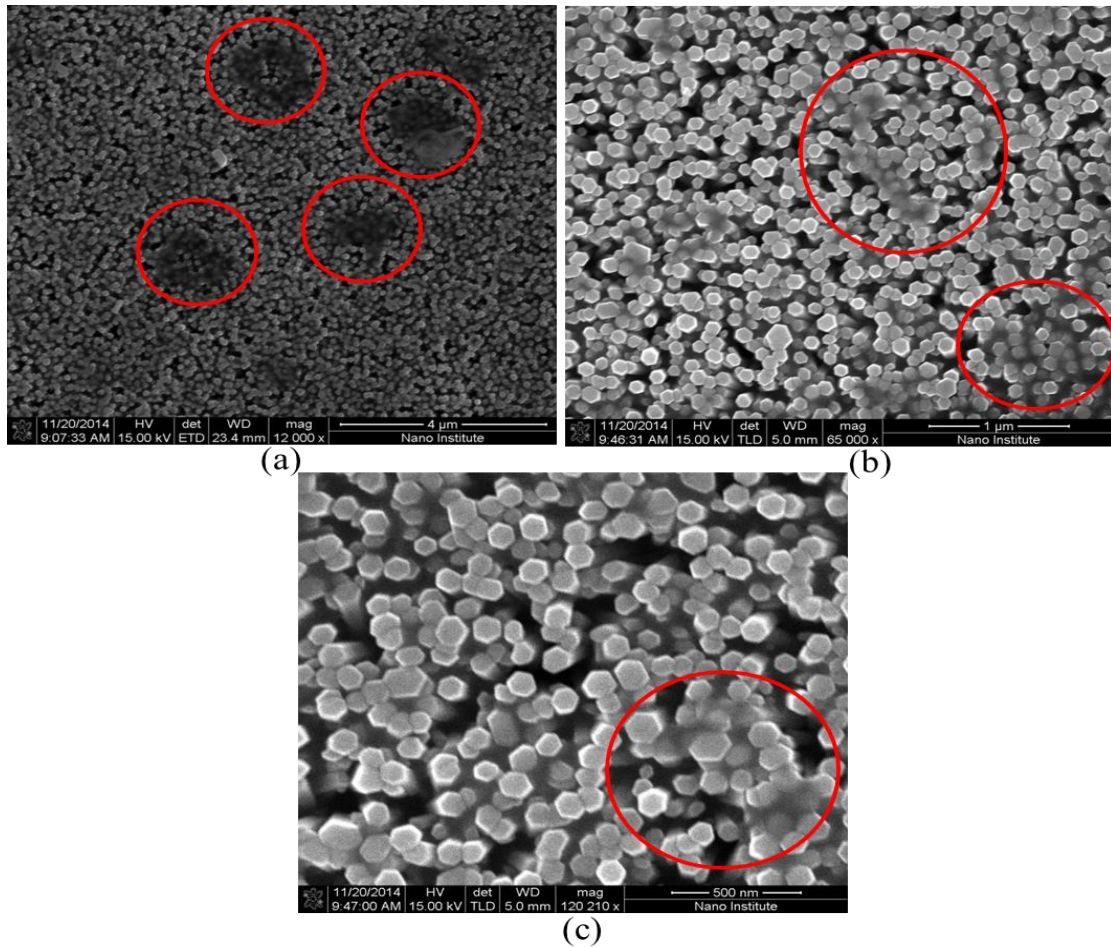
Figure 3.1. The scanning electron microscopy images of the first trial of synthesizing ZnO NRs using the hydrothermal and sol-gel method explained in Chapter 2.

box under nitrogen ambient before it was used to synthesize ZnO NRs on top of the ITO surfaces. The surfaces of the as-synthesized ZnO NRs were clear and no chemicals were observed to contaminate the surface of the grown nanostructure. Scanning electron microscopy images were again taken to evaluate the impact of the adjusted steps on the synthesis recipe. Figure 3.2 a and b shows the clear surfaces of the as-grown ZnO NRs at different magnifications. It was very important to obtain the new SEM images at the same magnification level that was used to obtain the previously shown images. In that case, one could compare between the two procedures and easily observe the enhancement in the new images.

(a)                                         (b)
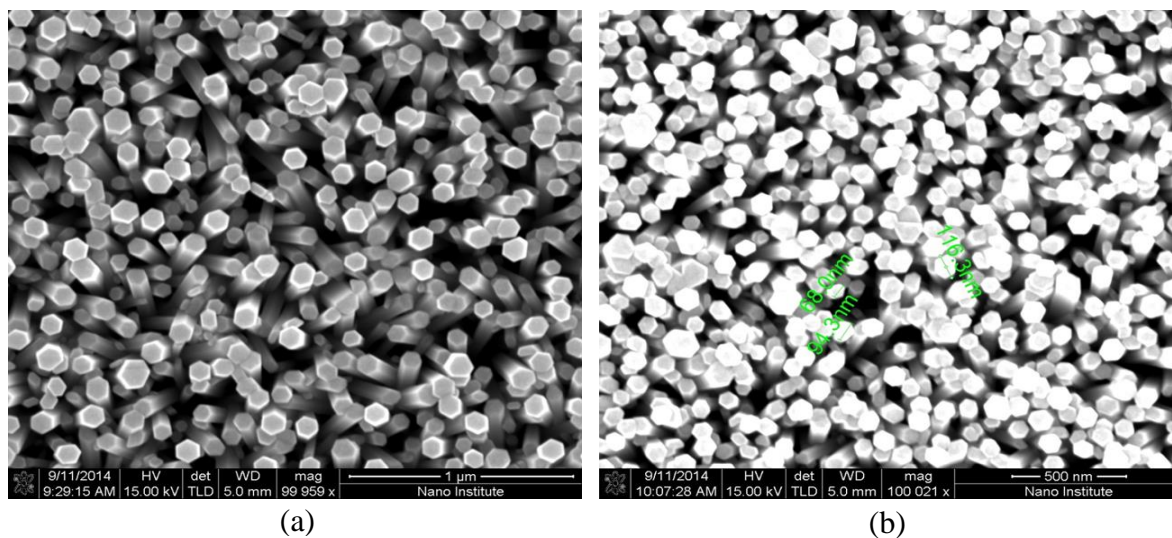
Figure 3.2.  SEM images of the as-synthesized ZnO NRs on top of ITO substrates dried at 300 $^{\circ}$C for 30 minutes and cleaned very carefully after the growth.  Image (b) is reprinted with permission from Marie, et al. [80].

From image (b), the as-synthesized ZnO NRs have slight differences in their diameters, which reflect the uniform distribution of the seed layer on top of the ITO substrates. It is clear from the SEM images in Figures 3.1 and 3.2 of the as-grown ZnO NRs, that the grown nanostructure provides a high surface-to-volume ratio which is very significant to fabricate a highly sensitive electrochemical glucose sensor. The high surface-to-volume ratio helps increase the electroactive area of the electrochemical glucose sensor out of the as-synthesized ZnO NRs. This means that more glucose oxidase can be adsorbed by the electroactive area of the as-synthesized ZnO NRs allowing an efficient direct electron transfer from the center of the enzyme to the surface of the working electrode. In addition, higher glucose concentrations are oxidized on the surface of the working electrode. As a result, a longer linear response can be observed as a function of different glucose concentrations. It is worth mentioning that the clean and uncontaminated surfaces of the as-grown ZnO NRs helped increase the selectivity of the electrochemical sensor and helped to produce uncontaminated signals during the amperometric

56

measurements of the fabricated glucose sensor.

The density, alignment, diameters, and lengths of the as-synthesized ZnO NRs were directly affected by the annealing process after deposition of the three layers of the so-gel solution on top of the ITO substrates. The growth of the seed layers on the ITO substrates was carried out following exactly the same recipe except there was no annealing after the deposition. Scanning electron microscopy images were taken to examine the surface of the grown ZnO NRs without annealing. The results in Figure 3.3 (a and b) showed a random distribution of the diameters and no alignment was observed. The growth was unsuccessful without the annealing as can be seen in Figure 3.3 (a and b). The main reason for that was the accumulation and clustering of the seed layer solution on the surface of the substrate.
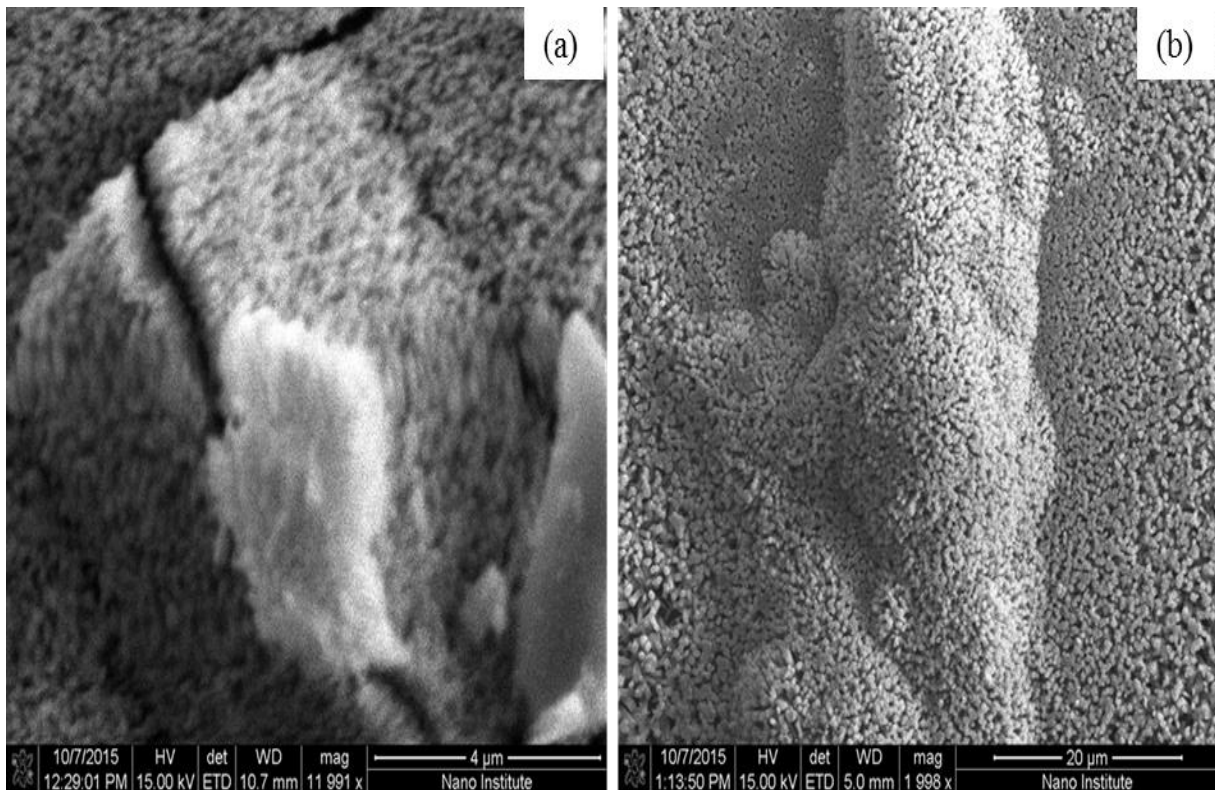


Figure 3.3. SEM images of the as-grown ZnO NRs on top of the ITO substrates without annealing the seed layer solution after the deposition of the three layers. Image (a) is reprinted with permission from Marie, et al. [104].

### 3.2.2 Absorbance spectrum of the grown ZnO NRs

The absorbance spectrum was measured to support the SEM images and to determine the exciton peak. The absorbance spectrum of the as-grown ZnO nanorods was measured after the annealing at 150 °C, and it is shown in Figure 3.4. It was very important to reduce the defects in the as-grown ZnO NRs and that could be done by annealing the coated seed layers on top of the substrate. Consequently, the grown nanostructure absorbed light more efficiently. Furthermore, single crystal ZnO NRs could be obtained by increasing the grain size of the as-synthesized ZnO NRs after annealing. The exciton peak was observed at 363 nm and that was due to the direct band gap of the as-grown ZnO NRs on top of the ITO substrate. The as-synthesized ZnO NRs absorbed all the energies higher than the band gap, which is 3.37 eV, and a rapid increase in the absorbance was noticed at lower wavelengths. The highest absorbance occurred around the edge of the visible region as can be seen in the figure [80].



Figure 3.4. The absorbance spectrum of the as-synthesized ZnO NRs on top of the ITO substrates. Reprinted with permission from Marie, et al. [80].

### 3.2.3 Raman spectrum of the grown ZnO NRs

The lattice and phonon vibration modes are shown in Figure 3.5. Raman spectroscopy provides information regarding the lattice vibration of the nanostructure materials. Raman spectroscopy can be explained as an inelastic scattering of monochromatic light (usually laser) in the material. The peak that belongs to the as-grown ZnO NR lattice vibration at 439 cm$^{-1}$ appears to be sharp and narrow, and it can be assigned as $E_2$ (or high mode). The oxygen vacancy peak of the as-synthesized ZnO NRs appeared on the right of the spectrum and it is associated with the wavenumber 582 cm$^{-1}$. The other peak at 334.4 cm$^{-1}$ can be assigned as a second-order phonon. The weakness of the peak can be explained by the oxygen vacancies during the growth process of the as-grown ZnO NRs, and can be an indicator of the high current obtained using the immobilized surface of the ZnO NRs as a working electrode. Measuring Raman spectroscopy of the as-grown ZnO NRs at low temperatures is very important. It provides an accurate estimation of ratio between zinc and oxygen. The natural lattice vibration of the ZnO NRs can be investigated at low temperatures because the phonons modes are easily noticed [80].

### 3.2.4 X-ray diffraction of the grown ZnO NRs

A Philips x-ray diffractometer was used to measure the x-ray (XRD) of the as-grown ZnO NRs on top of the surface of the ITO substrates. The wavelength of the x-ray used in the experiment was 1.54 Å, which was suitable to estimate the grain sizes of the as-synthesized ZnO NRs. In addition, x-ray measurement is a valid test to evaluate the purity of the synthesized ZnO nanorods. The x-ray pattern of the grown ZnO NRs is shown in Figure 3.6. The strongest peak appeared at 34.364°, which belongs to the as-synthesized ZnO NRs. (002) are the Miller indices associated to the ZnO peak that appeared at ~ 35$^{\circ}$. Classical Scherrer equation was utilized to calculate the grain size of the as-grown ZnO nanorods [105].
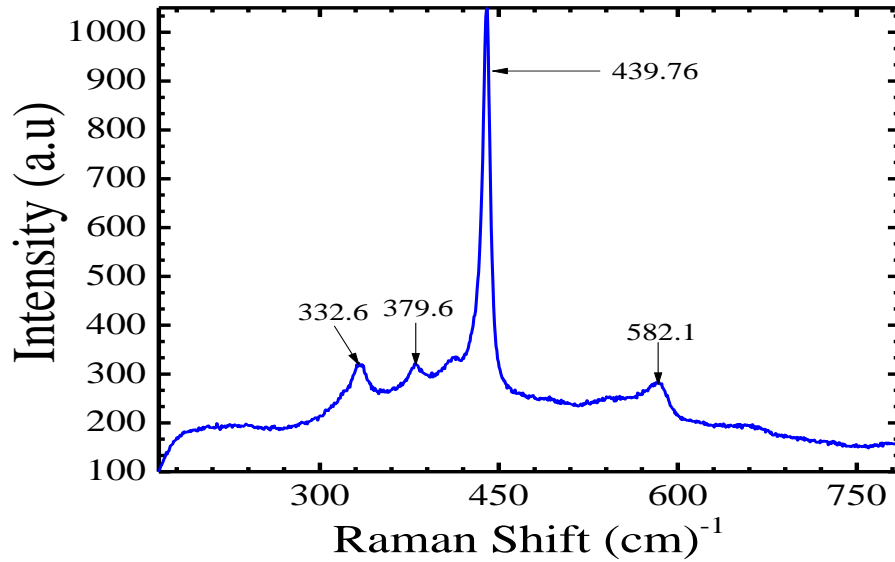
Figure 3.5. Raman spectrum of the as-grown ZnO nanorods on top of the ITO substrates and the observed peaks that correspond to the phonon vibration at room temperature. Reprinted with permission from Marie, et al. [80].



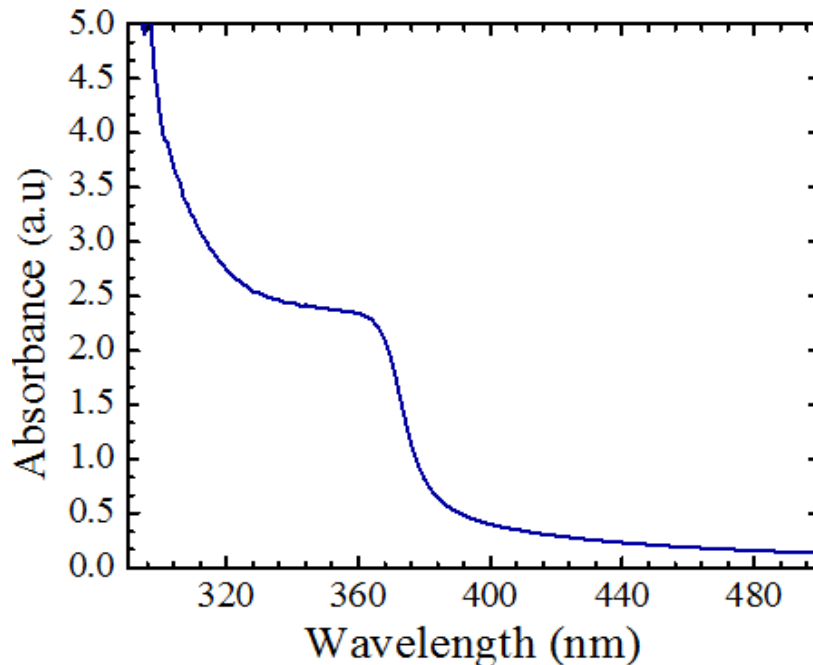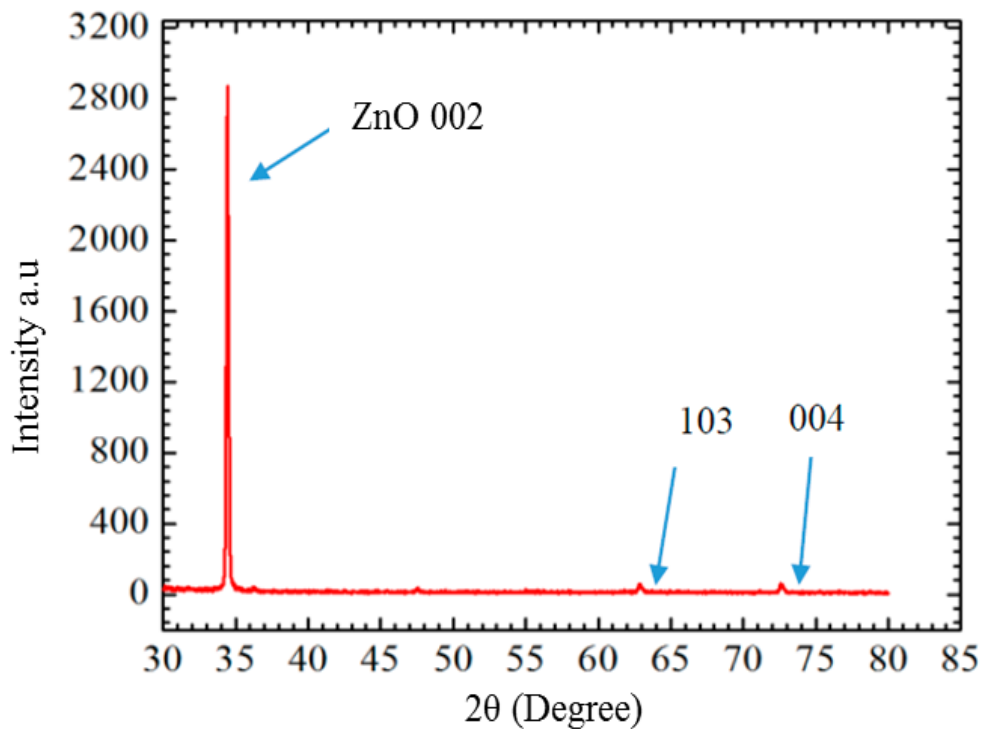Figure 3.6. The XRD patterns of the as-synthesized ZnO NRs on top of the ITO substrates. Reprinted with permission from Marie, et al. [80].

$$G = \frac{k\lambda}{\beta cos\theta} \qquad \text{(Equation 3.1)}$$

where $k$ is the Scherrer constant that has a value in the order of 0.9. G is the grain size of the nanostructure in the unit of Å, $\lambda$ is the wavelength of the x-rays, $\beta$ is the full width at the half maximum of the peak, and $\theta$ is the angle that is associated with the peaks during the measurements. The calculated grain size was on the order of 1.6 nm. The crystallinity of the as-synthesized ZnO NRs was evaluated to be single crystal based on the obtained grain size. The x-ray pattern also showed other weak peaks to the right of the main peak in the pattern. Those two peaks at $62.756^\circ$ and $72.429^\circ$ are associated with the Miller indices (103) and (004), respectively. No phases that are due to the impurities were observed from the XRD measurements of the as-grown ZnO NRs. That was an indication that the hydrothermal growth method was an effective approach to grow pure ZnO NRs which could be used to fabricate electrochemical glucose sensors [80].

### 3.3 The enzymatic glucose sensor based on ZnO NRs coated $GO_x$/BSA/nafion on ITO

### 3.3.1 The linear amperometric response of the sensor

The working electrode of the electrochemical glucose sensor was modified with a Bovine Serum Albumin (BSA) to increase the selectivity of the sensor toward different glucose concentrations. An amount of 4 g of the protein was dissolved in the PBS solution and dropped on top of the as-grown ZnO NRs. The working electrode was left over night at $4\ ^\circ C$ to dry and to adsorb the protein on the surface of the working electrode. Next, $GO_x$ and a nafion membrane were dropped on top of the modified electrode as it was illustrated in Chapter 2. The fabricated enzymatic electrochemical glucose sensor was characterized amperometrically using the Keithley SourceMeter 2410 of and the electrochemical Gamry potentiostat.

The linear response of the fabricated enzymatic electrochemical glucose sensor based on

glass/ITO/ZnO NRs/BSA/GO$_x$/nafion membrane is shown in Figure 3.7. The analytical solution

used to test the glucose sensor is the phosphate buffer solution (PBS) at pH 7.4. Two electrodes

were used in the amperometric measurements, the platinum plate as a counter electrode and the

fabricated working electrode. Both electrodes were placed in the analytical solution (PBS) with a

fixed distance between them. The concentrations of glucose were increased continuously during

the amperometric measurement starting with zero glucose concentration. The concentration of

the glucose was changed from 0.4-2.4 mM to test the linear response of the enzymatic glucose

sensor. The sensor showed a linear response to changes in the glucose concentration from 0.6 to

1.4 mM and the slope of the linear response was the sensitivity of the sensors toward changes in

the glucose concentration. To test the sensing ability of the glucose sensor toward very small

changes in the glucose concentration, the lower limit of detection $LOD$ was calculated using the

Equation 3.2.

$$LOD = 3 \times \frac{\sigma}{slope} \qquad \text{(Equation 3.2)}$$

where $\sigma$ is the standard deviation of the intercept. The $LOD$ was calculated to be on the order of

0.22 µM. The smaller the limit of detection meant the higher the ability of the sensors to detect

small changes in the glucose concentration during the amperometric measurements [80].
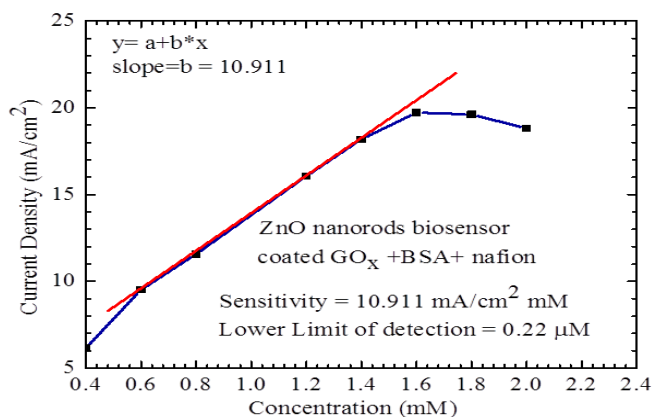


Figure 3.7. The linear response of the fabricated enzymatic electrochemical glucose sensor for different glucose concentrations in the PBS solution. Reprinted with permission from Marie, et al. [80].

### 3.3.2 The cyclic voltammetry measurements

Cyclic voltammetry measurements were conducted to evaluate the oxidation and reduction potentials of the glass/ITO/ZnO NRs/BSA/GO$_x$/nafion membrane-based enzymatic glucose sensor. A Gamry potentiostat was utilized to perform the measurement in the absence and the presence of 1 mM and 2 mM concentrations of glucose. Both the working and the counter electrodes were placed in the PBS analytical solution at zero glucose concentration. The measurements were conducted at 100 mV/s scan rate. The applied potential was swept from 1 to -1 volt to investigate the oxidation and reduction peaks of the glucose on the surface of the working electrode. In the absence of glucose in the PBS, the sensor showed no dependency on the swept potential, which meant that the sensor had a high selectivity toward the glucose. The maximum observed current was on the order of 0.045 μA as shown in Figure 3.8 a. Figure 3.8 b is the cyclic voltammetry measurement in the presence of 1 mM glucose in the PBS. The potential was swept from 1 to -1 volt in the PBS analytical solution. The maximum current observed was 0.8 volt, which is known as the oxidation peak of the sensor. At the reverse direction of the swept potential, the glucose sensor exhibited a reduction peak around -0.8 volts. The maximum observed current in the presence of 1m M of the glucose in the PBS was on the order of 0.11 μA.

The electrochemical reaction during the cyclic voltammetry measurements has two different directions depending on the oxidation time of the hydrogen peroxide, $H_2O_2$, to oxygen, hydrogen, and free electrons. In addition, it also depends on the reduction time of hydrogen and oxygen to reproduce $H_2O_2$. The electrochemical reaction in the presence of glucose can be either a forward (oxidation) reaction or backward (reduction) reaction, so it is a reversible reaction. In the presence of 2 mM of glucose in the analytical solution, the sensor showed high oxidation and

63
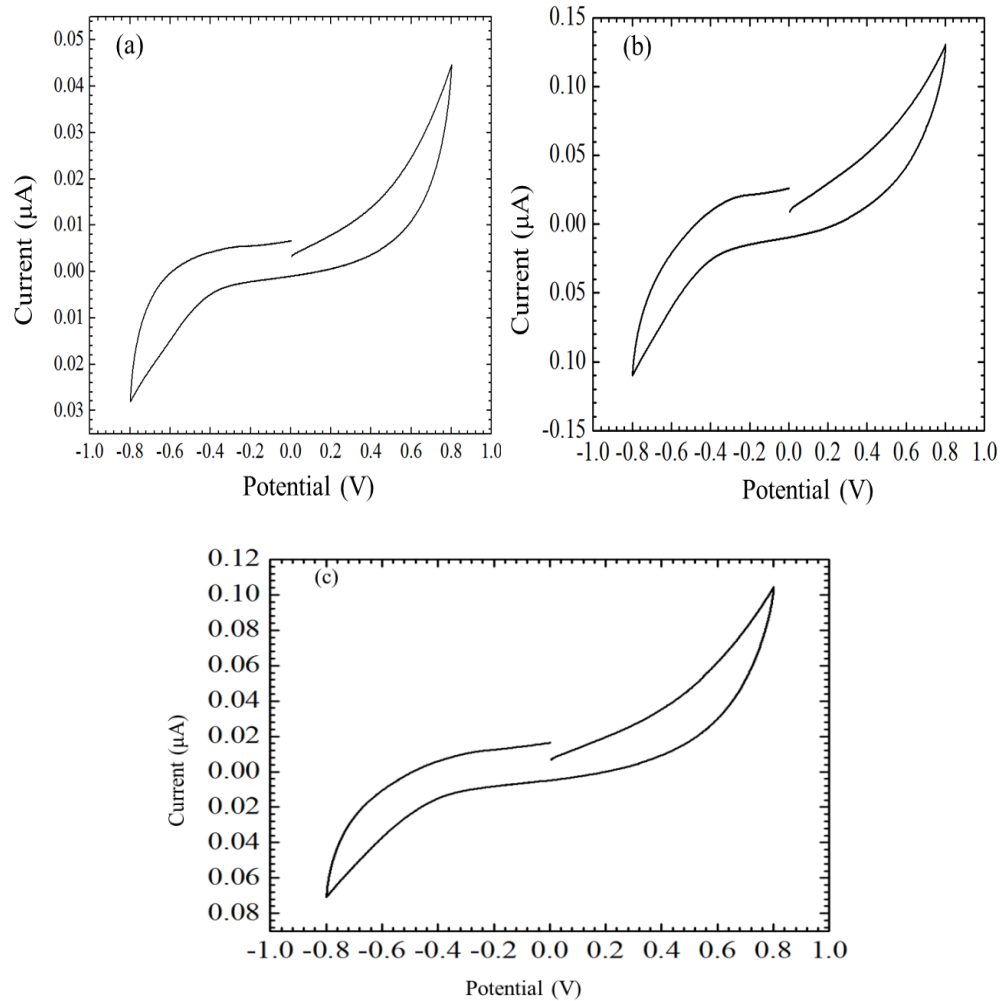
Figure 3.8. Cyclic voltammetry measurements of the enzymatic electrochemical glucose sensor, (a) in the absence of glucose, (b) at 1 mM of glucose, and (c) at 2 mM of glucose. Reprinted with permission from Marie, et al. [80].

reduction peaks at 0.8 and -0.8 volts, respectively, as can be seen in Figure 3.8 c. The maximum current at 2 mM of glucose was on the order of 0.125 μA. It was an indication that the fabricated sensor was sensitive to the changes in the glucose concentrations [80].

### 3.3.3 The time response characteristics

The amperometric time response measurement was carried out to test the detection capability of the enzymatic glucose sensor toward changes in the glucose concentration. This

capability to sense changes in the glucose concentration in the analytical solution was translated to a current response as a function to the time response. The amperometric time response of the sensors is shown in Figure 3.9. A potential on the order of 0.8 volt was applied between the working electrode, which is glass/ITO/ZnO NRs/BSA/GO$_x$/nafion membrane, and the counter electrode, which is a platinum plate. The amperometric test was conducted using the SourceMeter 2410. Continuous changes in the glucose concentrations were made in PBS during the amperometric measurement. The constant time interval between each two different glucose concentrations was 25 seconds. The software was set to read one value of the current each second and the average of the 25 measurements was calculated and plotted as a function of time. Each set of 25 values (measurements) represented a certain concentration of glucose in the PBS. The amperometric time response of the sensor was calculated to be on the order of 3 seconds. It was calculated from the time that the current started to increase after adding a new glucose concentration to the time when the amperometric current reaches the steady-state level.

The sharp and fast time response of the sensor was an indication that the current reaches 95% of the steady-state value in only 3 seconds. This was an indication of the fast electron exchange between the surface of the modified working electrode and the center of the enzyme in the PBS. The concentration of the glucose was changed from 1 mM to 4 mM during the amperometric measurement in the PBS. The GO$_x$ helped in catalyzing the glucose and producing hydrogen peroxide, and the latter will oxidize to hydrogen, oxygen, and free electrons. The nafion membrane that was used to coat the surface of the working electrode helped in increasing the stability of the sensor during the amperometric measurement. As a result, this helped in increasing the selectivity of the glucose sensors toward changes in the glucose in the PBS [80].
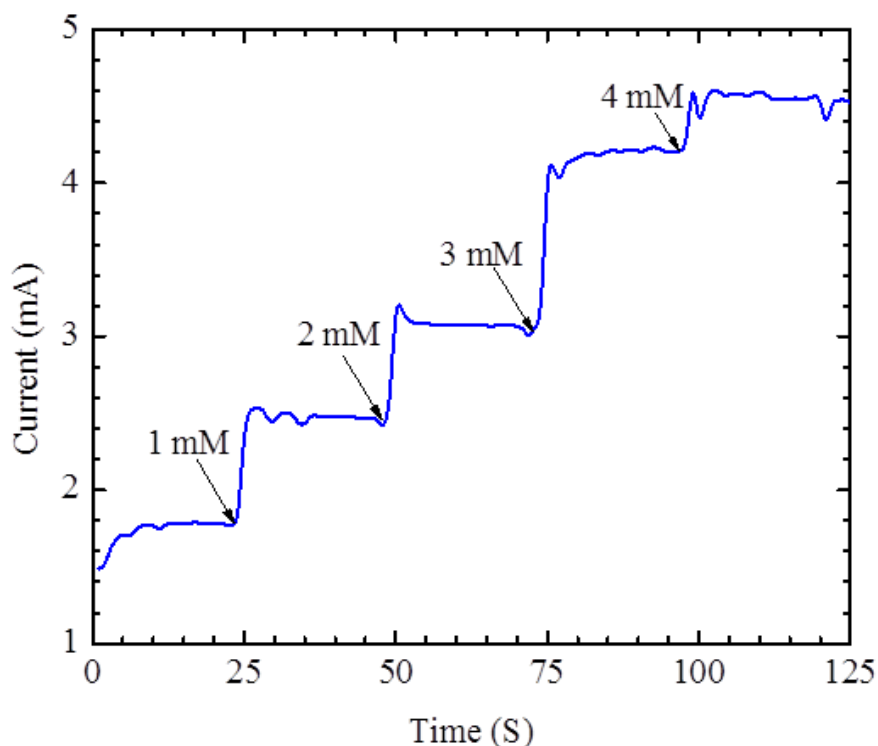
Figure 3.9. Amperometric time response of the fabricated enzymatic electrochemical sensor to different concentrations of glucose with 3 s response time. Reprinted with permission from Marie et al. [80].

### 3.3.4 Different concentrations of the enzyme, $GO_x$

To study the ability of the as-synthesized ZnO NRs for adsorbing different concentrations of the enzyme, $GO_x$, the surface of the fabricated electrochemical sensor was immobilized with different amounts of $GO_x$ and a fixed amount of the protein, bovine serum albumin (BSA). The surface of the working electrode was covered with a nafion membrane to increase the stability of the device and to reduce the noise of the detected signal. Figure 3.10 is the current versus different glucose concentrations of the immobilized working electrode with different concentrations of the enzyme, $GO_x$ and without immobilization with $GO_x$. It can be seen clearly that the device showed a higher sensitivity with higher amounts of $GO_x$, which meant that higher concentrations of the enzyme, $GO_x$, were adsorbed in the three dimensional nanostructural

reaction area. The non-immobilized $GO_x$ was taken away from the surface of the working electrode by the covalent method with a higher ionic solution as was explained in Chapter 2. The device showed a higher sensitivity when the working electrode was immobilized with 40 mg of $GO_x$. In addition, immobilizing the working electrode with 30 mg of $GO_x$ gave almost a similar result to the one with 40 mg. It meant that the three dimensional nanostructural area provided by the as-grown ZnO NRs was saturated and no more $GO_x$ could be adsorbed. Thus, increasing the aspect ratio, which is the length over the diameter of the as-synthesized ZnO NRs, helped in pushing the saturated level of the three dimensional area and helped in adsorbing higher amounts of $GO_x$. The direct growth of ZnO NRs helped in transferring electrons from the center of the enzyme to the surface of the as-grown ZnO NRs. The oxidation-reduction reaction of the glucose on the surface of the electrode depended on the adsorbed amount of $GO_x$ in the three dimensional area provided by the as-grown ZnO NRs.
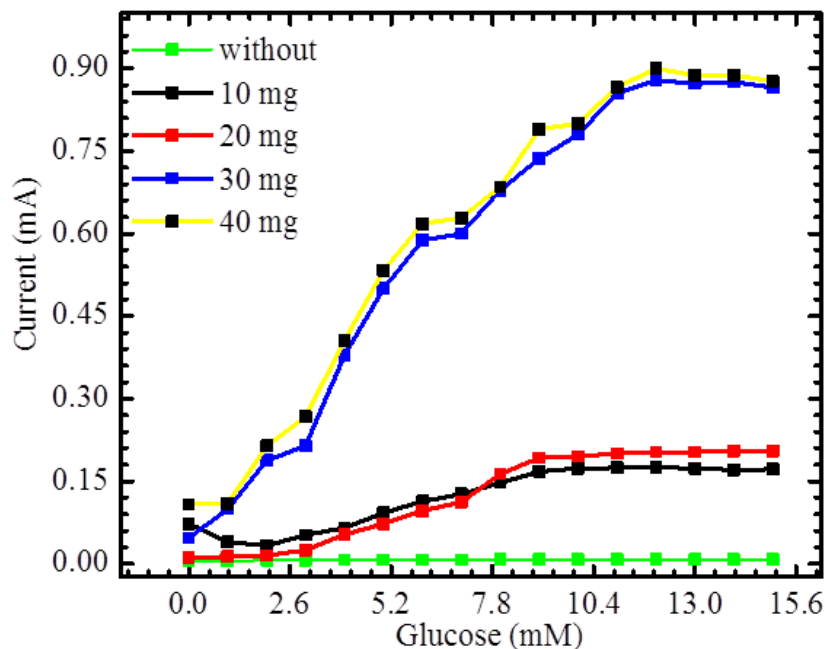


Figure 3.10. The amperometric measurement of the current on the surface of the working electrode as a function of glucose concentration at different concentrations of $GO_x$.

### 3.4  The enzymatic glucose sensor based on ZnO NRs grown on Si/SiO$_2$/Au substrate

### 3.4.1  Introduction

An enzymatic electrochemical glucose sensor was fabricated by using a silicon substrate coated with a silicon dioxide layer. The Si/SiO$_2$ substrate was covered with a 100 nm thin film of gold using an e-beam evaporator [101]. ZnO NRs were grown on top of the Si/SiO$_2$/Au substrate using the so-gel and hydrothermal method. To characterize the device, amperometric and cyclic voltammetry measurements were performed in the phosphate buffer solution at different glucose concentrations. Before running the amperometric and cyclic voltammetry measurements, the working electrode was coated with the enzyme, GO$_x$, and a nafion membrane. The final structure of the working electrode was as Si/SiO$_2$/Au/ZnO NRs/GO$_x$/nafion membrane. All the measurements were carried out at room temperature using the Keithley SourceMeter and Gamry potentiostat. Si/SiO$_2$/Au/ZnO NRs/GO$_x$/nafion membrane was used as the working electrode, while a platinum plate was utilized as the counter electrode in the electrochemical cell.

### 3.4.2  Time response measurement

The time response of the electrochemical sensor was performed in two different ways. First, the time response measurement was carried out only for the substrate. In other words, the time measurement was done for Si/SiO$_2$/Au/GO$_x$/nafion membrane without growing the ZnO NRs on top of the working electrode. The same amperometric time measurements were repeated under the same conditions but after the growth of ZnO NRs on top of the Si/SiO$_2$/Au substrate. The amperometric time measurements of glucose sensor with and without the as-grown ZnO NRs are shown in Figure 3.11. Measurements both with and without the growth of ZNO NRs were carried out at different glucose concentrations from 1–20 mM as shown in Figure 3.11. Glucose concentrations were increased by adding 1 mM of glucose to the PBS every 50 seconds.
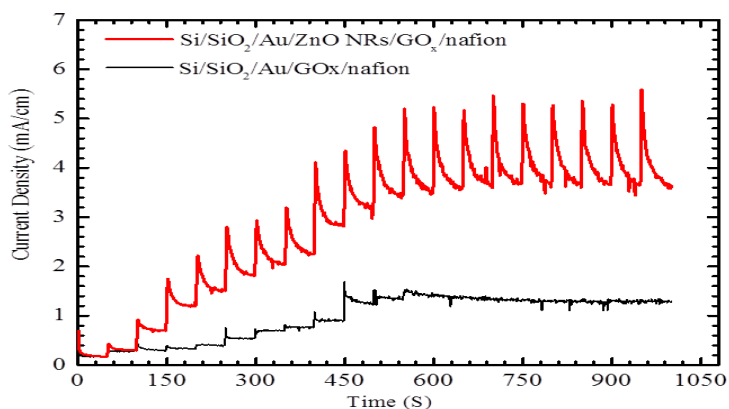
Figure 3.11. The time response measurement of the electrochemical glucose sensor with and without the growth of ZnO NRs on top of Si/SiO$_2$/Au.

The substrate Si/SiO$_2$/Au/GO$_x$/nafion membrane showed a very small and almost a negligible increase in the current density with changes in the glucose concentration (black line). The average increase in the current density with different glucose concentrations was on the order of ~0.1 mA/cm$^2$. A fast and a sharp amperometric time response was observed after applying the as-grown ZnO NRs to the surface of the working electrode. The time response of the electrochemical glucose sensor with the as-grown ZnO NRs applied to the surface of the working electrode was calculated to be on the order of 2 seconds. In addition, the glucose sensor based on Si/SiO2/Au/ZnO NRs/GOx/nafion showed a lower level of noise compared with the working electrode with the as-grown ZnO NRs. The as-synthesized ZnO NRs helped in increasing the signal to noise ratio by adsorbing higher concentrations of the enzyme, GO$_x$, on the surface of the working electrode. Furthermore, the response of the Si/SiO$_2$/Au/ZnO NRs/GOx/nafion membrane based electrochemical glucose sensor went to saturation at high glucose concentrations. The glucose sensor with ZnO NRs showed an average increase in the amperometric current density around 0.45 mA/cm$^2$. It can be seen in Figure 3.11 (the red line) that the time response of the electrochemical sensor did not go to saturation even at high glucose concentrations.

69

### 3.4.3 Cyclic voltammetry measurement

A Gamry potentiostat was utilized to run the cyclic voltammetry measurements on the fabricated glucose sensor after applying the as-synthesized ZnO NRs to the surface of the working electrode. The measurements were conducted at different scan rates and in the absence and the presence of the glucose. The cyclic voltammetry results with and without the glucose are shown in Figure 3.12 a and b. The applied voltages were swept from 1 to -1 volts at scan rates 50, 100, and 200 mV/s for the working electrode and the counter electrode in the PBS analytical solution. The electrochemical sensor showed no dependency on the different scan rates in the absence of the glucose. Although there was slight increase in the current density at different scan rates, it did not mean that there was a response from the electrochemical sensor.

As can be seen in Figure 3.12 a, the oxidation and reduction peaks were not observed in the absence of glucose. The oxidation and reduction peaks of the glucose sensor in the presence of 2 mM of glucose were clear at different scan rates as shown in Figure 3.12 b. The applied potential was swept from 1 to -1 volt at 50, 100, and 200 mV/s. The device showed a clear dependency on the scan rates in the presence of 2 mM of glucose. The strongest oxidation peak appeared at the scan rate of 200 mV/s with an amperometric current density on the order of 0.4 mA/cm$^2$. The electrochemical reaction could be considered as a forward reaction when $H_2O_2$ was oxidized to hydrogen, oxygen, and free electrons. It is clear from Figure 3.12 b that the oxidation peaks at different scan rates were much stronger than the reduction peaks at the same scan rates. The nafion membrane that was used to cover the working electrode helped enhance the stability of the sensor during the cyclic voltammetry measurement [101].

### 3.4.4 The linear amperometric measurement

The linear amperometric response of the electrochemical glucose sensor is shown in
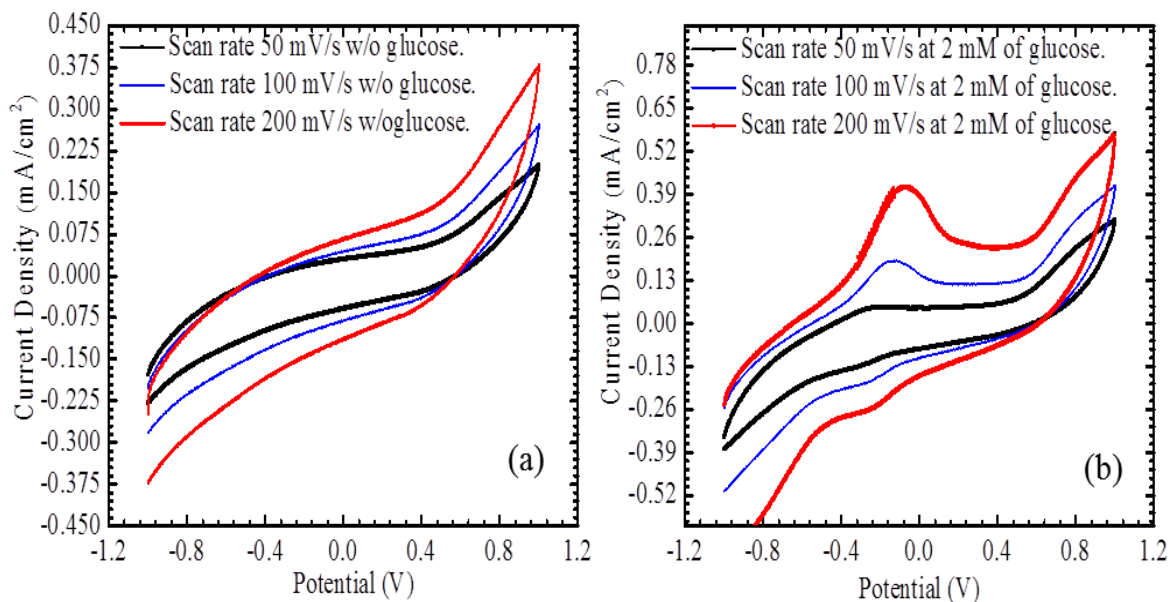
Figure 3.12. The cyclic voltammetry of the electrochemical glucose sensor based on Si/SiO$_2$/Au/ZnO NRs/GO$_x$/nafion in the absence of glucose (a) and in the presence of 2 mM of glucose (b) at different scan rates. Reprinted with permission from Marie et al. [101].

Figure 3.13. The working electrode without the growth of ZnO NRs showed a very weak response to changes in the glucose concentration. The working electrode without the as-grown ZnO NRs was saturated even at the low concentrations of glucose. From the black line in Figure 3.1, the response of the sensor was almost the same at different glucose concentrations starting from 3 mM to 10 mM. After introducing the as-synthesized ZnO NRs to the surface of the working electrode, the electrochemical glucose sensor exhibited a linear amperometric response to changes in the glucose concentrations as shown in Figure 3.13 (the red line). The device showed a linear response to changes in the glucose concentration from 1-8 mM. Comparing the amperometric response of working electrodes both with and without the ZnO NRs, one can highlight the importance of the electroactive area of the sensor provided by the as-grown ZnO NRs. Higher concentrations of the enzyme GO$_x$ were adsorbed in the nanostructured area created by ZnO NRs.
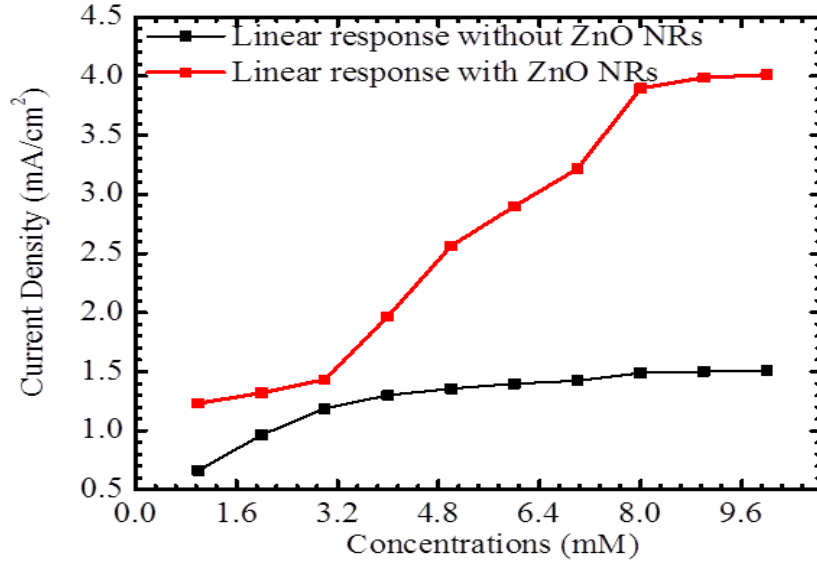
Figure 3.13. The amperometric response of the electrochemical glucose sensor based on $Si/SiO_2/Au/GO_x/nafion$ with and without the growth of ZnO NRs on top of the surface of the working electrode. Reprinted with permission from Marie, et al. [101].

In the absence of ZnO NRs on top of the working electrode, $GO_x$ was getting adsorbed on the two dimensional area on the surface of the working electrode. Glucose reacted with the enzyme, $GO_x$, and produced $H_2O_2$ on the surface of the working electrode. Hydrogen peroxide was oxidized to $H_2$, $O_2$, and free electrons. The produced electrons transferred from the center of the enzyme, $GO_x$, to the surface of the working electrode throughout the as-grown ZnO NRs. Since the as-grown ZnO NRs provided high surface-to-volume ratio to the surface of the working electrode, more $GO_x$ was adsorbed effectively on the electrochemical active area of the working electrode. Without the growth of ZnO NRs on top of the working electrode, less $GO_x$ reacted with glucose since only a lower concentration of the enzyme was getting adsorbed effectively by the surface of the gold thin film. The fabricated electrochemical glucose sensor based on $Si/SiO_2/Au/GO_x/nafion$ was saturated at lower glucose concentrations while the device with ZnO NRs on top of the gold thin film went to saturation at higher glucose concentrations [101].

**3.5 Enzyme-free electrochemical sensor based on ZnO NRs modified with ferric oxide**

Although the enzymatic electrochemical glucose sensors are very sensitive to changes in glucose concentrations, the lifetime of the enzyme, glucose oxidase, is one of the biggest issues that shorten the lifetime of these sensors. It is because of the biological degradation of the FAD in the center of the enzyme with time. Enzyme-free glucose sensors have less selectivity toward changes in glucose concentrations. However, those kinds of sensors are more stable with a longer lifetime. The fabricated enzyme-free electrochemical glucose sensor was based on ZnO NRs coupled with ferric oxide to work as a mediator for the redox of glucose on the surface of the nanostructure. The working electrode was coated with a nafion membrane to increase the stability of the glucose sensor. The device was characterized amperometrically using Keithley SourceMeter and Gamry potentiostat at different glucose concentrations.

**3.5.1 SEM images of ZnO NRs before and after modification with $Fe_2O_3$**

SEM images of the as-synthesized ZnO NRs on top of the FTO substrates with and without ferric oxide are shown in Figure 3.14. The images (a) and (b) are the pure ZnO NRs as a top view and a cross section, while the pictures in (c) and (d) are the top view and the cross section of the modified ZnO NRs with ferric oxide. The grown ZnO NRs have a good alignment and a high density. This is a direct reason for having a high volume-to-surface ratio of the electroactive area of the fabricated enzyme-free glucose sensor. After modifying the as-synthesized ZnO NRs with ferric oxide, SEM images were taken to evaluate the coupling between ZnO NRs and $Fe_2O_3$ as can be seen in images (c) and (d). ZnO NRs provided a three dimensional sensing area of the surface of the working electrode.

Higher concentrations of ferric oxide were attached successfully to the walls of the as-grown ZnO NRs on top of the FTO substrates. Higher concentrations of the glucose reacted with
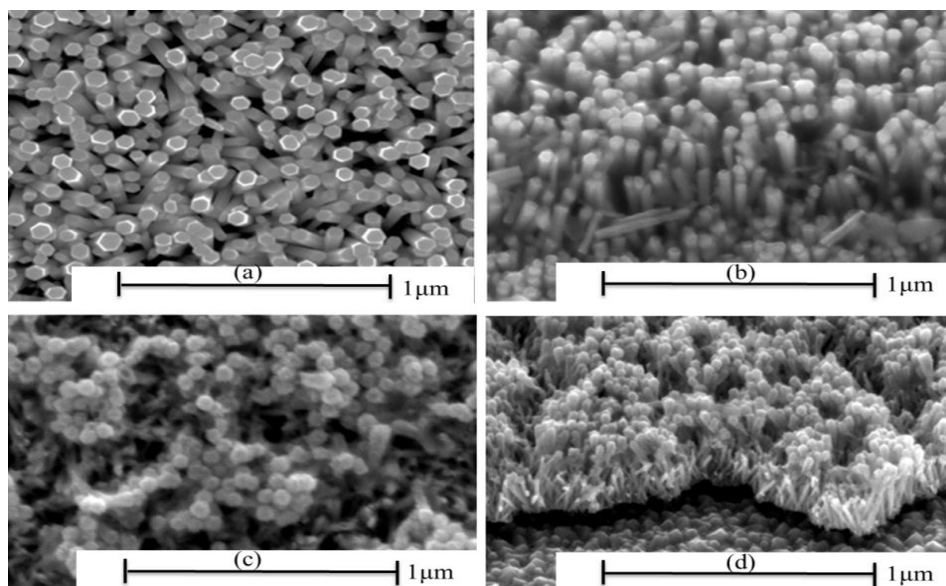
Figure 3.14. SEM images of the pure and modified ZnO NRs with ferric oxide where (a) is the top view of the pure as-synthesized ZnO NRs, (b) is the cross section of the pure ZnO NRs, (c) is the top view of ZnO NRs after coupling with $Fe_2O_3$ and (d) is the cross section of the ZnO NRs/$Fe_2O_3$. Reprinted with permission from Marie, et al. [95].

ferric oxide on the surface of the working electrode to produce the free electrons. The three dimensional area provided by the as-grown ZnO NRs can be expressed as (No. of ZnO NRs/area) $\times$ (area of substrate) $\times$ ($2\pi rl$), where l and r are the length and the radius of the ZnO NRs, respectively. The isoelectric point of ZnO NRs is on the order of 10.3, which is higher than the IEP of ferric oxide. This provides a good affinity between ZnO NRs and ferric oxide on the surface of the working electrode. During the electrochemical reaction, Fe (III) is oxidized to Fe (II) in the electroactive area of the electrochemical glucose sensor. The high electrocatalytic ability of ferric oxide helped in oxidizing higher concentrations of the glucose on the surface of the working electrode. In addition, Fe (II) is reduced to Fe (III) during the electrochemical reaction which helped enhance the linear amperometric response of the sensor. As a result, higher glucose concentrations were sensed easily and accurately on the surface of the glucose sensor [95].

## 3.5.2 XRD measurement of ZnO NRs before and after modification with Fe$_2$O$_3$

X-ray diffraction measurement was conducted to investigate the crystal structure of the as-grown ZnO NRs on FTO substrate after the modification with ferric oxide. The hexagonal wurtzite structure of the as-grown ZnO NRs along the c-axis plane showed a peak at 34.4° as shown in Figure 3.15. The peak of the wurtzite crystal structure of the ZnO NRs was attributed to the plane (002). The peak that belonged to the FTO substrate was observed at 37.8° and it was attributed to the (200) plane. The as-grown ZnO NRs on top of the FTO substrate were effectively textured to the x-ray radiation with the planes (002) and (200) and that was perpendicular to the surface normal, respectively. The texture coefficient, T$_{(hkl)}$, that describes the relative degree of the preferred orientation among many different crystal planes is known as:

$$T_{(khl)} = \frac{I_{(khl)}/I_{o(khl)}}{\frac{1}{n}\sum \frac{I_{(khl)}}{I_{o(khl)}}}$$

(Equation 3.3)

Where $I_{o(khl)}$ and $I_{(khl)}$ are the standard integrated intensity and the measured intensity for the plane (*hkl*) reflection, respectively, and *n* is the number of reflections. The texture coefficient, T$_{(002)}$, for ZnO NRs was calculated to be on the order of ~14. This was an indication that the as-synthesized ZnO NRs were grown in the c-axis direction. This was the direction normal to the surface and (200) planes of the FTO grains. In addition, the Scherrer equation (Equation 3.1) was utilized to calculate the lateral coherence lengths of the FTO and the synthesized ZnO NRs. The coherence lengths of the FTO substrate and ZnO NRs were on the order of ~30 nm and ~35 nm, respectively.

The crystal structure of the substrate FTO had an influence on the as-grown ZnO NRs in terms of the orientation and  grain size. It is worth mentioning that the ferric oxide that was used
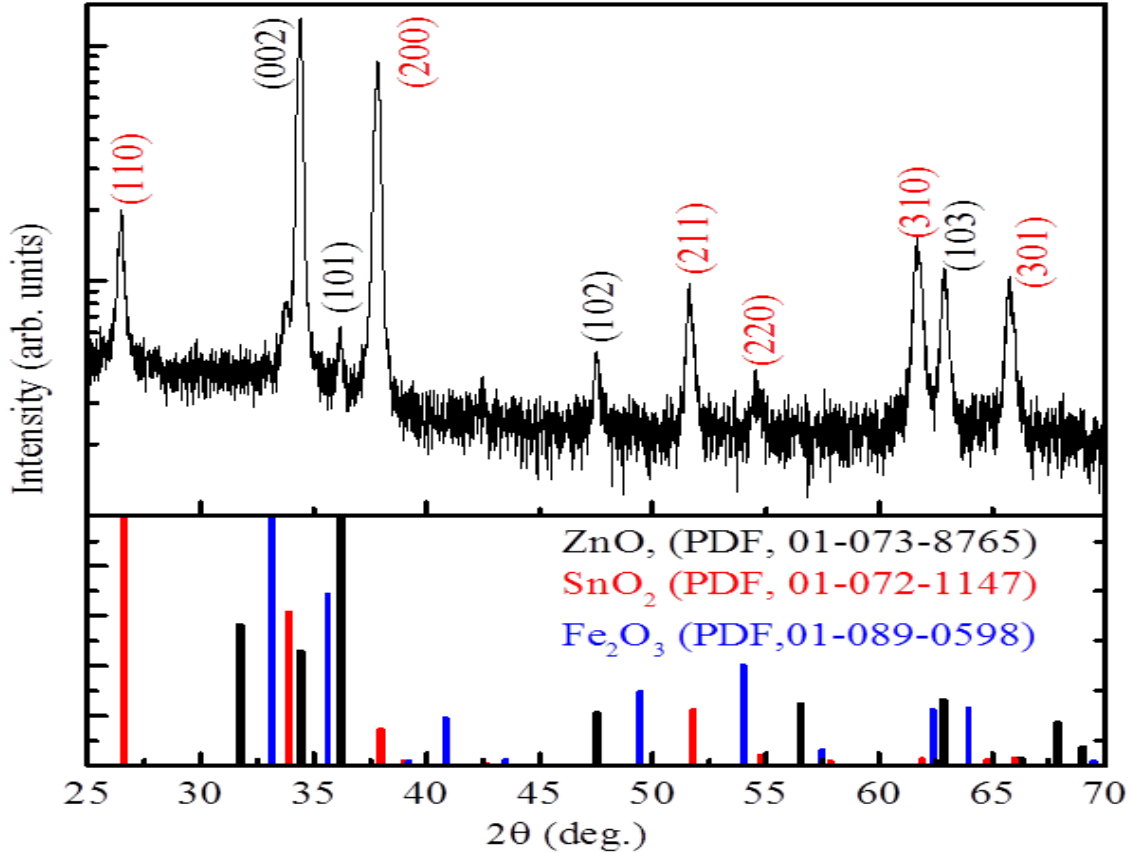
Figure 3.15. XRD pattern of the ZnO NRs after the coupling with $Fe_2O_3$. Reprinted with permission from Marie, et al. [95].

to modify the as-synthesized ZnO NRs had small grain sizes compared with the grain sizes of ZnO NRs and FTO substrates. The x-ray pattern showed that ferric oxide was attached to the walls of the as-grown ZnO NRs randomly. This made it difficult to observe the peaks that belong to the ferric oxide due to the smaller grain sizes and the random orientation. This is why the peaks belonging to ferric oxide were overlapped with the ZnO NR and FTO peaks. The advantage of the smaller grain sizes of the ferric oxide was that higher concentrations of ferric oxide could be attached to the walls of the ZnO NRs effectively. Because of the mentioned reasons, tunneling electron microscopy might have been useful to accurately evaluate the modification of as-grown ZnO with ferric oxide [95].

### 3.5.3 Cyclic voltammetry measurement of ZnO NRs modified with $Fe_2O_3$

Cyclic voltammetry measurements were conducted at room temperature to examine the modification of the surface of the working electrode with ferric oxide. The measurements were carried out the absence and presence of glucose. A three electrochemical cell consisting of glass/FTO/ZnO NRs/$Fe_2O_3$/nafion membrane as the working electrode, platinum plate and silver/silver chloride as the counter and the reference electrodes, respectively, was prepared to carry out the measurements. Silver/silver chloride was the reference electrode that the potential was swept against. The applied potential was swept from 1 to -1 volt to cover the oxidation and reduction peaks of the glucose during the cyclic voltammetry measurements.

The electrochemical sensor was tested under two different scan rates, 100 and 200 mV/s. Figure 3.16 a shows the cyclic voltammetry measurement at 100 and 200 mV/s scan rates in the absence of glucose. The fabricated electrochemical sensor showed no dependency on the two different scan rates in the absence of glucose. From Figure 3.16 a, one can see that the same current was obtained at the two scan rates meaning that the sensed current did not depend on the scan rate in the absence of the glucose. A 100 mg/dL of the glucose was added to the PBS analytical solution to evaluate the ability of the enzyme-free glucose sensor to sense the changes in the concentration. The cyclic voltammetry measurement was conducted at two scan rates, 200 and 300 mV/s, in the presence of 100 mg/dL of glucose. An oxidation peak was clearly observed around 0.7 volt for the scan rate of 300 mV/s and around 0.4 volt for the scan rate of 200 mV/s as shown in Figure 3.16 b. When the direction of the swept potential was reversed, the enzyme-free glucose sensor exhibited a reduction peak around 0.4 volt at the scan rate of 300 mV/s.

The oxidation reaction or the forward reaction, was faster than the reduction reaction or the backward reaction. It was an indication that the oxidation of Fe (III) to Fe (II) on the surface
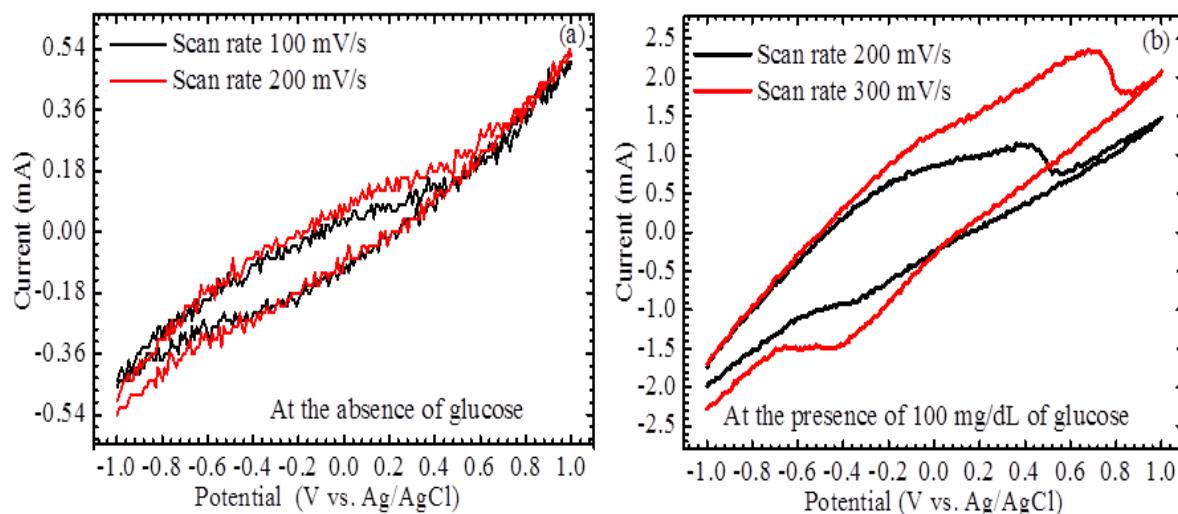
Figure 3.16. The cyclic voltametry measurements of the modified enzyme-free glucose sensor at different scan rates (100, 200, 300 mV/s) in the absence of glucose (a) and in the presence of 100 mg/dL glucose (b). Reprinted with permission from Marie et al. [95].

of the as-synthesized ZnO NRs was faster than the reduction of Fe (II) to Fe (III) on the same surface. When the direction of the swept potential was reversed at the scan rate of 200 mV/s, the sensor showed a reduction peak at -0.4 volt. At the scan rate of 200 mV/s, one can see that Fe (III) was oxidizing to Fe (II) and Fe (II) was reducing to Fe (III) at the same reaction speed. The shift in the peak positions at the scan rates 200 and 300 mV/s in the presence of 100 mg/dL of glucose was an indication that the sensor was sensitive to changes in the glucose concentration. Since the characterized enzyme-free electrochemical sensor exhibited the maximum glucose oxidation peak at 0.7 volt, all other amperometric measurements, such as the amperometric response, the time response, and the calculation of the apparent Michaelis-Menten constant, were carried out at 0.7 volt [95].

### 3.5.4 The time response measurement of ZnO NRs modified with $Fe_2O_3$

An amperometric time response measurement was performed using the Gamry potentiostat and the three electrodes setup. The measurement was conducted at different glucose

concentrations dissolved in the PBS solution at pH 7.4 as shown in Figure 3.17. The glucose

concentrations were changed in the phosphate buffer solution from 100 to 900 mg/dL. After

every 20 seconds, a new concentration of glucose was introduced to the solution during the

amperometric measurement. The amperometric current was plotted as a function of the

electrochemical reaction time for each glucose concentration. The average of each 20 values of

the sensed current was plotted versus time. Each 20 values of the current were associated with

one concentration of glucose. A sharp and a fast response time, ~1 s, was calculated from the

amperometric time measurement.
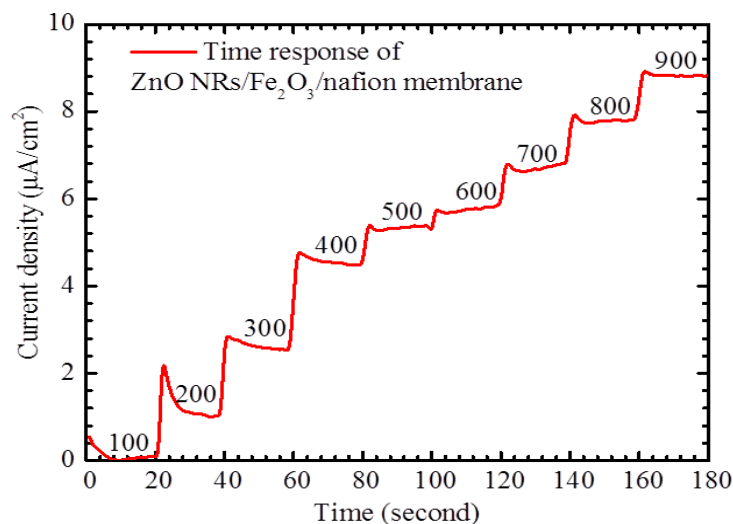


Figure 3.17. The amperometric time response of the enzyme-free glucose sensors at different
glucose concentrations from 100 to 900 mg/dL at 7 volt. Reprinted with permission from Marie
et al. [95].

The fabricated enzyme-free electrochemical glucose sensor out of glass/FTO/ZnO

NRs/Fe$_2$O$_3$/nafion exhibited a steady-state current with each glucose concentration. One can see

from Figure 3.17 that the sensor showed no decay in the current response during the

measurement indicating the high stability of the sensor toward the changes in the glucose

concentrations. There was a slight decay in the current at the 200, 300, and 400 mg/dL of the

glucose concentrations. A steady-state current was noticed during the measurements for the other different concentrations of the glucose. The sensing area of the enzyme-free sensor had a high surface to volume ratio provided by the as-synthesized ZnO NRs on the surface of the working electrode. Consequently, the glucose sensor exhibited a high signal-to-noise ratio that can be seen from the time response measurement. In addition, the continous oxidation of $Fe_2O_3$ which was attached to the walls of the ZnO NRs was another reason for the stability of time response. The nafion membrane provided a good isolation to the surface of the working electrode and that helped in enhancing the stability of the fbricated sensor during the amperometric time measurements [95].

### 3.5.5 The linear response measurement of ZnO NRs modified with $Fe_2O_3$

The amperometric linear response of the modified glucose sensor was measured using the amperometric method at different glucose concentrations. The phosphate buffer solution was utilized to host the electrochemical reaction and glucose concentrations were changed from 100 to 900 mg/dL. The measurement was conducted at 0.7 volt extracted from the cyclic voltammetry test. Continuous changes were made in the glucose concentrations during the amperometric measurements. A working electrode based on pure ZnO NRs on top of the glass/FTO coated with a nafion membrane was used in the measurement as can be seen in Figure 3.18 a (the red line). It can be seen from the figure that the working electrode based on glass/FTO/ZnO NRs/nafion membrane exhibited almost no dependency on the changes of the glucose concentrations from 100 to 900 mg/dL. The same glucose concentrations from 100 to 900 mg/dL were used to measure the amperometric response of the modified working electrode with $Fe_2O_3$. A wide linear response of the modified glucose sensor was observed at different glucose concentrations as in Figure 3.18 a (the black line). The linear amperometric response of

80

the modified electrode was observed from 100 to 400 mg/dL.
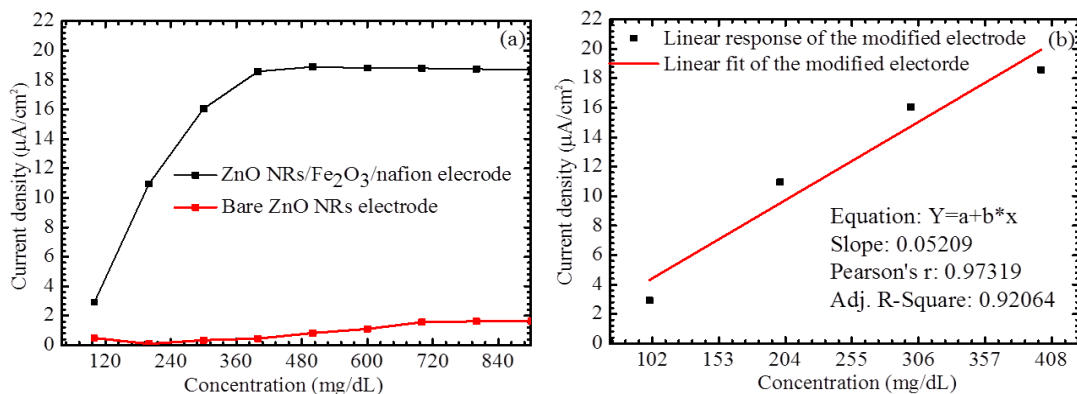


Figure 3.18. The amperometric response of the glucose sensor where (a) is the response of the sensor with and without ferric oxide and (b) is extracted linear response of the sensor. Reprinted with permission from Marie et al [95].

The response of the glass/FTO/ZnO NRs/$Fe_2O_3$/nafion membrane working electrode went to saturation at high glucose concentrations. The high electrocatalyst capability of the $Fe_2O_3$ helped in oxidizing higher concentrations of glucose which is the direct result of the wide linear response of the sensor. The wide amperometric linear response of the sensor covered the physiological range of the glucose. The oxidation and reduction ferric oxide on the surface of the working electrode helped in producing more free electrons and the numbers of the produced electrons was associated with the glucose concentrations. The high surface to volume ratio provided by ZnO NRs helped in attaching more ferric oxide to the walls of ZnO NRs on the surface of the sensing electrode. Sensitivity on the order of 0.052 $\mu A\ cm^{-2}\ (mg/dL)^{-1}$ was calculated from the slope of the amperometric linear response of the enzyme-free glucose sensor. The linear amperometric response of the sensor to changes of the glucose concentration was extracted from the total amperometric response to changes from 100-900 mg/dL. As shown in Figure 3.18 b, the linear response of the sensor was from 100 to 400 mg/dL. The sensitivity was calculated using Equation 3.4.

$$\text{Sensitivity} = \frac{\text{current density } (\frac{\mu A}{cm^2})}{\text{glucose concentrations (mg/dL)}} \qquad \text{(Equation 3.4)}$$

The lower limit of detection of the modified enzyme-free glucose sensor was calculated using

Equation 3.2 and it was on the order of 17.15 mg/dL which is equivalent to 0.95 mmol/L [95].

### 3.5.6  The apparent Michaelis-Menten constant

The apparent Michaelis-Menten constant is the way to determine the affinity between the

as-grown ZnO NRs and ferric oxide as in Figure 3.19. The double reciprocals of the current

versus the glucose concentrations were plotted to examine the attachment of $Fe_2O_3$ to the walls

of ZnO NRs. Before introducing the glucose to the phosphate buffer solution, the concentration

of ferric oxide was the dominant parameter and small changes in the current were observed.

When the concentration of glucose equaled the concentration of $Fe_2O_3$, the velocity of the

electrochemical reaction was half the rate of the maximum velocity. The increase in response of

the sensor was due to the increase in the glucose concentration. At higher glucose concentrations,

the concentration of glucose became much higher than the concentrations of ferric oxide. As a

result, the velocity of the electrochemical reaction reached the maximum velocity. At that level,

the electrochemical sensor worked in the saturation region.

The apparent Michaelis-Menten constant was calculated utilizing the Lineweaver-Burk

equation (Equation 2.7) to accurately estimate the affinity between the as-grown ZnO NRs and

$Fe_2O_3$. The extracted data from Figure 3.19 showed a higher correlation coefficient, $R^2$, on the

order of 0.998 (99.8%). In addition, the obtained adjusted $R^2$ was on the order of 0.996 (99.6%).

The small difference between $R^2$ and the adjusted $R^2$ indicated the high linearity between

changes in the glucose concentrations and the associated current to those changes. In addition, it

reflected the high affinity between ferric oxide and ZnO NRs.
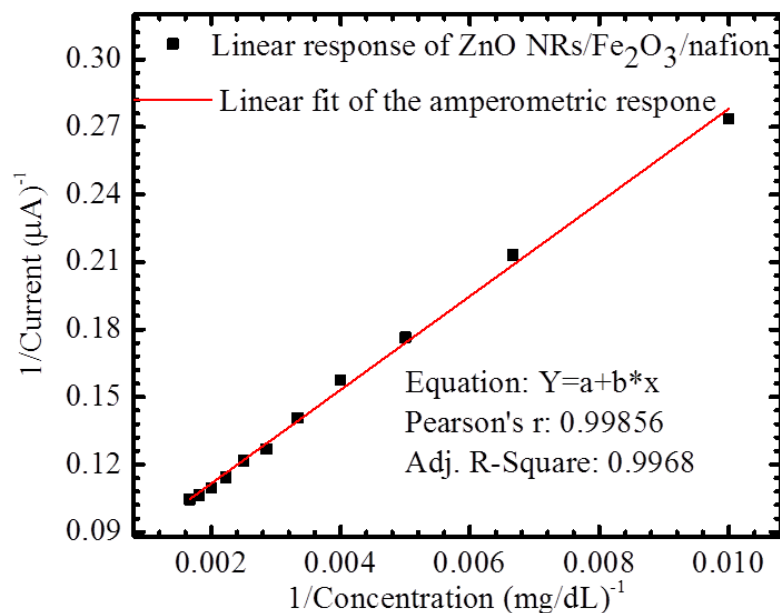
Figure 3.19. The reversed current as a function of the reversed glucose concentration as a method to determine the affinity between ZnO NRs and ferric oxide. Reprinted with permission from Marie et al. [95].

### 3.5.7 The reproducibility test of the enzyme-free sensor

The modified working electrode based on glass/FTO/ZnO NRs/$Fe_2O_3$/nafion membrane was kept at the room temperature before and after performing the amperometric measurements in order to evaluate the reusability of the sensor. Four amperometric measurements were conducted weekly for one month. Figure 3.20 shows the obtained sensitivity for the modified electrochemical glucose sensors as a function of time. At the first amperometric measurement which was conducted directly after the fabrication and modification of the glucose sensor, the sensor exhibited sensitivity to changes in the glucose concentrations on the order of 0.052 μA $cm^{-2}$ $(mg/dL)^{-1}$.

For the second week measurement, the sensitivity was calculated to be 0.02 μA $cm^{-2}$ $(mg/dL)^{-1}$ for the same sensor. For the third week measurement, a further 30% decline in the sensitivity had occurred and the calculated sensitivity was on the order of 0.014 μA $cm^{-2}$

83
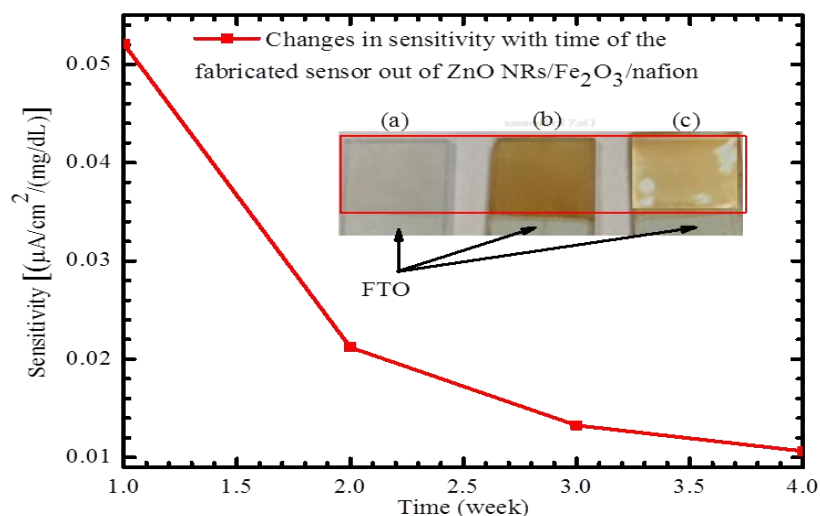
Figure 3.20. The reusability test of the enzyme-free glucose sensor for one month. The inset showed (a) the bare ZnO NRs, (b) ZnO NRs/Fe$_2$O$_3$ before use, and (c) ZnO NRs/Fe$_2$O$_3$/nafion membrane after 4 amperometric measurements for one month. Reprinted with permission from Marie et al. [95].

(mg/dL)$^{-1}$. For the last amperometric measurement after one month, the sensitivity of the modified electrochemical glucose sensor was ~ 0.0106 μA cm$^{-2}$ (mg/dL)$^{-1}$. The image (a) in the inset of Figure 3.20 was the pure ZnO NRs based working electrode before modification with ferric oxide. In image (b), one can see the ZnO NR-based working electrode after the modification with ferric oxide. In the image (b) of the inset, the modified working electrode was not used in any amperometric measurement. Image (c) in the inset of Figure 3.20 shows the modified working electrode after 4 amperometric measurements were performed in one month [95].

## 3.6  Silicon NWs based enzymatic glucose sensors

Silicon NWs are of great interest because of their optical, structural, mechanical, and electrical properties. Silicon NWs were grown by the nanospheres lithography method using both RIE and wet etching. The etching method used to grow the Si NWs was explained in detail in Chapter 2.

### 3.6.1 SEM images of the etched Si NWs

The etched Si NWs using the RIE system and the nanospheres lithography are shown in Figure 3.21. A high density of Si NWs were obtained on the surface of the silicon substrate. The etched Si NWs showed a uniform distribution in their lengths and diameters. This was a direct result of the uniform distribution of the polystyrene nanospheres after they were etched by the plasma inside the reactive ion etching system. Figure 3.21 a at 2755 x magnification, shows the alignment and the density of the etched Si NWs, while Figure 3.21 b at 25000 x magnification shows the distribution of the diameters and the lengths of the Si NWs. The etched Si NWs provided a high surface-to-volume ratio which was a crucial factor in glucose sensing. In addition, it helped in enhancing the signal-to-noise ratio, which meant increasing the capability of the electrochemical sensor to sense small changes in glucose concentrations. The high surface-to- volume ratio provided by etched Si NWs was the key factor in adsorbing higher amounts of the enzyme, $GO_x$, which was essential in glucose detection. Adsorbing higher concentrations of the enzyme on the surface of the working electrode (Si NWs/Si) helped in oxidizing higher concentrations of the glucose by the electrochemical sensor.
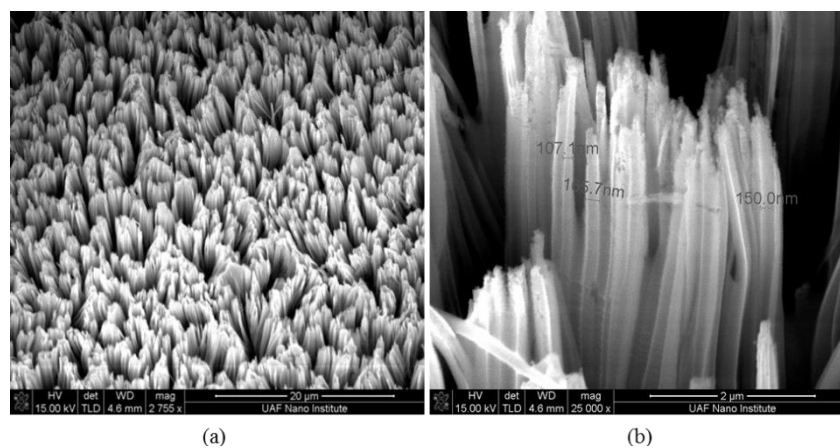


(a)  (b)

Figure 3.21. SEM images of the grown Si NWs etched by the nanosphere lithography using the RIE system. The image (a) is at low magnification and (b) at high magnification to show the diameters and lengths of the Si NWs.

### 3.6.2  The time response of Si NWs/GO$_x$/nafion glucose sensor

To run the amperometric measurement over the fabricated electrochemical glucose sensor based on Si NWs, the surface of the working electrode was modified with glucose oxidase, GO$_x$, and a nafion membrane. The enzyme-treated working electrode (Si NWs/GO$_x$/nafion membrane) was left at 4 $^\circ$C for one day. The enzyme helped in increase the sensitivity and selectivity of the electrode. To enhance the chemical stability of the working electrode and to increase the ion exchange between the glucose dissolved in phosphate buffer solution (PBS) and the surface of the electrode, a nafion membrane was spin-coated on the surface of the modified working electrode. To test the sensor, a platinum plate was used as a counter electrode, and the measurements were performed under 0.8 V. Amperometric measurements were done using a Keithley SourceMeter 2410 and Gamry potentiostat. The electrochemical glucose sensor was characterized at different glucose concentrations from 1-20 mM.

The measurements were started by using 1 mM of glucose dissolved in the PBS. After 50 seconds, the concentration of glucose was increased by adding another 1 mM. The concentrations of the glucose were added to the PBS after each 50 seconds. The electrochemical glucose sensor showed a fast response time towards changes in the glucose concentrations. The result of the time response measurement of the sensor can be seen in Figure 3.22. From the graph, one can see that the electrochemical sensor based on Si NWs modified with GO$_x$ and nafion membrane reached the maximum response in around 2 seconds. This was considered a fast and sharp response time to changes in the glucose concentrations.  However, the amperometric response declined after it reached the maximum level. This might have been due to the chemical wet etching to the Si NWs using the nanospheres lithography.

The stability of the time response of the Si NWs based glucose sensor was clear from the figure. The Si NWs glucose sensor showed a similar behavior during all measurements until all

86

Figure 3.22. The amperometric time response of the fabricated electrochemical glucose sensor based on Si NWs/ $GO_x$/nafion tested at 0.8 V for different glucose concentrations.

the glucose concentrations were added to the PBS. At the last measurement, when 20 mM of glucose was added to the solution, there was a jump in the time response of the electrochemical sensor based on Si NWs/$GO_x$/nafion. This was a result of some damage to the nafion membrane. The nafion membrane is very critical during the electrochemical measurement to protect the surface of the modified working electrode from the degradation that might occur from the chemical solution. It was noticed that the nafion membrane started to become damaged when the phosphate buffer solution became very concentrated. The other factor that affected the nafion membrane was the applied potential to the electrochemical cell during the amperometric measurement. It was desired to use a lower potential during the amperometric measurement to protect the nafion membrane and to lower the chance of the other electroactive species from being oxidized.

87

### 3.6.3 The linear response of Si NWs/GO$_x$/nafion glucose sensor

The fabricated electrochemical glucose sensor was characterized amperometrically to test the linear response of the working electrode at different glucose concentrations. Different glucose concentrations were introduced to the solution continuously from 1 to 20 mM. The average of each 50 data point set was calculated and plotted as a function to glucose concentration. The modified working electrode based Si NWs/GO$_x$/nafion membrane showed a linear response to a wide range of changes in the glucose concentration as can be seen in Figure 3.23 a and b. The high surface-to-volume ratio provided by the silicon nanowires helped in adsorbing higher concentrations of the enzyme glucose oxidase. As a result, higher concentrations of the glucose were oxidized on the surface of the working electrode.
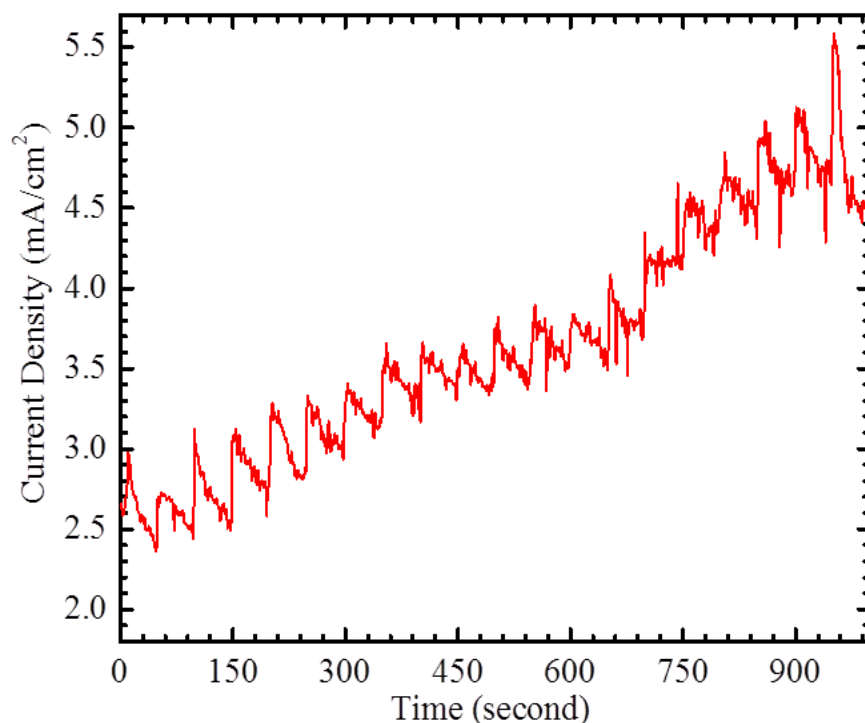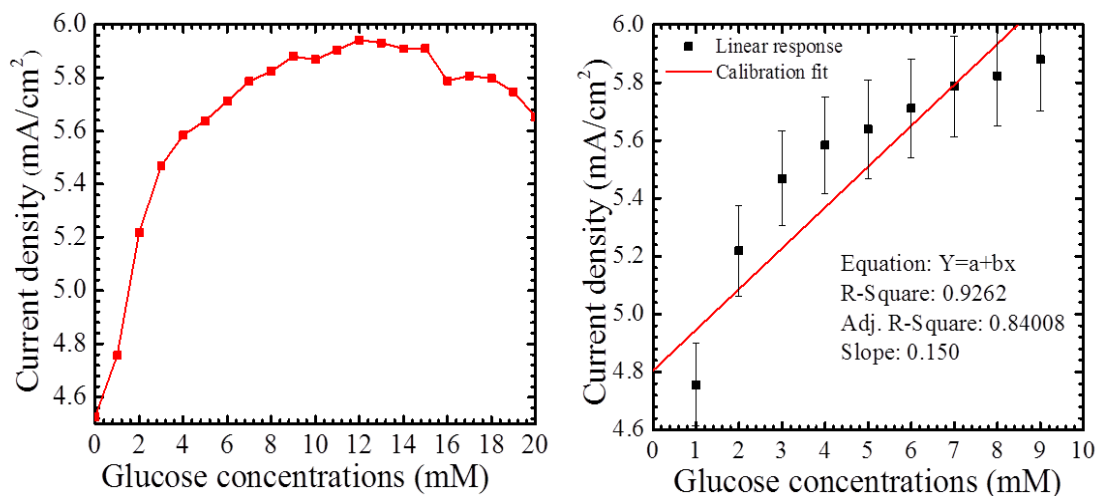


Figure 3.23. The amperometric linear response of the fabricated electrochemical glucose sensor based on Si NWs/GO$_x$/nafion, where (a) is the whole range of the amperometric response and (b) is the linear amperometric response from 1-10 mM.

Silicon nanowires provided the nanoenvironmental area of the glucose molecules since the sizes of the glucose molecules and the Si NWs were comparable. This provided a fast

electron transfer between the center of the enzyme glucose oxidase and the surface of the etched silicon nanowires. The fabricated glucose sensor showed a linear response to changes in the glucose concentrations from 1-10 mM before the amperometric current went to saturation as shown in Figure 3.23 b. At the saturation level, all the enzyme glucose oxidase was consumed and the amperometric response of the electrochemical sensor did not depend anymore on the accumulated concentrations of glucose in the PBS solution. The electrochemical glucose sensor showed sensitivity on the order of 0.15 mA cm$^{-2}$ mM$^{-1}$ to changes in the glucose concentration. The sensitivity of the measurement is the slop of the amperometric response of the sensors.

**Chapter 4  Conclusions and future work**

**4.1  Conclusions**

Enzymatic electrochemical glucose sensors were fabricated based on the nanostructure of semiconductor materials. Zinc oxide nanorods were synthesized hydrothermally using sol-gel solution at low temperatures. The controlled diameters, density, and lengths of the as-grown ZnO NRs resulted in synthesizing highly dense and well-aligned ZnO NRs. The high surface-to-volume ratio obtained by the as-grown ZnO NRs was a direct result to the controlled hydrothermal and sol-gel growth methods. The optimized growth method of ZnO NRs was utilized to synthesize ZnO NRs on top of the surface of the working electrode of the electrochemical glucose sensor. The electrochemical glucose sensors fabricated from the as-synthesized ZnO NRs exhibited high signal- to-noise ratio. The high signal-to-noise ratio was an essential parameter for glucose detection. The high signal-to-noise ratio meant higher the capability of the electrochemical sensor to detect lower concentrations of glucose. In other words, the high signal-to-noise ratio helped in reducing the lower limit of detection, which was the lowest concentration of the glucose that could be detected by the electrochemical sensor. The fabricated enzymatic electrochemical glucose sensors out of ZNO NRs were sensitive to small changes of the glucose concentration.

The enzymatic electrochemical sensors showed a high sensitivity and selectivity toward changes in glucose in the phosphate buffer solution due to the high affinity between the enzyme glucose oxidase, $GO_x$, and the glucose. The enzyme, $GO_x$, has the flavin adenine dinucleotide (FAD) in its center as an electron acceptor. This makes the electrons produced by the oxidation of glucose transfer directly from the center of the enzyme to the

surface of the working electrode through the as-grown ZnO NRs. This direct electron transfer resulted in a fast amperometric response of the electrochemical glucose sensors. In short, the fabricated enzymatic electrochemical glucose sensors were sensitive, selective, and had a fast response to the changes in the glucose concentration. However, the lifetime of the enzyme makes it difficult to reuse these kinds of the glucose sensors due the biological degradation of the enzyme with time.

Silicon nanowires were used to fabricate enzymatic electrochemical glucose sensors. Nanospheres lithography method was utilized to etch the Si NWs by using the reactive ion etching (RIE) system. The obtained Si NWs were dense with a high aspect ratio, which is the ratio between the lengths to the diameters of the etched Si NWs. In addition, the grown Si NWs showed a high surface-to-volume ratio with good alignment. The working electrode fabricated from Si NWs was modified with the enzyme, $GO_x$, and casted with the nafion membrane to enhance the stability of the sensor during the electrochemical reaction. The fabricated electrochemical sensors showed a high sensitivity and selectivity toward changes in the glucose concentration. In addition, the amperometric response of the sensors was fast and sharp when higher glucose concentrations were introduced to the analytical solution.

An enzyme-free electrochemical glucose sensor was fabricated using the as-grown ZnO NRs modified with ferric oxide. Ferric oxide, $Fe_2O_3$, was prepared and dipped coated on top of the as-grown ZnO NRs. ZnO NRs were grown on glass/FTO substrates using the same hydrothermal and sol-gel methods. The dip-coater technique was utilized to modify the surface of the working electrode with ferric oxide. The glass/FTO/ZnO NRs/$Fe_2O_3$/nafion membrane structure resulted in an enzyme-free electrochemical glucose

91

sensor. During the electrochemical reaction between the ferric oxide and glucose, Fe (III)

is oxidized to Fe (II) and produces free electrons. The free electrons produced transfer to

the surface of the working electrode under the effect of the electrical field. Ferric oxide has

a high electrocatalytic capability which means that more glucose can be oxidized on the

surface of the working electrode. The fabricated enzyme-free glucose sensor showed a

good sensitivity and a longer lifetime compared with the enzymatic glucose sensors

fabricated using ZnO NRs and Si NWs.

## 4.2  Future work

Metal oxide semiconductor field effect transistor (MOSFET) based glucose sensor

is a promising approach to sense glucose efficiently. These kinds of devices are usually

called BioFET glucose sensors. They depend on changes in the drain current due to the

charges produced by oxidizing the glucose in the channel between the source and the drain.

The channel between the source and the drain can be modified by applying either ZnO NRs

or Si NWs. In addition, a back metallic gate can be easily deposited to induce all the

possible charges in the channel. These BioFET-based glucose sensors can be characterized

by sweeping the drain voltage and fixing the gate voltage. The drain current that is

associated with the concentrations of the glucose can be studied as a function of the drain

voltages.

Impedance-based glucose sensors are another promising approach for glucose

detection. They work based on changes in the dielectric constant of the analytical solution

during the electrochemical impedance measurements. The glucose sensor can be designed

as an interdigital structure with different channel widths. The impedance that is in a direct

proportion to the concentrations of glucose can be studied as a function of different

92

frequencies. There will be three regions of frequencies: low, medium, and high. In each one of these regions, the impedance can be measured and analyzed to determine the concentrations of the glucose.

## References

[1]     V. Pahurkar, Y. Tamgadge, A. Gambhire, and G. Muley, "Glucose oxidase immobilized PANI cladding modified fiber optic intrinsic biosensor for detection of glucose," *Sensors and Actuators B-Chemical,* vol. 210, pp. 362-368, 2015.

[2]     M. Rahman, A. Ahammad, J. Jin, S. Ahn,  and J. Lee, "A Comprehensive review of glucose biosensors based on nanostructured metal-oxides, *Sensors,* Review vol. 10, no. 5, pp. 4855-4886, 2010.

[3]     I. Torres, M. Baena, M. Cayon, J. Ortego-Rojo, and M. Aguilar-Diosdado, "Use of sensors in the treatment and follow-up of patients with diabetes mellitus," *Sensors,* vol. 10, no. 8, pp. 7404-7420, 2010.

[4]     S. K. Vashist, "Continuous glucose monitoring systems: A Review," *Diagnostics,* vol. 3, no. 4, pp. 386-412, 2013.

[5]     H. Wang and A. Lee, "Recent developments in blood glucose sensors," *Journal of Food and Drug Analysis,* vol. 23, no. 2, pp. 191-200,  2015.

[6]     X. Du, Y. Li, J. Motley, W. Stickle, and G. Herman, "Glucose sensing using functionalized amorphous In−Ga−Zn−O field-effect transistors," *Applied materials and interfaces,* vol. 8, no. 12, pp. 7631-7637, 2016.

[7]     S. Wild, G. Roglic,  A. Green, R. Sicree, and H. King, "Global prevalence of diabetes," *Diabetes Care,* vol. 27, no. 5, pp. 1047-1053, 2004.

[8]     Z. Bloomgarden, "Type 1 diabetes and glucose monitoring," *Diabetes Care,* vol. 30, no. 11, pp. 2965-2971, 2007.

[9]     G. Cappon, G. Acciaroli, M. Vettoretti, A. Facchinetti, and G. Sparacino, "Wearable continuous glucose monitoring sensors: A revolution in diabetes treatment,"*Electronics,* vol. 6, no. 3, pp. 65-80, 2017.

[10]    M. Davidson,  "Counterpoint: self-monitoring of blood glucose in type 2 diabetic Patients not receiving insulin," *Diabetes Care,* vol. 28, no. 6, pp. 1531-1533, 2005.

[11]    L. Murtaugh, "Pancreas and beta-cell development: from the actual to the possible," *Development,* vol. 134, no. 3, pp. 427-438,  2007.

[12]    B. McAdams and A. Rizvi, "An overview of insulin pumps and glucose sensors for the generalist," *Journal of Clinical Medicine,* vol. 5, no. 1, pp. 5-21, 2016.

[13]    L Welsche, E. Bloemendal, G. Nijpels, J. Dekker, R. Heine, W. Stalman, and L. Bouter, "Self-monitoring of blood glucose in patients with type 2 diabetes who are not using insulin," *Diabetes Care,* vol. 28, no. 6, pp. 1510-1517, 2005.

[14]    A. Xiang, R. Peters, S. Kjos, A. Marroquin, J. Goico, C. Ochoa, M. Kawakubo, and T. Buchanan, "Effect of pioglitazone on pancreatic β-cell function and diabetes risk in

hispanic women with prior gestational diabetes," Diabetes, vol. 55, no, 2, pp. 517-522, 2006.

[15]    E. Yoo and S. Lee, "Glucose biosensors: An overview of use in clinical practice," *Sensors,* vol. 10, no. 5, pp. 4558-4576, 2010.

[16]    A. Turner, "Biochemistry - biosensors sense and sensitivity," *Science,* vol. 290, no. 5495, pp. 1315-1317, 2000.

[17]    A. Hiratsuka, K. Fujisawa, and H. Muguruma, "Amperometric biosensor based on glucose dehydrogenase and plasma-polymerized thin films," *Analytical Sciences,* vol. 24, no. 4, pp. 483-486, 2008.

[18]    K. Wintergerst, B. Buckingham, L. Gandrud, B. Wong, S. Kache, and D. Wilson, "Association of hypoglycemia, hyperglycemia, and glucose variability with morbidity and death in the pediatric intensive care unit,"*Pediatrics,*vol. 118, no. 1, pp. 173-179, 2006.

[19]    A. Sieg, R. Guy, and M. Delgado-Charro, "Noninvasive and minimally invasive methods for transdermal glucose monitoring," *Diabetes Technology & Therapeutics,* vol. 7, no. 1, pp. 174-197, 2005.

[20]    J. Klonoff, "Continuous glucose monitoring," *Diabetes Care,* vol. 28, no. 5, pp. 1231-1239, 2005.

[21]    R. Pandey, S. Paidi, T. Valdez, C. Zhang, N. Spegazzini, R. Rao Dasari, and I. Barman, "Noninvasive Monitoring of blood glucose with Raman spectroscopy,"*Accounts of Chemical Research,* vol. 50, no. 2, pp. 264-272, 2017.

[22]    A. Heller and B. Feldman, "Electrochemistry in diabetes management," *Accounts of Chemical Research,* vol. 43, no. 7, pp. 963-973, 2010.

[23]    P. Barone and M. Strano, "Single walled carbon nanotubes as reporters for the optical detection of glucose," *Journal of Diabetes Science and Technology,* vol. 3, no. 2, pp. 242-252, 2009.

[24]    C. Amaral and B. Wolf "Current development in non-invasive glucose monitoring," *Medical Engineering & Physics* vol. 30, no. 5, pp. 541-549, 2008.

[25]    A. Lin, Y. Mayzel, K. Horman, and K. Bahartan, "Non-invasive glucose monitoring: A review of challenges and recent advances," vol. 6, no. 5, pp. 1-7, 2017.

[26]    J. Bantle and W. Thomas, "Glucose measurement in patients with diabetes mellitus with dermal interstitial fluid," *Journal of Laboratory and Clinical Medicine,* vol. 130, no. 4, pp. 436-441, 1997.

[27]    S. Sharma, Z. Huang, M. Rogers, M. Boutelle, and A. Cass, "Evaluation of a minimally invasive glucose biosensor for continuous tissue monitoring," *Analytical and Bioanalytical Chemistry,* vol. 408, no. 29, pp. 8427-8435, 2016.

[28]  T. Gross, D. Einhorn, D. Kayne, J. Reed, N. White, and J.Mastrototaro, "Performance evaluation of the minimed and continuous glucose monitoring system during patient home use," vol. 2, no. 1, pp. 49-56, 2004.

[29]  G. McGarraugh, "The chemistry of commercial continuous glucose monitor," *Diabetes technology and therapeutics,* vol. 11, no. s1, pp. 17-24, 2009.

[30]  K. Rebrin and G. Steil, "Can interstitial glucose assessment replace blood glucose measurements?," *Diabetes Technology & Therapeutics,* vol. 2, no. 3, pp. 461-472, 2004.

[31]  R. Tanenberg, B. Bode, W. Lane, C. Levetan, J. Mestman, A. Harmel, J. Gross, and J. Mastrototaro, "Use of the continuous glucose monitoring system to guide therapy in patients with insulin-treated diabetes: A randomized controlled trial," *Mayo Clinic Proceedings,* vol. 79, no. 12, pp. 1521-1526, 2004.

[32]  W. Zhang, Y. Du, and M. Wang,"Noninvasive glucose monitoring using saliva nano-biosensor," *Sensing and Bio-Sensing Research,* vol. 4, pp. 23-29, 2015.

[33]  S. Vashist, "Non-invasive glucose monitoring technology in diabetes management: A review," *Analytica Chimica Acta,* Review vol. 750, pp. 16-27, 2012.

[34]  N. Oliver, C. Toumazou, A. Cass, and D. Johnston, "Glucose sensors: a review of current and emerging technology," *Diabetic Medicine,* vol. 26, no. 3, pp. 197-210, 2009.

[35]  J. Wang, "Electrochemical glucose biosensors," *Chemical Reviews,* vol. 108, no. 2, pp. 814-825, 2008.

[36]  A. Sieg, R. Guy, and M. Delgado-Charro, "Noninvasive glucose monitoring by reverse iontophoresis in vivo: Application of the internal standard concept," *Clinical Chemistry,* vol. 50, no. 8, pp. 1383-1390, 2004.

[37]  M. Tierney, H. Kim, M. Burns, J. Tamada, and R. Potts, "Electroanalysis of glucose in transcutaneously extracted samples," *Electroanalysis,* vol. 12, no. 9, pp. 666-671, 2000.

[38]  A. Bandodkar, W. Jia, C. Yardimci, X. Wang, J. Ramirez, and J. Wang, "Tattoo-based noninvasive glucose monitoring: A proof-of-concept study," *Analytical Chemistry* vol. 87, no. 1, pp. 394-398, 2015.

[39]  G. Rao, P. Gilkfeld, and R. Guy, "Reverse iontophoresis: development of a noninvasive approach for glucose monitoring," *Pharmaceutical Research,* vol. 10, no. 12, pp. 1751-1755, 1993.

[40]  S. Haxha and J. Jhoja, "Optical based noninvasive glucose monitoring sensor prototype," *IEEE Photonics Journal,* vol. 8, no. 6, pp. 1-11, 2016.

[41]  R. Gabbay and S. Sivarajah, "Optical coherence tomography-based continuous noninvasive glucose monitoring in patients with diabetes," *Diabetes Technology & Therapeutics,* vol. 10, no. 3, pp. 188-193, 2008.

[42]   M. Kinnunen, R. Myllyla, T. Jokela, and S. Vainio, "In vitro studies toward noninvasive glucose monitoring with optical coherence tomography," *Applied Optics,* vol. 45, no. 10, pp. 2251-2260, 2006.

[43]   Y. Pan, R. Birngruber, J. Rosperich, and R. Engelhardt, "Low-coherence optical tomography in turbid tissue-theoretical analysis," *Applied Optics,* vol. 34, no. 28, pp. 6564-6574, 1995.

[44]   M. Wróbel, "Non-invasive blood glucose monitoring with Raman spectroscopy: prospects for device miniaturization," *Materials Science and Engineering*, vol. 104, p. 012036, 2016.

[45]   A. Aggidis, J. Newman, and G. Aggidis, "Investigating pipeline and state of the art blood glucose biosensors to formulate next steps," *Biosensors and Bioelectronics*, vol. 74, pp. 243-262, 2015.

[46]   N. Abd Salam, W. Mohd Saad, Z. Manap, and F. Salehuddin, "The evolution of non-invasive blood glucose monitoring system for personal application," *Journal of Telecommunication, Electronic and Computer Engineering,* vol. 8, no. 1, pp. 59-65, 2016.

[47]   A. Giada, V. Martina, F. Andrea, S. Giovanni, and C. Claudio, "From two to one per day calibration of dexcom G4 platinum by a time-varying day-specific bayesian prior," *Diabetes Technol Ther,* vol. 18, no. 8, pp. 472-479, 2016.

[48]   O. Amir, D. Weinstein, S. Zilberman, M. Less, D. Perl-Treves, H. Primack, A. Weinstein, E. Gabis, B. Fikhte, and A. Karasik, "Continuous noninvasive glucose monitoring technology based on "occlusion spectroscopy," *Journal of Diabetes Science and Technology,* vol. 1, no. 4, pp. 463-469, 2007.

[49]   I. Wentholt, J. Hoekstra, A. Zwart, and J. DeVries, "Pendra goes dutch: lessons for the CE mark in Europe," *Diabetologia,* vol. 48, no. 6, pp. 1055-1058, 2005.

[50]   A. Enejder, T. Scecina, J. Oh, M. Hunter, S. Sasic, G. Horowitz, and M. Feld, "Raman spectroscopy for noninvasive glucose measurements," *Journal of Biomedical Optics,*vol. 10, no. 3, pp. 1114-1123, 2005.

[51]   J. Shao, M. Lin, Y. Li, X. Li, J. Liu, J. Liang, and H. Yao,"In Vivo blood glucose quantification using raman spectroscopy," *Plos One,* vol. 7, no. 10, 2012.

[52]   I. Barman, C. Kong, G. Singh, R. Dasari, and M. Feld, "Accurate spectroscopic calibration for noninvasive glucose monitoring by modeling the physiological glucose dynamics," *Analytical Chemistry* vol. 82, no. 14, pp. 6104-6114, 2010.

[53]   A. Heller and B. Feldman, "Electrochemical glucose sensors and their applications in diabetes management," *Chemical Reviews* vol. 108, no. 7, pp. 2482-2505, 2008.

[54]   A. Chaubey and B. Malhotra, "Review mediated biosensors," *Biosensors & Bioelectronics,* vol. 17, no. 6-7, pp. 441-456, 2002.

[55]    Y. Wang, H. Xu, J. Zhang, and G. Li, "Electrochemical sensors for clinic analysis," *Sensors,* vol. 8, no. 4, pp. 2043-2081, 2008.

[56]    P. D'Orazio, "Biosensors in clinical chemistry," *Clinica Chimica Acta,* vol. 334, no. 1-2, pp. 41-69, 2003.

[57]    C. Chang, H. Cheng, and A. Chao, "Applying the Nernst equation to simulate redox potential variations for biological nitrification and denitrification processes," *Environmental Science & Technology,* vol. 38, no. 6, pp. 1807-1812, 2004.

[58]    B. Wu, S. Hou, F. Yin, Z. Zhao, Y. Wang, X. Wang, and Q. Chen, "Amperometric glucose biosensor based on multilayer films via layer-by-layer self-assembly of multi-wall carbon nanotubes, gold nanoparticles and glucose oxidase on the Pt electrode," *Biosensors & Bioelectronics,*vol. 22, no. 12, pp. 2854-2860, 2007.

[59]    J. Wang, "Amperometric biosensors for clinical and therapeutic drug monitoring: a review," *Journal of Pharmaceutical and Biomedical Analysis,* vol. 19, no. 1-2, pp. 47-53, 1999.

[60]    A. Caduff, F. Dewarrat, M. Talary, G. Stalder, L. Heinemann, and Y. Feldman, "Non-invasive glucose monitoring in patients with diabetes: A novel system based on impedance spectroscopy," *Biosensors & Bioelectronics,* vol. 22, no. 5, pp. 598-604, 2006.

[61]    M. Khan and S. Kang, "Highly sensitive multi-channel IDC sensor Array for low concentration taste detection," *Sensors,* vol. 15, no. 6, pp. 13201-13221, 2015.

[62]    S. Huang, C. Chou, T. Chen, P. Chiou, V. Hsiao, C. Ching, and T. Sun,"Enhanced sensitivity using microfluidic interdigitated microelectrode based capacitance glucose sensor measured at 4 MHz," *Journal of the Electrochemical Society,* vol. 161, no. 5, pp. B102-B105, 2014.

[63]    R. Igreja and C. Dias, "Dielectric response of interdigital chemocapacitors: The role of the sensitive layer thickness," *Sensors and Actuators B-Chemical,* vol. 115, no. 1, pp. 69-78, 2006.

[64]    C. Koopal and R. Nolte, "Highly stable first-generation biosensor for glucose utilizing latex-particles as the enzyme-immobilization matrix," *Enzyme and Microbial Technology,* vol. 16, no. 5, pp. 402-408, 1994.

[65]    H. Zhu, L. Li, W. Zhou, Z. Shao, and X. Chen, "Advances in non-enzymatic glucose sensors based on metal oxides," *Journal of Materials Chemistry B,* vol. 4, no. 46, pp. 7333-7349, 2016.

[66]    I. Willner and E. Katz, "Integration of layered redox proteins and conductive supports for bioelectronic applications," *Angewandte Chemie-International Edition,* Review vol. 39, no. 7, pp. 1180-1218, 2000.

[67]    M. Shichiri, Y. Yamasaki, R. Kawamori, N. Hakui, and H. Abe, "Wearable artificial endocrine pancreas with needle-type glucose sensor, " *The lancet,* vol. 320, no. 8308,  pp. 1129-1131, 1982.

[68]    A. Cass, G. Davis, G. Francis, and H. Hill " Ferrocene-mediated enzyme electrode for amperometric determination of glucose," *Analytical Chemistry,* vol. 56, no. 4, pp. 667-671, 1984.

[69]    H. Yang and Y. Zhu, "Size dependence of $SiO_2$ particles enhanced glucose biosensor," *Talanta,* vol. 68, no. 3, pp. 569-574, 2006.

[70]    Z. Zhu, L. Garcia-Gancedo, A. Flewitt, H. Xie, F. Moussy, and W. Milne, "A critical review of glucose biosensors based on carbon nanomaterials: carbon nanotubes and graphene," *Sensors,* vol. 12, no. 5, pp. 5996-6022, 2012.

[71]    S. Liu and H. Ju, "Reagentless glucose biosensor based on direct electron transfer of glucose oxidase immobilized on colloidal gold modified carbon paste electrode," *Biosensors & Bioelectronics,* vol. 19, no. 3, pp. 177-183, 2003.

[72]    M. Hasan, M. Huq, and Z. Mahmood, "A review on electronic and optical properties of silicon nanowire and its different growth techniques," *SpringerPlus,* vol. 2, no. 1, pp. 51-59, 2013.

[73]    C. Hsu, W. Feng, F. Su, and G. Wang, "An Electrochemical Glucose Biosensor with a Silicon Nanowire Array Electrode," *Journal of the Electrochemical Society,* vol. 162, no. 10, pp. B264-B268, 2015.

[74]    Z. Huang, H. Fang, and J. Zhu, "Fabrication of silicon nanowire arrays with controlled diameter, length, and density," *Advanced Materials,* vol. 19, no. 5, pp. 744, 2007.

[75]    A. Nusir, S. Bauman, M. Marie, J. Herzog, and M. Manasreh, "Silicon nanowires to enhance the performance of self-powered near-infrared photodetectors with asymmetrical Schottky contacts," *Applied Physics Letters,* vol. 111, no. 17, pp. 1103-1106, 2017.

[76]    T. Stelzner, M. Pietsch, G. Andra, F. Falk, E. Ose, and S. Christiansen, "Silicon nanowire-based solar cells," *Nanotechnology,* vol. 19, no. 29, pp. 5203-5206, 2008.

[77]    C. Hsu, Y. Liao, Y. Tsai, H. Yeh, and C. Wu, "Multiple silicon nanowires with enzymatic modification for measuring glucose concentration," *Micromachines*, vol. 6, no. 8, pp. 1135-1142, 2015.

[78]    S. Su, Y. He, S. Song, D. Li, L. Wang, C. Fan, and S. Lee "A silicon nanowire-based electrochemical glucose biosensor with high electrocatalytic activity and sensitivity," *Nanoscale,* vol. 2, no. 9, pp. 1704-1707, 2010.

[79]    W. Chen, H. Yao, C. Tzang, J. Zhu, M. Yang, and S. Lee, "Silicon nanowires for high-sensitivity glucose detection," Applied Physics Letters, vol. 88, no. 21, pp. 3104-3106, 2006 .

[80]   M. Marie, S. Mandal, and M. O. Manasreh, "An electrochemical glucose sensor based on zinc oxide nanorods," *Sensors,* vol. 15, no. 8, pp. 18714-18723, 2015.

[81]   C. Xia and W. Ning, "A novel non-enzymatic electrochemical glucose sensor modified with FeOOH nanowire," *Electrochemistry Communications,* vol. 12, no. 11, pp. 1581-1584, 2010.

[82]   K. Schugerl, B. Hitzmann, H. Jurgens, T. Kullick, R. Ulber, and B. Weigal, "Challenges in integrating biosensors and FIA for on-line monitoring and control," *Trends in Biotechnology,* vol. 14, no. 1, pp. 21-31, 1996.

[83]   C. Zhu, G. Yang, H. Li, D. Du, and Y. Lin, "Electrochemical sensors and biosensors based on nanomaterials and nanostructures," *Analytical Chemistry*, *vol.* 87, no. 1, pp. 230-249,  2015.

[84]   X. Liu, Q. Hu, Q. Wu, W. Zhang, Z. Fang, and Q. Xie, "Aligned ZnO nanorods: A useful film to fabricate amperometric glucose biosensor," *Colloids and Surfaces B-Biointerfaces,* vol. 74, no. 1, pp. 154-158, 2009.

[85]   Y. Zhang, Z. Kang, X. Yan, and Q. Liao, "ZnO nanostructures in enzyme biosensors," Science China-Materials, vol. 58, no. 1, pp. 60-76, 2015.

[86]   C. Xu, G. Xu, Y. Liu, and G. Wang, "A simple and novel route for the preparation of ZnO nanorods," *Solid State Communications,* vol. 122, no. 3-4, pp. 175-179, 2002.

[87]   P. Rai, H. Song, Y. Kim, M. Song, P. Oh, J.Yoon, and Y. Yu, "Microwave assisted hydrothermal synthesis of single crystalline ZnO nanorods for gas sensor application," *Materials Letters,* vol. 68, pp. 90-93, 2012.

[88]   M. Ahmad, C. Pan, Z. Luo, and J. Zhu, "A Single ZnO nanofiber-based highly sensitive amperometric glucose biosensor," *Journal of Physical Chemistry C,* vol. 114, no. 20, pp. 9308-9313, 2010.

[89]   Q. Zhao, X. Xu, X. Song, Z. Zhang, and D. Yu,"Enhanced field emission from ZnO nanorods via thermal annealing in oxygen," *Applied Physics Letters,* vol. 88, no. 3, pp. 3102-3104, 2006.

[90]   J. Wu and S. Liu, "Catalyst-free growth and characterization of ZnO nanorods," *Journal of Physical Chemistry B,* vol. 106, no. 37, pp. 9546-9551, 2002.

[91]   A. Umar, M. Rahman, M. Vaseem, and Y. Hahn, "Ultra-sensitive cholesterol biosensor based on low-temperature grown ZnO nanoparticles," *Electrochemistry Communications,* vol. 11, no. 1, pp. 118-121, 2008.

[92]   Y. Wei, Y. Li, X. Liu, Y. Xian, G. Shi, and L. Jin, "ZnO nanorods/Au hybrid nanocomposites for glucose biosensor," *Biosensors & Bioelectronics,* vol. 26, no. 1, pp. 275-278, Sep 15 2010.

[93]   Y. Zhao, W. Li1, L. Pan, D. Zhai, Y. Wang, L. Li, W. Cheng, W. Yin, X. Wang, J. Xu, and Y. Shi, "ZnO-nanorods/graphene heterostructure: a direct electron transfer glucose biosensor," *Scientific Reports,*  vol. 6, no. 32, pp. 327-333, 2016.

[94]   C. Zhou, L. Xu, J. Song, R. Xing, S. Xu, D. Liu, and H. Song, "Ultrasensitive non-enzymatic glucose sensor based on three-dimensional network of ZnO-CuO hierarchical nanocomposites by electrospinning," *Scientific Reports,* vol. 4, no. 73, pp. 82-91, 2014.

[95]   M. Marie, A. Manoharan, A. Kuchuk, S. Ang, and M. O. Manasreh, "Vertically grown zinc oxide nanorods functionalized with Ferric oxide for in-vivo and non-enzymatic glucose detection," *Nanotechnology,* vol. 29, no. 11, pp. 5501-5509, 2018.

[96]   R. Chung, A. Wang, Q. Liao, and K. Chuang, "Non-enzymatic glucose sensor composed of carbon-coated cano-zinc oxide," *Nanomaterials,* vol. 7, no. 2, pp. 36-45, 2017.

[97]   R. Ahmad, M. Vaseem, N. Tripathy, and Y. Hahn, "Wide linear-range detecting nonenzymatic glucose biosensor based on CuO Nanoparticles inkjet-printed on electrodes," *Analytical Chemistry,* vol. 85, no. 21, pp. 10448-10454, 2013.

[98]   S. Baruah and J. Dutta, "Hydrothermal growth of ZnO nanostructures,"*Science and Technology of Advanced Materials,* vol. 10, no. 1, pp. 3001-3018, 2009.

[99]   B. Liu and H. Zeng, "Hydrothermal synthesis of ZnO nanorods in the diameter regime of 50 nm," *Journal of the American Chemical Society,* vol. 125, no. 15, pp. 4430-4431, 2003.

[100]  Y. Sun, N. Ndifor-Angwafor, D. Riley, and M. Ashfold, "Synthesis and photoluminescence of ultra-thin ZnO nanowire/nanotube arrays formed by hydrothermal growth," *Chemical Physics Letters,* vol. 431, no. 4-6, pp. 352-357, 2006.

[101]  M. Marie and M.O. Manasreh "Investigation of the influence of the as-grown ZnO  nanorods and applied potentials on an electrochemical sensor for in-vitro glucose monitoring" C*hemosensors,* vol. 5, no. 1, pp. 4-16, 2017.

[102]  F. Zhou, W. Jing, P. Liu, D. Han, Z. Jiang, and Z. Wei, "Doping Ag in ZnO Nanorods to Improve the Performance of Related Enzymatic Glucose Sensors," *Sensors,* Article vol. 17, no. 10, pp. 2214-2225, 2017.

[103]  R. Ahmad, N. Tripathy, M. Ahn, and Y. Hahn, "Solution Process synthesis of high aspect Ratio ZnO nanorods on electrode surface for sensitive electrochemical detection of uric acid,"*Scientific Reports,* Article vol. 7, 2017.

[104]  M. Marie, S. Mandal, and M. O. Manasreh, "An enzymatic glucose detection sensor using ZnO nanostructure," *MRS Advances,* vol. 1, no. 13, pp. 847-853, 2016.

[105]  V. Prasad, C. D'Souza, D. Yadav, A. Shaikh, and N. Vigneshwaran, "Spectroscopic characterization of zinc oxide nanorods synthesized by solid-state reaction," *Spectrochimica Acta Part a-Molecular and Biomolecular Spectroscopy,* vol. 65, no. 1, pp. 173-178, 2006.

**Appendix A: Description of Research for Popular Publication**

Diabetes mellitus is one of the main reasons for death and disabilities all around the world. It is the main reason for kidney failure, heart attack, high blood pressure, and other chronic diseases. It costs people a lot of money and it requires daily glucose checks. In addition, a certain diet should be followed to avoid any possible complications. Glucose sensors are the tools to measure and test the glucose level in the blood. Tremendous attention has been given to fabricating glucose sensors that one can use to measure the glucose level in the blood accurately, safely, and cost-effectively. Most of the produced glucose sensors depend mainly on the affinity between the glucose and the enzyme, glucose oxidase, and these devices are known as enzymatic glucose sensors. The main challenge in fabricating these kinds of glucose sensors is controlling the way that the produced electrons can be transferred. A direct electron transfer is the desirable approach that could lead to fast, accurate, selective, and sensitive glucose sensors.

In the recent years, nanostructured materials-based glucose sensor has been studied extensively to fabricate electrochemical sensors for glucose monitoring. Different enzymatic glucose sensors have been fabricated and used to test glucose levels in the blood. The biological degradation of the enzyme, glucose oxidase, is a drawback that shortens the lifetime of the fabricated glucose sensors. The sensitivity and the reproducibility of these electrochemical glucose sensors needs to be improved, so the enzymatic glucose sensors can be used repeatedly with the same sensitivity toward changes in the glucose concentrations.

Enzymatic and enzyme-free electrochemical glucose sensors based on zinc oxide (ZnO) nanorods, (NRs) have been investigated by Mohammed Marie, a Ph.D. student in the Microelectronics -Photonics graduate program at the University of Arkansas/Fayetteville. The research, conducted in the optoelectronics lab in the Electrical Engineering Department, University of Arkansas, was led by Dr. Omar Manasreh. The main focus was on fabricating and

characterizing sensitive, selective, fast, and accurate enzymatic and non-enzymatic glucose sensors based on pure ZnO NRs, modified ZnO NRs, and modified silicon nanowires. Highly sensitive and selective electrochemical glucose sensors were fabricated based on highly dense and well-aligned ZnO NRs grown on indium tin oxide (ITO) and fluorine doped tin oxide (FTO) and glass coated gold substrates. In addition, zinc oxide nanorods (ZnO NRs) modified with ferric oxide was utilized to fabricate enzyme-free electrochemical glucose sensor with high sensitivity and selectivity toward glucose. The successful modification of ZnO NRs and ferric oxide was the key point in producing an enzyme-free glucose sensor with high sensitivity and longer lifetime. Finally, silicon nanowires coupled with the enzyme, glucose oxidase, and covered with a nafion membrane were utilized to fabricate glucose sensors with high sensitivity, lower detection limit, and high selectivity toward changes in the glucose concentrations.

**Appendix B: Executive Summary of Newly Created Intellectual Property**

1- The modification of ZnO NRs with ferric oxide and the fabricated enzyme-free electrochemical glucose sensor out of the structure glass/FTO/ZnO NRs/$Fe_2O_3$/nafion membrane.

2- The coupling between Si NWs grown by the nanospheres lithography and RIE system, glucose oxidase, and nafion membrane has led to a sensitive and selective electrochemical glucose sensor.

**Appendix C: Potential Patent and Commercialization Aspects of Listed Intellectual Property Items**

C. 1 Patentability of the newly created intellectual property

1. The amperometric sensor based on ZnO NRs modified with ferric oxide and casted with a nafion membrane is not a patentable newly created intellectual property since the growth methods of ZnO NRs are well-known to researchers in the field. The coupling between ZnO and ferric oxide is known to researchers in the same field. Furthermore, the dip-coating technique used to immobilize the surface of ZnO NRs with ferric oxide is known to researchers in the field. The combinations of technologies used in this research would be obvious to those skilled in the art.

2. The etched Si NWs using RIE system and nanosphere lithography cannot be patented because it should be known to those skilled in the art.

C. 2 Commercialization Prospects

1. The short lifetime of the working electrode makes it difficult to compete with other commercialized glucose sensors.

2. Not applicable.

C. 3 Possible Prior Disclosure of IP

1. The results of item one has already been disclosed to the public: M. Marie, A. Manoharan, A. Kuchuk, S. Ang, and M. O. Manasreh, "Vertically grown zinc oxide nanorods functionalized with Ferric oxide for in-vivo and non-enzymatic glucose detection," *Nanotechnology,* vol. 29, no. 11, pp. 5501-5509, 2018.

2. Not applicable.

**Appendix D: Broader Impact of Research**

D.1 Applicability of Research Methods to Other Problems

Controlling the growth of ZnO NRs is of interest since the ZnO NRs is a cost-effective, biocompatible, environment friendly, and easy to synthesize material. Well-aligned and highly dense ZnO NRs grown at low temperatures can be used in different applications, such electrochemical glucose sensors, cholesterol sensors, DNA sequencing, and pacemakers for heart problems. The coupling between ZnO NRs and ferric oxide is a great approach to fabricate enzyme-free sensors that can be sued in different biological and electrochemical applications.

D2. Impact of Research Results on U.S. and Global Society

Diabetes mellitus is a widespread disease in the United States and worldwide. Fabricating enzyme-free electrochemical glucose sensors based on ZnO NRs and ferric oxide is a perfect approach that can be used to sense glucose accurately with a high sensitivity and selectivity. The fabricated enzyme-free glucose sensor can be utilized clinically for in-vivo glucose monitoring. The research was focused on the fabrication of the third generation of the glucose sensors. It is extremely important to replace the harmful (invasive) method of glucose detection with a less harmful method. Diabetic people need to be able to monitor their glucose level easily, accurately, and with less harm. The research was directed to investigate different nanostructured semiconductor materials for a glucose sensor that can address all the points above.

D.3 Impact of Research Results on the Environment

Since ZnO is a biocompatible material, glucose sensors based on ZnO NRs are not toxic devices and can be used safely to monitor glucose. In addition, ZnO material can be

disposed safely with no environmental issues. The fabricated glucose sensors are important for diabetic people and using these kinds of glucose sensors will help in reducing some medical tools that might be harmful and difficult to dispose. Furthermore, the chemical materials used in the research were organic chemicals that dissolve in water without causing problems.

**Appendix E: Microsoft Project for Ph.D. microEP Degree Plan**

| | ❶ | Task Mode | Task Name | Duration | Start | Finish |
|---|---|---|---|---|---|---|
| 1 | ✓ | ⟱ | Mohammed Marie | 1 day | Wed 12/11/13 | Wed 12/11/13 |
| 2 | ✓ | 📌 | Searching for major advisor | 46 days | Sun 9/1/13 | Fri 11/1/13 |
| 3 | ✓ | 📌 | Training in the optoelectronics lab | 101 days | Fri 1/10/14 | Fri 5/30/14 |
| 4 | ✓ | 📌 | Finish the written candidacy exam | 30 days | Mon 3/23/15 | Fri 5/1/15 |
| 5 | ✓ | 📌 | Defending the candidacy research proposal | 56 days | Mon 6/1/15 | Sat 8/15/15 |
| 6 | ✓ | 📌 | writing a paper in one of the technical journals about ZnO biosensor | 174 days | Fri 5/1/15 | Wed 12/30/15 |
| 7 | ✓ | 📌 | Attending the MRS Fall meeting | 5 days | Mon 11/2/15 | Fri 11/6/15 |
| 8 | ✓ | 📌 | Fabricating the electrochemical sensor | 89 days | Sun 9/20/15 | Wed 1/20/16 |
| 9 | ✓ | 📌 | Characterizing the device | 66 days | Wed 1/20/16 | Wed 4/20/16 |
| 10 | ✓ | 📌 | Non – enzymatic electrochemical sensor (Fabrication and characterization). | 262 days | Wed 4/20/16 | Thu 4/20/17 |
| 11 | ✓ | 📌 | Synthesizing Si NWs using RIE system and nanospheres lithography | 219 days | Mon 5/1/17 | Thu 3/1/18 |
| 12 | ✓ | 📌 | Attending the APS march meeting | 5 days | Mon 3/5/18 | Fri 3/9/18 |
| 13 | ✓ | 📌 | Writing my PH.D. dissertation | 67 days | Tue 3/20/18 | Wed 6/20/18 |
| 14 | ✓ | 📌 | Defending my Ph.D. dissretation | 1 day | Tue 10/9/18 | Tue 10/9/18 |
| 15 | ✓ | 📌 | Graduation | 39 days | Wed 10/10/18 | Sat 12/1/18 |

GANTT CHART

**Appendix F: Identification of All Software Used in Research and Dissertation Generation**

Computer #1:

       Model Number: acer
       Serial Number: 14131953217
       Location: ELEG
       Owner: Electrical Engineering department/University of Arkansas

Software #1:

       Name: Microsoft Office 2010
       Purchased by: Electrical Engineering Department, University of Arkansas

Software #2:

       Name: Origin 8.6Bit
       Serial number: GF3S4-6078-7604856

Software #3:

       Name: AutoCad
       Purchased by Electrical Engineering department, University of Arkansas (Blackmesa).

Software #4:

       Google SketchUp

       Downloaded for free from https://www.sketchup.com/download

Software #5:

       Name: Gamry Echem Analyst version 5.61

       Downloaded for free from https://www.gamry.com/support/software-updates-3/

Computer #2:

       Model: Dell

       Serial Number: HZ221F1

       Location: Electrical Engineering department, Optoelectronics lab.

       Owner: Electrical Engineering Department.

Software #1:

       Name:Varian UV Scan application.

       Version:  3.00(339).

       Serial number: EL99093019

Software #2:

       Name: Microsoft office 2007.

Purchased by:  Electrical Engineering department.

Computer #3:

Model: Dell

Serial Number: CP9RVV1

Location: Electrical Engineering department, Optoelectronics lab.

Owner: Electrical Engineering Department.

Software #1:

Name: LabSpec

Version: 5.7824

Computer #4:

Model: Trion Minilock Phantom III

Serial number: (MNLIII 8423)

Location:Electrical Engineering Department, Optoelectronics lab.

Owner: Electrical Engineering Department.

Software #1:

Name: PLC

**Appendix G: All Publications Published, Submitted and Planned**

G.1. List of the published articles.

1. **M. Marie**, S. Mandal, and M. O. Manasreh, "An Electrochemical Glucose Sensor Based on Zinc Oxide Nanorods," *Sensors,* Article vol. 15, no. 8, pp. 18714-18723, AUG 2015.

2. **M. Marie** and M. O. Marasreh, "Investigation of the Influence of the As-Grown ZnO Nanorods and Applied Potentials on an Electrochemical Sensor for In-Vitro Glucose Monitoring," *Chemosensors,* vol. *5*, no. 1, 2017.

3. **M. Marie**, A. Manoharan, A. Kuchuk, S. Ang, and M. O. and Manasreh, "Vertically grown zinc oxide nanorods functionalized with Ferric oxide for in-vivo and non-enzymatic glucose detection," *Nanotechnology,* vol. 29, no. 11, 2018.

4. S. Mandal, **M. Marie**, A. Kuchuk, M. O. Manasreh and M. Benamara "Sensitivity enhancement in an in-vitro glucose sensor using gold nanoelectrode ensembles," *J Mater Sci: Mater Electron,* vol. 28, no. 7, 2017.

5. **M. Marie**, S. Mandal and M. O. Manasreh (2016). "An enzymatic glucose detection sensor using ZnO nanostructure," *MRS Advances*, vol. 1, pp 847-853, 2016.

6. A. Nusir, S. Bauman, **M. Marie**, J. Herzog and M. O.Manasreh, "Silicon nanowires to enhance the performance of self-powered near-infrared photodetectors with asymmetrical Schottky contacts," *Applied Physics Letters*, vol. 111, 2017.

G.2. List of the submitted articles.

1. Rao, Lei; **Marie, Mohammed**; Nusir, Ahmad; Vasan, Ramesh; Benamara, Mourad; Manasreh, M. Omar, Manuscript ID: jp-2017-09393a, Mechanisms of Metal-Assisted Chemical Etching of Si Covered by Perforated-Au and Continuous-Au Films as Catalysts, submitted to The Journal of Physical Chemistry, Sep-22-2017.